

Fundamental stellar parameters for selected T-Tauri stars in the Chamaeleon and Rho Ophiuchus star-forming regions

D. J. James^{1*}, A. N. Aarnio², A. J. W. Richert³, P. A. Cargile⁴, N. C. Santos^{5,6}, C. H. F. Melo⁷ and

¹*Cerro Tololo InterAmerican Observatory, Casilla 603, La Serena, Chile*

²*University of Michigan Department of Astronomy, 403 West Hall, 1085 S. University Ave, Ann Arbor, MI 48109, USA*

³*Department of Astronomy and Astrophysics, The Pennsylvania State University, 525 Davey Lab, University Park, PA 16802, USA*

⁴*Harvard-Smithsonian Center for Astrophysics, 60 Garden St, Cambridge, MA 02138, USA*

⁵*Instituto de Astrofísica e Ciências do Espaço, Universidade do Porto, CAUP, Rua das Estrelas, 4150-762 Porto, Portugal*

⁶*Departamento de Física e Astronomia, Faculdade de Ciências, Universidade do Porto, Rua do Campo Alegre, 4169-007 Porto, Portugal*

⁷*European Southern Observatory (ESO), Casilla 19001, Santiago 19, Chile*

⁸*Laboratoire d'Astrophysique, Observatoire de Grenoble, BP 53, 38041 Grenoble, France*

Accepted XXX. Received YYY; in original form ZZZ

ABSTRACT

We present the results of an optical photometry and high-resolution spectroscopy campaign for a modest sample of X-ray selected stars in the Chamaeleon and Rho Ophiuchus star forming regions. With $R \sim 50000$ optical spectra, we establish kinematic membership of the parent association and confirm stellar youth for each star in our sample. With the acquisition of new standardized $BVIc$ photometry, in concert with near-infrared data from the literature, we derive age and mass from stellar positions in model-dependent Hertzsprung-Russell diagrams. We compare isochronal ages derived using colour-dependent extinction values finding that, within error bars, ages are the same irrespective of whether $E(B - V)$, $E(V - Ic)$, $E(J - H)$ or $E(H - K)$ is used to establish extinction, although model ages tend to be marginally younger for redder E_{colour} values. For Cham I and η Cha members we derive ages of $\lesssim 5$ -6 Myr, whereas our three η Cha candidates are more consistent with a $\gtrsim 25$ Myr post-T Tauri star population. In Rho Ophiuchus, most stars in our sample have isochronal ages < 10 Myr. Five objects show evidence of strong infrared excess ($Av > 5$) in the 2MASS colour-colour diagram, however in terms of $H\alpha$ emission, all stars except RXJ1625.6-2613 are consistent with being weak-lined T-Tauri stars. Spectral energy distributions (SEDs) over the range $\simeq 4000\text{\AA} < \lambda < 1000\mu\text{m}$, show that only one Chamaeleon star (RXJ1112.7-7637) and three Rho Ophiuchus stars (ROXR1 13, RXJ1625.6-2613 & RXJ1627.1-2419) reveal substantial departures from a bare photosphere.

Key words: stars: circumstellar matter, stars: fundamental parameters, stars: evolution, stars: Hertzsprung-Russell and colour-magnitude diagrams, stars: pre-main-sequence, stars: late-type.

1 INTRODUCTION

Star forming regions (SFRs) and young star clusters seed a variety of empirical and theoretical investigations into the fundamental physical processes governing how stars form and evolve. Exemplar domains of study include proto-stellar formation and evolution (Bate 1998; Wuchterl & Tscharnuter 2003), circumstellar disc dynamics (Haisch, Lada & Lada 2001; Bate 2011), extra-solar planet formation (e.g. Pollack et al. 1996; Tsukamoto et al. 2013), and

exoplanet orbital mechanics (Trilling et al. 1998; Armitage 2003; Nelson & Benz 2003a,b). Observational efforts, through optical and infrared photometric and spectroscopic surveys, are required to understand such processes and generally necessitate a large sample of confirmed members of parent SFRs or young clusters with well-constrained fundamental stellar parameters.

Young stellar objects (YSOs) fall into four main classes generally denoted 0–III, representing an evolutionary sequence from protostar shrouded by natal molecular cloud material through to a discless system possibly hosting an evolved planetary system. Embedded class 0–I objects (Lada 1987; André et al. 1993) transition to class II when the surrounding envelope has cleared. Class II objects correspond with classical T Tauri stars (CTTS), defined by

* Visiting astronomer, Cerro Tololo Inter-American Observatory, National Optical Astronomy Observatory, which is operated by the Association of Universities for Research in Astronomy (AURA) under a cooperative agreement with the National Science Foundation

their enhanced infrared (disc) emission, excess blue emission from accretion luminosity, and numerous spectral features in emission; further, broad and complex line morphologies are observed which are due to circumstellar material. Class III YSOs show little or no near-infrared excess, and correspond to weak-lined T-Tauri stars (WTTS), which also exhibit little spectral line emission above expected chromospheric activity levels, consistent with the cessation of circumstellar disc accretion as the inner disc has been depleted.

More remains unknown than known concerning the evolution of circumstellar discs; in particular the mechanisms most responsible for driving accretion (i.e. outward angular momentum transport) and dissipation in Class I and II systems. Circumstellar discs are also important testbeds for theories of planet formation and migration. Near-infrared spectral energy distributions (SEDs) of so-called *transition discs* (Forest et al. 2004) have long been thought to reveal the presence of gaps cleared by massive planets, as in type II planet migration (e.g. Nelson & Benz 2003a,b). This has been confirmed in several cases via direct imaging and interferometry (e.g. Skemer et al. 2014; Brogan et al. 2015). Nearby systems showing excess infrared emission consistent with the presence of a disc therefore make logical targets for followup imaging to probe disc structure, search for signs of protoplanet–disc interactions, and possibly direct detection of embedded protoplanets. Measuring stellar ages will therefore be key in observationally constraining planet formation timescales.

Circumstellar disc evolution, especially with regard to planet formation and migration, is a high priority science driver of the current and next-generation optical, infrared and sub-mm observatories such as the Transiting Exoplanet Survey Satellite (*TESS*), the Atacama Large Millimeter/submillimeter Array (ALMA), and the James Webb Space Telescope (e.g. Wolf et al. 2012; Flock et al. 2015; Cowan et al. 2015). Given that the relatively bright stars, in nearby SFRs such as Chamaeleon and Rho Ophiuchus¹, are most likely to be included in the *TESS* mission input catalogue, it is vitally important to fully characterize the fundamental physical properties of their solar-type members. Broadly speaking, complete membership catalogues and well-constrained stellar parameters – especially mass and age – in coeval SFRs and clusters are essential for understanding the time evolution of fundamental physics which govern disc evolution, and thus planet formation and evolution.

In this manuscript, we detail a photometric and spectroscopic campaign of X-ray selected candidate members of the Chamaeleon and Rho Ophiuchus associations, exploiting the dataset to characterize their physical properties and evolutionary status. In § 2, we discuss target selection, telescope observations and data reduction procedures in producing standardized *BVIc* photometry, spectroscopic kinematics and spectral line equivalent widths. We present our results and data catalogues in § 3, using them to confirm membership, and establish youth, of each star of its parent association. In concert with 2MASS and WISE near- and mid-infrared photometry, we construct theoretical Hertzsprung–Russell diagrams to infer stellar age and mass for each object in our sample. In § 4, we detail a programmatic search for the presence of circumstellar accretion discs of our sample, exploiting optical and infrared photometric data in order to construct SEDs for each candidate member of Chamaeleon and Rho Ophiuchus. In concluding, we deliver a discussion and summary of our research program in § 5.

2 TARGET SELECTION AND OBSERVATIONS

Young, low-mass stellar objects are oftentimes associated with super-solar levels of magnetic activity, which is manifest through elevated X-ray and radio emission (Feigelson & Montmerle 1999; James et al. 2000; James et al. 2006; Cargile et al. 2009). For our study into the properties of both the Chamaeleon and Rho Ophiuchus SFRs, mirroring the strategy in our earlier studies (James et al. 2006 – [J06], Santos et al. 2008 – [S08]), we selected candidate SFR stars within positional error circles of detections in the ROSAT All-Sky Survey [RASS]. For each candidate WTTS, physical properties such as proper motions, radial velocities [RVs], Lithium abundances and near infrared colours are used to ascertain membership of their parent association, details of which are presented in § 3.1.

In order to investigate the fundamental properties of each SFR member, specifically mass and age, we pursued photometric and spectroscopic observing campaigns in the optical to complement existing near- and mid-infrared all sky survey photometry now available in the literature. Observations, data reduction and analysis for each campaign are discussed below.

2.1 Photometry

BVIc photometric data for individual fields containing X-ray selected candidates of Chamaeleon and Rho Ophiuchus were obtained using the 1.0m SMARTS telescope (the former YALO telescope) situated at the Cerro Tololo InterAmerican Observatory [CTIO], Chile, on the night of UT20070630. The data were acquired with the quad-amplifier Y4KCAM CCD camera, equipped with Johnson-Cousins filters, which with its 15 μm pixels and 0.289 arcsec/pixel plate scale results in an on-sky areal coverage of $19'.3 \times 19'.3$. We note that during the 2007 observing season, one of the quad-amplifiers of Y4KCAM was inoperable in the North-West corner of the array, resulting in a reduced field of view per image. An observing log of the Chamaeleon and Rho Ophiuchus Y4KCAM observations is presented in Table A1.

All science and standard star images were processed for over-scan region subtraction, master-bias subtraction and flat fielding, using twilight sky images, employing standard procedures in the IRAF² suite of data reduction algorithms. Substantial use was also made of two batch processing IRAF scripts, written by Phil Massey of Lowell Observatory, whose protocol specifically handles the FITS headers and quad-amplifier readout of the Y4KCAM CCD frames. The low space density of the SFRs allows us to employ aperture photometry for science images as well as the standard star field images. Source searching and aperture photometry, with an aperture radius of 13-pixels, were achieved using the DAOPHOT II package in IRAF (Stetson et al. 1990; Stetson 1993).

Equatorial *BVIc* standard stars catalogued in Landolt (1992), with a broad dynamic range of photometric magnitude and colour, and located at a wide distribution of airmass, were observed in order to correct for atmospheric extinction and to transform extinction corrected, instrumental magnitudes onto the standard system. Modified forms of Bouguer’s law, see Eqs. 1–4, were used to de-

¹ Rho Ophiuchus has already been observed in Field 2 of the Kepler2 mission

² IRAF, in our case through <http://iraf.net>, is distributed by the National Optical Astronomy Observatories, which are operated by the Association of Universities for Research in Astronomy, Inc., under cooperative agreement with the National Science Foundation.

fine the relationship between standard and instrumental magnitudes for the ensemble of standard stars.

$$V = v + \varepsilon(B - V) + \xi_v - \kappa_v.X \quad (1)$$

$$V = v + \phi(V - I) + \xi_v - \kappa_v.X \quad (2)$$

$$(B - V) = \mu(b - v) + \xi_{bv} - \mu \kappa_{bv}.X \quad (3)$$

$$(V - I)_c = \psi(v - i)_c + \xi_{vi} - \psi \kappa_{vi}.X \quad (4)$$

where

- V , $(B - V)$ and $(V - I)_c$ are magnitudes/indices on the *BVI*_c standard system.
- v , $(b - v)$, and $(v - i)_c$ are measured, instrumental magnitudes/indices.
- κ_v , κ_{bv} and κ_{vi} are wavelength (filter) dependent extinction coefficients.
- ε , ϕ , μ and ψ are colour transformation coefficients.
- ξ_v , ξ_{bv} and ξ_{vi} are zero-point coefficients.
- X = airmass of target [$\simeq \sec z$ - where z is the zenith distance]

Unknown extinction coefficients, colour transformation coefficients and zeropoints were determined by solving the self-similar series of linear simultaneous algebraic equations detailed in Eqs. 1–4. For the ensemble of standard star observations, solutions were derived using a least-squares fit algorithm³ which processes the numeric parameters via an iterative refinement method. Comparing calculated magnitudes and colours of Landolt standard stars to their published values allows an iterative rejection process to take place, thereby eliminating seriously discrepant standard star measurements. Standard star measurements were eliminated from the fit if the difference between their calculated and published magnitudes were $\gtrsim 3\sigma$ away from equality, with a final solution being accepted if the RMS of these differences was $\lesssim 0.02$ magnitudes. In this way, approximately 70-80 standard stars were observed, with 60-70 stars used in the final solution. In order to test whether the solutions to the colour equations have parameter dependencies on magnitude, colour, airmass or time of observation, we compared calculated and published values of the observed Landolt standard star fields searching for parameter correlations. None were found.

Solutions to the colour equations are listed in Table 1. Target star photometry is easily determined by substituting the derived extinction, transformation and zero-point coefficients, and measured instrumental magnitudes into Eqs. 1–4. Comparing our colour equation coefficients to similar data acquired with the exact same instrument set up (*c.f.*, Cargile & James 2010), we find that our colour transformation coefficients agree to within $\simeq 1 - 2$ per cent of the Cargile & James values, except for the B-V one, where the difference is of order 5 per cent. Judging the similarity of extinction coefficients and zero-points is very difficult because of the way we solve the colour equations, calculating all three coefficients simultaneously, allowing the least-squares solution to *see-saw* about the colour-transformation coefficient as a fulcrum. What we can say is that comparing our coefficient values in Table 1 with those

in table 2 of the Cargile & James paper shows that there are no obviously deviant coefficient data points. In any case, we are able to reproduce the colours and magnitudes of Landolt standard stars throughout the UT20070630 night to the $\simeq 1 - 2$ per cent level (*e.g.*, see RMS delta-magnitudes in both studies).

Initial stellar coordinates (RA, DEC) were calculated using 6-coefficient fits to CCD X,Y values using Digitized Sky Survey [DSS] red plates; Object matches were subsequently made with 2MASS catalogues, using a 2-arcsec matching radius, and we employ these 2MASS J2000 sexagesimal coordinates for each SFR candidate member (columns 4-5 in table A1).

2.2 Spectroscopy

With the express goals of deriving radial velocities and detection of the resonance doublet of neutral Lithium at 6708Å, facilitating SFR kinematic membership and youth assessments, we have obtained high-resolution échelle spectra of our SFR candidate members in Chamaeleon and Rho Ophiuchus. The high resolution ($R \equiv \lambda/\Delta\lambda \sim 50000$) spectra were acquired in service mode with the UVES spectrograph on the Kueyan 8.2-m telescope located at the Paranal site of the European Southern Observatory (programme ID 075.C-0272). The observations were made using the Red 580 mode of cross disperser #3, with a spectral window of 4800–7000Å (with a small gap between 5700–5840Å), using the SHP700 filter, employing a 0.9-arcsec slit and 2×2 binning of the MIT/LL EEV detector (CCD-44). An observing log of the Chamaeleon and Rho Ophiuchus UVES observations is presented in Table A2.

Data reduction in the form of removal of instrumental effects (de-biasing, flat-fielding), spectral extraction and wavelength calibration (using corresponding ThAr lamp spectra) of the UVES spectra was performed using the instrument's dedicated reduction pipelines. Heliocentric radial velocities [RVs] were calculated by cross-correlation techniques (Tonry & Davis 1979) relative to the slowly-rotating IAU and GAIA velocity standard star HD 76151 (Nordström et al. 2004; Soubiran et al. 2013) using the spectral range 5000-5350Å. This spectral window is ideal for RV determinations because it contains many deep metal absorption lines (especially the Mg I triplet) and little telluric contamination. Cross correlation of the HD 76151 UVES spectrum against other IAU velocity standards reveal that external errors on the standard system are $\simeq 0.4 \text{ km s}^{-1}$. Random errors were calculated in a similar manner to the J06 study, and vary from 0.2 km s^{-1} for slowly rotating stars increasing to $\simeq 2 - 3 \text{ km s}^{-1}$ for more rapidly rotating objects ($\gtrsim 20 \text{ km s}^{-1}$).

In order to measure equivalent widths [EW] of the Li I resonance doublet at 6708Å, we first normalized target UVES spectra by division of a $\simeq 25^{th}$ -order cubic spline fit to the data over the 6600-6800 Å spectral window, masking out the Balmer series H α region from the fit. We employ both the direct integration and Gaussian fitting methods (*e.g.* see J06), so our EW values encompass contributions from the small Fe I+CN lines at 6707.44Å, leading to measured Lithium EWs that result in a minorly ($10 - 20 \text{ mÅ}$) overestimated photospheric Li presence (Soderblom et al. 1993 report that this Fe line blend has an empirical $\text{EW} = [20(B - V)_0 - 3] \text{ mÅ}$, for main sequence, solar-type stars). In the case of H α , we followed the same procedure as J06 in that the normalized spectrum of an old, slow rotating, minimum-activity standard star of similar spectral type was first subtracted from the Chamaeleon and Rho Ophiuchus candidate's spectrum. This methodology is powerful because it takes account of (at least to first order) telluric contamination and acts to remove the photospheric contribution to the

³ The algorithm, F04AMF, is distributed by the Numerical Algorithms Group (NAG)

Table 1. Calculated extinction, transformation and zero-point coefficients on the standard *BVIc* system for photometric observations using the CTIO SMARTS 1.0m telescope+Y4Kcam during the night of UT20070630.

| Colour Equation | Extinction ^b Coefficient | CTC ^{a,b} | Zero ^b Point | RMS ^c Δ mag | No of. Standards ^d |
|-----------------|-------------------------------------|--------------------|-------------------------|-------------------------------|-------------------------------|
| $V [B - V]$ | 0.1077 | 0.0366 | -2.0593 | 0.0160 | 84, 69 |
| $V [V - Ic]$ | 0.1065 | 0.0277 | -2.0552 | 0.0176 | 81, 70 |
| $B - V$ | 0.1137 | 0.8306 | -0.0857 | 0.0186 | 77, 62 |
| $V - Ic$ | 0.0332 | 1.0076 | 0.7515 | 0.0158 | 84, 64 |

a – CTCs are colour transformation coefficients.

b – Extinction coefficients (magnitudes/airmass), CTCs and zeropoints, as described in Eqs. 1–4.

c – RMS of differences between measured and published magnitudes of Landolt (1992) standard stars.

d – Initial and final numbers of standard stars used in fits to colour equations.

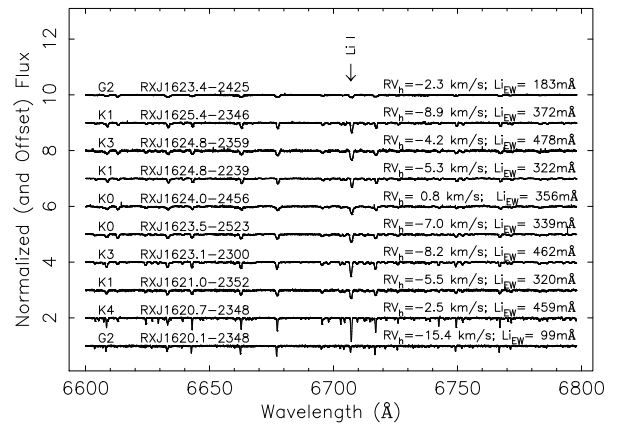
H α line. In our case, we used UVES spectra of the slowly rotating stars HD 76151 (G3V, Prot=15days, Barnes 2007), HD 196761 (G8V, Prot=31days, Wright et al. 2004) and HD 191408 (K2.5V, Prot=45days, Barnes 2007), whose spectral types were verified by cross-correlation against the digital spectral library presented in James (2013).

Finally, we exploit our UVES spectra in order to calculate spectroscopic projected equatorial rotation rates, $v \sin i$, for our SFR targets by cross correlation with similar spectra of the minimum activity, slowly rotating late-type stars listed above (c.f., James & Jeffries 1997). Calibration of the width of the inverse cross correlation function is achieved by artificially broadening (Gray 1992; limb-darkening fixed at 0.6) a high-S/N spectrum of a given minimum activity star, and cross-correlating it with its un-broadened original for a series of incremental $v \sin i$ values. By measuring the width of the central peaks in the resulting inverse cross-correlation functions, as a function of rotation rate in the broadening kernel, a relationship between rotation rate and cross correlation function width is readily produced. Empirical simulations, similar to those detailed in J06, were performed to show that UVES $v \sin i$ values are reproducible at the ± 10 per cent level down to an upper limit of $\simeq 4 - 5 \text{ km s}^{-1}$.

3 RESULTS

Optical *BVIc* and infrared *JHK* photometry, from Y4KCAM observations and 2MASS, respectively, are presented for our candidate members of the Chamaeleon and Rho Ophiuchus SFRs in Table 2; accompanying table notes detail data sources for each object. Data products for our UVES observations are presented in Table 3, which include spectral types drawn from the literature. Equivalent widths for the H α and Li I 6708Å spectral lines are provided using both Gaussian fit and direct integration methods. A representative sample of normalized UVES spectra, in the 6700Å region, for candidate members of Rho Ophiuchus is shown in Figure 1.

Each subset of the observational data can be engaged in deriving fundamental properties for each candidate SFR member and of the parent SFR itself. We will investigate five cornerstone characteristics of the observational data in the following manner. **First**, our UVES spectra provide radial velocities and Lithium detections for each star, which assist us in assigning kinematic membership of each SFR and in assessing stellar youth. **Second**, optical and infrared photometry, in concert with spectral types, allows us to measure colour-dependent reddening vectors, which contribute to

**Figure 1.** Normalized (and offset) rest-frame UVES spectra for a sample of candidate members of the Rho Ophiuchus SFR are shown. Heliocentric radial velocities and Gaussian-fit Li I 6708Å EWs are annotated for each star (c.f. Table 3).

our spectral energy distribution analysis of Chamaeleon and Rho Ophiuchus members suspected of being classical T Tauri stars (see § 4). **Third**, JHK photometry can be exploited to search for excess infrared emission, indicative of the presence of a circumstellar accretion disc around young stars, and represents one of the key demarcation signatures between classical and weak-line T Tauri stars. Extremely high levels of H α emission can also be indicative of circumstellar material, allowing us to use our UVES spectra to correlate infrared excess with strong H α emission. **Fourth**, employing effective temperatures and bolometric corrections (for bolometric luminosity determinations) derived from spectral types, facilitating the construction of theoretical Hertzsprung-Russell diagrams [HRDs] leading to determinations of stellar mass and age. **Fifth**, combining optical and near-to-mid infrared photometry with radiative transfer models, we construct spectral energy distributions [SEDs] for each candidate SFR member observed to search for, and characterize, signature evidence of circumstellar discs and blueward excesses indicative of ongoing accretion. The following sections are dedicated to describing each observational dataset in terms of the fundamental nature of our target stars, culminating in a commentary for each of these five investigative avenues.

Table 2. Optical $BVIc$ (Y4Kcam) and infrared (2MASS) photometry for SFR candidate members

| Object | $^a V \pm \text{err}$ | $^a (B - V) \pm \text{err}$ | $^a (V - I)c \pm \text{err}$ | $J \pm \text{err}$ [2MASS] ^b | $H \pm \text{err}$ [2MASS] ^b | $K' \pm \text{err}$ [2MASS] ^b | Err Code ^b |
|-----------------------------|-----------------------|-----------------------------|------------------------------|--|--|---|--------------------------|
| Chamaeleon | | | | | | | |
| RXJ0850.1-7554 | 10.617 \pm 0.001 | 0.747 \pm 0.002 | 0.845 \pm 0.001 | 9.259 \pm 0.026 | 8.848 \pm 0.025 | 8.704 \pm 0.019 | AAA |
| RXJ0951.9-7901 | 10.202 \pm 0.001 | 0.831 \pm 0.002 | ... ^e | 8.587 \pm 0.032 | 8.138 \pm 0.034 | 8.040 \pm 0.029 | AAA |
| RXJ1112.7-7637 | 11.583 \pm 0.002 | ... ^d | 1.344 \pm 0.003 | 9.275 \pm 0.030 | 8.524 \pm 0.055 | 7.999 \pm 0.031 | AAA |
| RXJ1129.2-7546 | 12.946 \pm 0.005 | 1.407 \pm 0.023 | 1.774 \pm 0.005 | 9.817 \pm 0.026 | 9.124 \pm 0.021 | 8.878 \pm 0.024 | AAA |
| RXJ1140.3-8321 | 11.472 \pm 0.002 | 1.142 \pm 0.006 | 1.289 \pm 0.002 | 9.328 \pm 0.023 | 8.709 \pm 0.045 | 8.635 \pm 0.019 | AAA |
| RXJ1158.5-7754a | 10.519 \pm 0.001 | 1.179 \pm 0.003 | ... ^e | 8.219 \pm 0.029 | 7.556 \pm 0.042 | 7.404 \pm 0.021 | AAA |
| RXJ1159.7-7601 | 11.181 \pm 0.002 | 1.150 \pm 0.005 | 1.307 \pm 0.002 | 9.140 \pm 0.027 | 8.469 \pm 0.038 | 8.304 \pm 0.027 | AAA |
| RXJ1201.7-7859 ^c | 8.56 \pm 9.999 | 0.67 \pm 9.999 | 0.75 \pm 9.999 | 7.263 \pm 0.027 | 6.967 \pm 0.044 | 6.848 \pm 0.018 | AAA |
| RXJ1233.5-7523 | 9.539 \pm 0.001 | 0.738 \pm 0.001 | ... ^e | 8.201 \pm 0.020 | 7.883 \pm 0.040 | 7.756 \pm 0.040 | AAA |
| RXJ1239.4-7502 | 10.344 \pm 0.001 | 0.997 \pm 0.002 | 1.093 \pm 0.001 | 8.434 \pm 0.021 | 7.953 \pm 0.033 | 7.777 \pm 0.021 | AAA |
| Rho Ophiuchus | | | | | | | |
| RXJ1620.1-2348 | 10.053 \pm 0.001 | 0.666 \pm 0.001 | 0.767 \pm 0.001 | 8.753 \pm 0.024 | 8.381 \pm 0.034 | 8.287 \pm 0.021 | AAA |
| RXJ1620.7-2348 | 12.668 \pm 0.004 | 1.374 \pm 0.009 | 1.645 \pm 0.005 | 9.867 \pm 0.023 | 9.141 \pm 0.021 | 8.927 \pm 0.019 | AAA |
| RXJ1621.0-2352 | 10.477 \pm 0.001 | 0.852 \pm 0.001 | 0.935 \pm 0.001 | 8.888 \pm 0.021 | 8.513 \pm 0.045 | 8.393 \pm 0.019 | AAA |
| RXJ1621.2-2347 | 16.015 \pm 0.026 | 2.282 \pm 0.287 | 2.889 \pm 0.027 | 10.728 \pm 0.024 | 9.498 \pm 0.029 | 8.962 \pm 0.023 | AAA |
| RXJ1623.1-2300 | 11.920 \pm 0.002 | 1.313 \pm 0.005 | 1.601 \pm 0.002 | 9.042 \pm 0.032 | 8.343 \pm 0.040 | 8.184 \pm 0.024 | AAA |
| RXJ1623.4-2425 | 12.720 \pm 0.004 | 1.133 \pm 0.014 | 1.692 \pm 0.005 | 9.708 \pm 0.024 | 9.060 \pm 0.024 | 8.762 \pm 0.021 | AAA |
| RXJ1623.5-2523 | 11.457 \pm 0.001 | 1.268 \pm 0.003 | 1.634 \pm 0.001 | 8.600 \pm 0.024 | 7.979 \pm 0.045 | 7.695 \pm 0.022 | AAA |
| RXJ1624.0-2456 | 13.140 \pm 0.003 | 1.577 \pm 0.014 | 2.100 \pm 0.004 | 9.445 \pm 0.022 | 8.597 \pm 0.044 | 8.280 \pm 0.020 | AAA |
| RXJ1624.8-2359 | 14.117 \pm 0.005 | 1.810 \pm 0.021 | 2.589 \pm 0.005 | 9.430 \pm 0.027 | 8.275 \pm 0.038 | 7.857 \pm 0.020 | AAA |
| RXJ1624.8-2239 | 9.781 \pm 0.001 | 0.974 \pm 0.001 | 1.138 \pm 0.001 | 7.779 \pm 0.027 | 7.280 \pm 0.027 | 7.084 \pm 0.018 | AAA |
| RXJ1625.0-2508 | 12.276 \pm 0.003 | 1.340 \pm 0.006 | 1.873 \pm 0.004 | 8.992 \pm 0.023 | 8.324 \pm 0.034 | 8.081 \pm 0.024 | AAA |
| RXJ1625.4-2346 | 11.989 \pm 0.002 | 1.238 \pm 0.005 | 1.707 \pm 0.002 | 8.833 \pm 0.027 | 8.081 \pm 0.021 | 7.822 \pm 0.027 | AAA |
| RXJ1625.6-2613 | 11.759 \pm 0.002 | 1.283 \pm 0.005 | 1.674 \pm 0.002 | 8.688 \pm 0.019 | 7.947 \pm 0.055 | 7.517 \pm 0.024 | AAA |
| ROXR1 13 | 13.881 \pm 0.005 | 2.185 \pm 0.028 | 3.096 \pm 0.005 | 8.090 \pm 0.021 | 6.862 \pm 0.046 | 6.227 \pm 0.018 | AAA |
| RXJ1627.1-2419 | 14.133 \pm 0.009 | 1.751 \pm 0.033 | 2.823 \pm 0.010 | 8.745 \pm 0.027 | 7.507 \pm 0.038 | 6.719 \pm 0.024 | AAA |

a – V , $(B - V)$ and $(V - I)c$ data are calculated using our UT20070630 Y4KCAM observations, with internal statistical errors annotated.

b – JHK data are taken from the 2MASS All-Sky Release Point Source catalogue (March 2003). [<http://irsa.ipac.caltech.edu/applications/Gator/>]

c – Optical $BVIc$ data for RXJ1201.7-7859 are taken from Torres et al. (2006).

d – The B-filter image had a corrupted readout.

e – The star was saturated in the I-filter image.

3.1 Membership of the parent SFR

An understanding of the age-rotation-magnetic activity paradigm (e.g. Hempelmann et al. 1995, Neuhäuser et al. 1995, Alcalá et al. 1996, J06, Cargile et al. 2009) already implies that these low-mass SFR candidate members, being optical counterparts to RASS X-ray detections, are either very young and rapidly rotating, are short-period multiple stars systems, or are both. Irrespective of whether each Chamaeleon and Rho Ophiuchus candidate is a classical or weak-lined T Tauri star, we can assign membership of each star relevant to their parent associations through a careful consideration of each one's astrometric and kinematic properties.

In Figure 2, we display astrometric data for each star in our sample to ascertain whether our targets are consistent with membership of any particular young SFR in their vicinity. In the left-hand plot, we show that all of our targets, as expected and without exception, fall into the expected regions of (l, b) , Galactic coordinate space, for both the Chamaeleon and Rho Ophiuchus SFRs (based on previous work and examples by Sartori et al. 2003 and Aarnio et al. 2008).

While SPM4 (Girard et al. 2011) and/or UCAC4 (Zacharias et al. 2012) proper motion data exist for about half of our Rho Ophiuchus sample, they are oftentimes neither

precise enough, nor unambiguous enough, to provide us with a definitive membership indication of their parent association (c.f. Mamajek 2008, Ducourant et al. 2005). Only one Rho Ophiuchus object is a clear proper motion non-member of the SFR, RXJ1620.1-2348, for which we show in § 3.3 is a probable field star. For the Chamaeleon sample however, a summary of high quality proper motion vectors are available in the literature (e.g. López Martí et al. 2013a; López Martí et al. 2013b), which we plot in the right-hand panel of Figure 2. A comparison to proper motion vectors of young stars in the vicinity allows us to allocate sub-group Chamaeleon membership for our targets.

Interestingly, this proper motion vector phase diagram reveals the following: Three of our Chamaeleon sample, RXJ0850.1-7554, RXJ0951.9-7901 and RXJ1140.3-8321, have two-dimensional kinematics broadly consistent with being members of the Eta Chamaeleon population, in agreement with the findings of López Martí et al. (2013a). On the other hand, Elliott et al. (2014) assert that RXJ0951.9-7901 and RXJ1140.3-8321 are in fact members of the older (30–40 Myr, Kraus et al. 2014; 45 Myr, Bell et al. 2015) Tucana-Horologium [Tuc-Hor] association. We further note that the position of RXJ0850.1-7554 in proper motion space lies several sigma away from the main Eta Cha clump, and in fact

Table 3. UVES spectroscopic data products for X-ray selected candidate members of the Chamaeleon and Rho Ophiuchus SFRs.

| Target | HJD [days] (+2450000) | Rad Vel. km s ⁻¹ | ΔRV^a km s ⁻¹ | $v\sin i$ km s ⁻¹ | SpTy ^b | ^c Li I 6708Å [mÅ] ^d Gauss ^e Integ. | | ^f H α [mÅ] ^f Fit ^e Integ. | | S/N ^g 6700Å |
|-----------------------------|--------------------------|--------------------------------|---------------------------------------|---------------------------------|-------------------|--|-----|---|------|---------------------------|
| Chamaeleon | | | | | | | | | | |
| RXJ0850.1-7554 ^h | 2712.590 | 17.1 | ... | 49 | G6 | 330 | 319 | 497 (G) | 493 | 87 |
| RXJ0951.9-7901 | 3452.6444 | 12.0 | -27.8 32.3 , -26.1 47.1 | 77 | G7 | 287 | 261 | 1928 (L) | 1855 | 120 |
| RXJ1112.7-7637 | 3453.5495 | 15.0 | 1.4, -0.2 | 31 | K2 | 417 | 408 | 2824 (L) | 2636 | 165 |
| RXJ1129.2-7546 | 3453.5691 | 15.0 | -0.9, -0.5 | 21 | K3 | 460 | 451 | 1067 (L) | 920 | 92 |
| RXJ1140.3-8321 | 3453.6973 | 12.9 | -1.1 | 11 | K3/4 | 203 | 204 | 1167 (G) | 1395 | 105 |
| RXJ1158.5-7754a | 3453.7078 | 13.3 | 2.9, 3.2 | 11 | K3 | 466 | 469 | 1593 (L) | 1305 | 100 |
| RXJ1159.7-7601 | 3453.7176 | 14.0 | -1.1 | 9 | K3 | 448 | 450 | 1043 (G) | 1274 | 105 |
| RXJ1201.7-7859 | 3453.7322 | 18.4 | 6.1, 4.8 | 23 | G5 | 238 | 231 | 325 (L) | 259 | 120 |
| RXJ1233.5-7523 | 3453.7368 | 15.1 | 0.3, -0.9 | 6.5 | K1 | 125 | 124 | 193 (G) | 170 | 150 |
| RXJ1239.4-7502 | 3453.7432 | 13.3 | -1.2, -0.9 | 21 | K2/3 | 412 | 400 | 808 (G) | 827 | 110 |
| RXJ1303.5-7701 | 3453.7485 | 7.9 | 129.0 | 118 | early | 17 | 13 | ... | ... | 95 |
| Rho Ophiuchus | | | | | | | | | | |
| RXJ1620.1-2348 | 3453.8995 | -15.4 | ... | 8.5 | G2 | 99 | 97 | 180 (G) | 138 | 70 |
| RXJ1620.7-2348 | 3456.7326 | -2.5 | ... | 9.5 | K4 | 459 | 449 | 1745 (G) | 2145 | 105 |
| RXJ1621.0-2352 | 3453.9050 | -5.5 | ... | 29 | K1 | 320 | 292 | 458 (G) | 436 | 65 |
| RXJ1623.1-2300 | 3456.7538 | -8.2 | ... | 24 | K3 | 462 | 448 | 1176 (G) | 1162 | 110 |
| RXJ1623.4-2425 | 3456.7774 | -2.3 | ... | 57 | G2 | 183 | 168 | 352 (G) | 334 | 125 |
| RXJ1623.5-2523 | 3466.8534 | -7.0 | ... | 34 | K0 | 339 | 319 | 625 (G) | 524 | 105 |
| RXJ1624.0-2456 | 3466.8706 | 0.8 | ... | 38 | K0 | 356 | 338 | 1620 (L) | 1411 | 100 |
| RXJ1624.8-2359 | 3481.6751 | -4.2 | ... | 40 | K3 | 478 | 452 | 1185 (L) | 1027 | 60 |
| RXJ1624.8-2239 | 3494.6352 | -5.3 | ... | 28 | K1 | 322 | 307 | 1688 (L) | 1290 | 155 |
| RXJ1625.0-2508 | 3466.8934 | -3.0 | ... | 48 | G1 | 167 | 158 | 250 (G) | 178 | 110 |
| RXJ1625.4-2346 | 3494.6471 | -8.8 | ... | 27 | K1 | 392 | 366 | ... | ... | 10 |
| RXJ1625.4-2346 | 3495.6345 | -9.0 | ... | 27 | K1 | 352 | 333 | 614 (G) | 513 | 130 |
| RXJ1625.6-2613 | 3476.7809 | -3.8 | -0.3 | 17 | K7Ve | 479 | 471 | >6400 (L*) | 5976 | 100 |
| ROXR1 13 | 3505.7105 | -7.3 | ... | 68 | K0 | 320 | 284 | 667 (G) | 712 | 55 |
| ROXR1 13 | 3505.7991 | -12.2 | ... | 69 | K0 | 296 | 268 | 1298 (L) | 1250 | 65 |
| RXJ1627.1-2419 | 3505.6780 | -5.0 | -2.3 | 60 | G1 | 194 | 174 | 3521 (L) | 2943 | 50 |

a – We compare our UVES RVs to those detailed in J06 [UVES - J06 values]. Two values listed represent two epochs in the J06 study, which for RXJ0951.9-7901, include its status as a double-lined spectroscopic binary (J06).

b – Spectral types for Chamaeleon stars are taken from Covino et al. (1997) and Alcalá et al. (2000), whereas Martín et al. (1998) data were used for Rho Ophiuchus stars, except for RXJ1625.6-2613, whose spectral type was reclassified as K7Ve in Torres et al. (2006).

c – Li/residual H α features were measured for EWs; by *residual*, we mean that the normalized spectrum of an old, slowly rotating minimum-activity standard star, of similar spectrum type, broadening if the target has $v \sin i > 10$ km s⁻¹, was first subtracted from the normalized spectrum of each target.

d – EWs measured using a Gaussian fit between the limits of where the Li feature approaches unity on either side of its central absorption feature.

e – EWs measured using direct integration between the same wavelength limits as for the Gaussian fitting method.

f – EWs of residual H α emission features were measured with either a Gaussian (G) or Lorentzian (L) function, with limits placed where the feature approaches the continuum level on the red and blue wings. For the Rho Ophiuchus target, RXJ1625.6-2613, the residual emission profile presented substantial non-uniform morphology and sub-structure, which was not adequately fitted by either a Gaussian or Lorentzian function.

g – Approximate S/N of continuum region around 6700Å.

h – UVES data were not obtained for this target; for reference, we reproduce here the measurements of J06.

Elliott et al. (2014) report that RXJ0850.1-7554 is a member of the 30 Myr Carina association.

A further four objects, RXJ1158.5-7754a, RXJ1159.7-7601, RXJ1201.7-7859 and RXJ1239.4-7502 are kinematic members of Eps Chamaeleon (in agreement with the recent Eps Cha membership allocations given by Murphy et al. 2013). Two stars, RXJ1112.7-7637 and RXJ1129.2-7546, have proper motion vectors consistent with the Cham I SFR (in accord with López Martí et al. 2013a), although we note that there is some overlap in this region of the kinematic phase diagram with the Cham II cloud and a wide slew of background sources. We further note that RXJ1303.5-7701 is kinematically consistent with membership of the Cham II association. Finally, RXJ1233.5-7523 has

a very discrepant proper motion vector compared to the any of the Chamaeleon sub-groups, and indeed many of the background sources in the region. We therefore judge this star to be a member of the field population, (concordant with the López Martí et al. 2013a findings) and do not consider it further in our analysis.

3.2 UVES Radial Velocities

One-dimensional kinematic membership of parent SFRs can be judged through assessment of their RV vectors, which are provided in Table 3. For the Chamaeleon candidates, except for RXJ1303.5-7701, this is a simple process because there is a clear grouping of values $\simeq 15$ km s⁻¹, within a scatter of a few km s⁻¹. This velocity

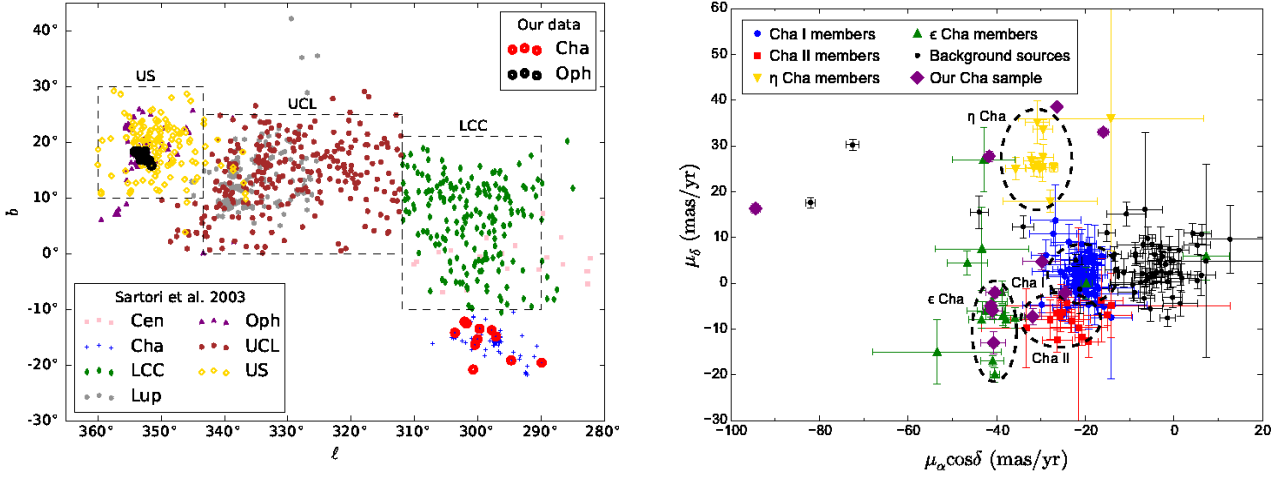


Figure 2. Left-hand panel: In units of degrees, Galactic longitude (l) and latitude (b) are plotted for our Chamaeleon (●) and Rho Ophiuchus (●) candidate SFR members. Comparable data for several well-described SFRs, taken from Sartori et al. (2003), are included for reference (US – Upper Scorpius; UCL – Upper Centaurus Lupus; Lup – Lupus; LCC – Lower Centaurus Crux). Right-hand panel: In concert with data for several sub-groups of the Chamaeleon SFR (López Martí et al. 2013a), proper motion vectors (in mas/yr) are plotted for stars in our Chamaeleon sample. The proper motion data for RXJ1233.5-7523 (middle-left of the plot) show that this star does not belong to any of the main sub-groups of the Chamaeleon SFR.

clumping correlates extremely well with extant RV measurements of objects in the Chamaeleon region (J06, Guenther et al. 2007, Nguyen et al. 2012; Biazzo et al. 2012; Frasca et al. 2015). We note that the Carina and Tuc-Hor associations have systemic RVs of 9.7 ± 0.5 and 20.9 ± 0.9 km s $^{-1}$ respectively (Kraus et al. 2014, Malo et al. 2013). For the Chamaeleon candidates RXJ0850.1-7554, RXJ0951.9-7901 & RXJ1140.3-8321, which are suspected of being members of either the Carina or Tuc-Hor associations instead of the η Cha associations, our UVES RVs cannot unambiguously distinguish between the three associations.

For RXJ1303.5-7701 however, this object is either a non-member of one of the Chamaeleon regions or a binary system, or both. Comparison of its UVES RV to the one reported by J06 shows that the object is binary in nature (RV variant). Moreover, our UVES spectrum confirms the James et al. finding that the object is of early-type spectral-type, having few metal lines and very broad H α and H β Balmer series line profiles, when indeed a G7 spectrum was expected (Alcalá et al. 2000). A zoom-in of a red-plate DSS image shows that, in fact, there is a visual double in the RASS X-ray error circle of RXJ1303.5-7701, one star extremely bright, the other one less so. Our spectroscopic observations (J06 and UVES data presented herein) may therefore not be for the correct optical counterpart in the RASS X-ray error circle, and in a case of *mistaken identity* of the brighter star with the fainter one, the true source of the X-ray emission remains elusive.

However for the Rho Ophiuchus stars in our sample, a 1-d kinematic analysis is a little more difficult to interpret – essentially through a paucity of existing data for our stars and the nature of their single-epoch measurements. However, while there are not extensive, programmatic velocity surveys of the Rho Ophiuchus region yet published, the 1-d radial velocity of its low-mass members is now quite well established to be -7.0 ± 0.7 km s $^{-1}$ (Kurosawa et al. 2006, Guenther et al. 2007, Prato 2007). With the obvious exceptions of RXJ1620.1-2348 and RXJ1624.0-2456, most of our Rho Ophiuchus stars do indeed have UVES RVs clustered around the SFR systemic velocity of -7.0 km s $^{-1}$, albeit with a scatter of ~ 4 km s $^{-1}$.

3.2.1 Radial Velocities: Comparison to J06

Because our UVES spectra were acquired approximately two years after the FEROS data presented in the J06 study, a comparison of their time-separated RVs allows us to identify obvious binary stars in our sample. In order to facilitate such a comparison, we have included a separate column in Table 3 detailing a star-by-star RV difference between the two studies. From two closely-spaced epochs in our UVES data, the RVs of ROXR1 13 are indicative of orbital motion over the course of about 2 hours, albeit that the per-datum precision is quite low (2-3 km s $^{-1}$) due to the high rotation velocity of the object. For the two Rho Ophiuchus stars common to our study and the J06 one, there is no strong evidence of RV variation.

Three Chamaeleon objects appear to be RV variable. The early-type star RXJ1303.5-7701 shows a very large Δ RV value and is clearly a spectroscopic binary star, although there is no evidence or a second or third set of spectral lines in our UVES spectra. Based on our studies alone, RXJ1201.7-7859 is consistent with being a single-lined spectroscopic binary star [SB1], with three RVs quite widely separated from each other, at values 4-5 times the per-datum measurement error. Combined with literature RV values however (Malaroda et al. 2006; Torres et al. 2006; López Martí et al. 2013a; Murphy et al. 2013; Elliott et al. 2014), its SB1 is confirmed.

One of the more interesting curiosities is that of RXJ0951.9-7901. Its J06 entry shows that it is a rapidly-rotating, double-lined spectroscopic binary [SB2], whose double-line features were detected over two different epochs of observation (separated by about 6-days). It is worth noting that K-band speckle interferometry and direct imaging of the system show that it has no nearby companions in the 0.13-6.0 arcsecond range (Köhler 2001), although its J06 K $_1$ and K $_2$ velocities are large enough that both components of an SB2 system at the distance of the Chamaeleon region would easily lie inside an 0.13'' annulus. Our UVES spectrum only shows a single peak in the cross-correlation function, which can be readily explained as having been observed at inferior or superior conjunction of an SB2 system. Based on a further three epochs of observations, Covino et al. (1997) and Guenther et al. (2007) list this star

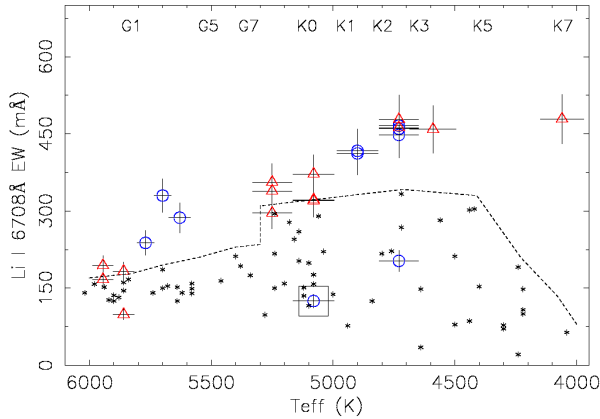


Figure 3. Lithium 6708 Å equivalent width is plotted against effective temperature for our candidate members of the Chamaeleon (◐) and Rho Ophiuchus (◓) SFRs. The boxed data-point represents the proper motion non-member of the Chamaeleon regions, RXJ1233.5-7523. The hand-drawn dashed black line indicates a by-eye estimate of the upper boundary of Lithium for their similar- T_{eff} counterparts in the 125 Myr Pleiades open cluster (*; Soderblom et al. 1993).

as RV-constant, whose RV values are within $\sim 1\text{--}2\text{ km s}^{-1}$ of our UVES value. Finally, Torres et al. (2006) report four epochs of RV measurements for this star, close to our RV value, albeit with quite a large scatter (6.1 km s^{-1}); for such a rapidly rotating star, such a scatter is not particularly unusual. Its J06 SB2 nature may therefore be in doubt, and further RV observations are necessary in order for us to confirm or refute its multiplicity status.

3.3 Lithium abundance of young stars

Fortunately, we can call on Lithium detection as a criterion in assessing youth, and by inference, membership of a young SFR. As both Chamaeleon and Rho Ophiuchus are considered to be active, or at least very recent, sites of star formation, one would expect that insufficient time has passed for substantial depletion of natal Lithium (by proton burning - Bodenheimer 1965) to have occurred. Members of young SFRs should therefore contain Lithium abundance levels far in excess of their typically-much older field star counterparts in the Galaxy.

Because determining precise and accurate ages of field stars is problematic at best, sometimes yielding different ages for different methods (e.g. Barnes 2007, Cargile & James 2010), we choose to compare Lithium levels in our young SFR candidate members to a main sequence open cluster of known age, such as the 125-Myr Pleiades (Basri et al. 1996; Stauffer et al. 1998). Plotted in Figure 3, we show the Lithium EWs of Chamaeleon and Rho Ophiuchus candidates (*c.f.*, Table 3), as a function of effective temperature (using the spectral type-temperature relation for main sequence stars reported by Kenyon & Hartmann 1995 - [KH95]); also included, are corresponding data for the Pleiades cluster (Soderblom et al. 1993). Clearly, most of the Chamaeleon and Rho Ophiuchus candidates are indeed Lithium rich, containing at least as much Lithium as their Pleiades counterparts, oftentimes far more.

There are three notable exceptions to this statement. In Rho Ophiuchus, RXJ1620.1-2348 exhibits a Lithium EW of only

99 mÅ, considerably below its Pleiades counterparts. Given that its RV is also considerably discrepant from the systemic 1-d velocity of Rho Ophiuchus, we postulate that this star is more likely to be a non-member of its parent SFR than a member, and do not consider it in further in our analyses. In the case of the two low-Lithium Chamaeleon candidates, simple explanations present themselves readily.

The proper motion data for RXJ1233.5-7523 (López Martí et al. 2013a – see also Figure 2) show that this star does not belong to any of the main sub-groups of the Chamaeleon SFR, and its low Lithium EW is indicative of its field star status. Star RXJ1140.3-8321 however is a proper motion member of the Eta Cha region (6-7 Myr old, Murphy et al. 2013), has a set of invariant radial velocities consistent with Eta Cha membership, and has a Li I 6708 Å EW within ± 10 per cent of the J06 study. However, as we have discussed previously in this section, there is evidence to suggest that this particular star in fact belongs to the considerably older (45 Myr) Tuc-Hor association. While Jeffries et al. (2009) warn that pre-main sequence [PMS] Lithium depletion in solar-type stars cannot be confidently employed as a *precise* age indicator in young kinematic groups, the Lithium abundance of RXJ1140.3-8321 strongly indicates a post-T Tauri star evolutionary status (*c.f.*, figure 6 of Jeffries et al. 2009 & figure 7 of Kraus et al. 2014). We henceforth consider RXJ1140.3-8321 as a Tuc-Hor candidate member.

In the cases of RXJ0850.1-7554 and RXJ0951.9-7901, adding in Lithium into the membership consideration, we still cannot distinguish between their belonging to η Cha or Carina/Tuc-Hor respectively. This is because even after 30-40 Myr of stellar evolution post birthline, mid-G stars still have not undergone substantial Lithium depletion, and their position in an abundance-temperature plot cannot be differentiated from that of very young T-Tauri stars (Jeffries et al. 2009). We return to their membership status in § 3.6 & 3.6.1.

3.3.1 Lithium: Comparison to J06

Naturally, we ought to compare the variation in Li I 6708 Å EWs for those stars common to the present study and that of J06 (see Figure 4), because outwith the different instruments used, the formalism of the data analysis procedures is identical. With the exception of a few systems, there is good agreement between the two campaigns. However in the case of the deviant Rho Ophiuchus datum (RXJ1627.1-2419) at $\simeq 250\text{ mÅ}$, the disagreement can likely be explained by comparison to the low quality spectrum ($S/N=14$) in the J06 study, manifested as a poor Gaussian fit to the data and/or poor continuum placement. For the two most deviant Cham stars, one is again likely due to a poor quality ($S/N=11$) J06 spectrum of the Cham I star RXJ1129.2-7546. The other, η Cham candidate RXJ0951.9-7601 (although, see also § 3.6.1 for details of its candidacy of the Tuc-Hor group), it is listed as a double-lined spectroscopic binary star in the J06 study, and moreover, of the late-type stars in our samples it is the fastest rotator. Potentially, this is an interesting system for a time-domain Lithium variation follow-up campaign, although line-blending due to rapid rotation and/or binarity make it a problematic system for detailed analysis.

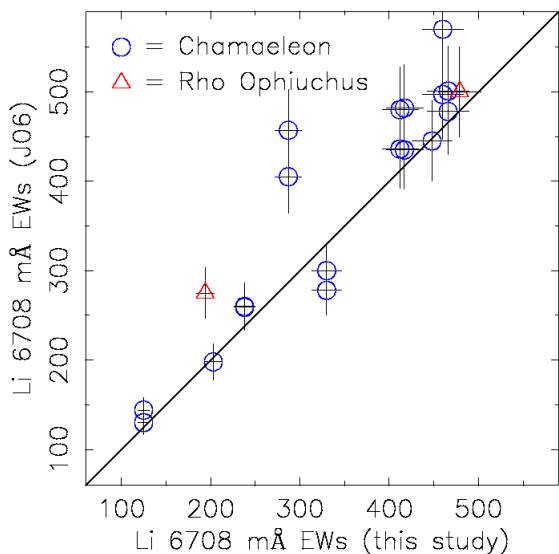


Figure 4. Comparison of Li I 6708 Å equivalent widths for stars in common between the present study and that of J06. Some stars are shown twice, representing multiple epochs of measurement in the J06 study. The solid line represents equality between the two studies and is not a fit to the data.

3.4 Reddening Vectors and Extinction

By comparing our target optical and near-infrared photometry (see Table 2) to theoretical colours based on their spectral type (see Table 3), we can determine photometric colour-dependent reddening and extinction vectors for each SFR candidate member; results of this analysis are presented in Table 4. We note that a small handful of stars yield astrophysically unrealistic negative reddening values, which may result from incorrect spectral type classifications and/or variable photometric data (presumably resulting from heightened stellar activity), and we decline to calculate extinction values for them. Furthermore, we remind the reader that our reddening/extinction analyses are founded upon KH95 model parameters, which are based on main sequence stellar properties. For stellar objects in young star formation regions, such an approach may not be entirely appropriate. In Appendix B, we re-perform our reddening/extinction analyses using the recent pre-main sequence model parameters presented by Pecaut & Mamajek (2013), with relevant discussion included therein.

For our targets in the Chamaeleon sub-regions, most stars exhibit modest A_v values ($A_v \ll 1$) derived from optical and near-infrared photometry. Two objects however, RXJ112.7-7637 & RXJ1129.2-7546, show elevated levels of extinction ($A_v > 1$) across the optical and near-infrared range. The case for Rho Ophiuchus is considerably more interesting however, with > 90 per cent of the sample showing elevated reddening and extinction values across the optical and near-infrared colours; such a result is hardly surprising when one considers the abundantly clear evidence of interstellar gas and dust to be found in the magnificent *true colour* images of the Rho Ophiuchus region (e.g. Hatchell et al. 2012). Four Rho Ophiuchus stars, RXJ1621.2-2347, RXJ1624.8-2359, ROXR1 13 & RXJ1627.1-2419, exhibit in high ($A_v > 5$) extinction values.

We note that irrespective of whether main-sequence or pre-main sequence theoretical data are used, the same stars in Chamaeleon and Rho Ophiuchus are shown to have high ($A_{v,\lambda} >$

5) extinction values (c.f. Tables 4 & B1). We posit that these high reddening/extinction stars are either (i) situated in heavy extinction regions of their parent clouds and/or (ii) systems hosting circumstellar accretion/debris discs, which act to mimic the effects of high reddening/extinction, especially in the near and mid-infrared. Further discussion and analysis of the high extinction stars are presented in § 3.5 & § 4.

3.5 Classical or Weak-Lined?

Exploiting near-infrared photometry can be an efficient, powerful, didactic method for triaging classical and weak-lined stars. A quick visual inspection of Figure 5 allows such a methodology to be easily understood, although caution must be used in interpreting high interstellar extinction cases. In this colour-colour diagram, we plot JHK photometry for our candidate members of the Chamaeleon and Rho Ophiuchus SFRs, as well as loci of field dwarfs and giants, and by extension, their high extinction loci. For comparison, we also plot the data for a sample of F → M-dwarfs on the main sequence (Nidever et al. 2002), as well as data for a sample of known Classical T Tauri stars in the very young ($\simeq 1 - 2$ Myr) Orion Nebula Cluster (e.g. Neuhäuser et al. 1995).

This colour-colour diagram, and the data presented in Table 4, show that one star in Chamaeleon and four stars in Rho Ophiuchus exhibit substantial infrared excess, having data positions well-displaced from un-reddened main-sequence late-type dwarf and giant loci. Interestingly, these five candidates, RXJ112.7-7637 (Cham), ROXR1 13 (ρ Oph), RXJ1621.2-2347 (ρ Oph), RXJ1624.8-2359 (ρ Oph) and RXJ1627.1-2419 (ρ Oph) yield $E(J - H)$ and/or $E(H - K)$ derived extinctions of $A_v > 5$. The remainder of our sample exhibits more moderate extinction, consistent with their having little or moderate infrared excess emission. A handful of stars have infrared colours that lie close to the giant locus, and in-between the giant and dwarf loci, which if confirmed as young members of their parent SFRs, one can imagine interpreting them as being sub-giant-like stars still in the very early pre-main sequence phase (< 10 Myr), having somewhat inflated radii thereby mimicking giant-like stellar properties.

These five high extinction objects ($A_v > 5$), are Lithium rich (see Table 3 and Martín et al. 1998), and are therefore good candidates for classical T-Tauri star status. Historically, albeit with some definition differences among various authors and specific SFRs, classical T-Tauri stars invariably exhibit very strong Balmer series $H \alpha$ emission ($EW_{H\alpha} > 5 - 10 \text{ Å}$ – Barrado y Navascués & Martín 2003, Martín et al. 1998). Only one of our targets, RXJ1625.6-2613, shows $H \alpha$ emission at these CTTS-like levels (see also § C4), and in fact, none of the five high extinction stars have $EW_{H\alpha} > 5 \text{ Å}$. The four high extinction Rho Ophiuchus stars are listed as being either WTTS or young solar-type stars in Martín et al. (1998). While several objects in our sample exhibit $H \alpha$ EWs of order $1 - 3 \text{ Å}$, these activity emission levels are consistent with rapidly rotating late-type stars early on the PMS and zero-age main sequence (e.g. Soderblom et al. 1993, James & Jeffries 1997, Martín et al. 1998, Jeffries et al. 2000, Jeffries et al. 2009).

3.5.1 $H \alpha$ Activity: Comparison to J06

The most likely scenario where activity in the Balmer series $H \alpha$ 6563 Å line is temporally variable for our targets is two-pronged. For such young stars, some combination of circumstellar

Table 4. Reddening and Extinction Vectors for Chamaeleon and Rho Ophiuchus Targets

| Target | $E(B - V)^a$ | $E(V - Ic)^a$ | $E(J - H)^{a,b}$ | $E(H - K)^{a,b}$ | A_v^c [$E(B - V)$] | A_v^c [$E(V - Ic)$] | A_v^c [$E(J - H)$] | A_v^c [$E(H - K)$] |
|-----------------------------|--------------|---------------|------------------|------------------|---------------------------|----------------------------|---------------------------|---------------------------|
| Chamaeleon | | | | | | | | |
| RXJ0850.1-7554 | 0.067 | 0.075 | 0.064 | 0.056 | 0.208 | 0.186 | 0.567 | 0.918 |
| RXJ0951.9-7901 | 0.121 | ... | 0.112 | 0.010 | 0.375 | ... | 0.991 | 0.167 |
| RXJ1112.7-7637 | ... | 0.334 | 0.306 | 0.407 | ... | 0.828 | 2.711 | 6.648 |
| RXJ1129.2-7546 | 0.437 | 0.694 | 0.209 | 0.128 | 1.355 | 1.721 | 1.850 | 2.095 |
| RXJ1140.3-8321 ^d | 0.172 | 0.209 | 0.135 | -0.044 | 0.533 | 0.518 | 1.194 | ... |
| RXJ1140.3-8321 ^d | 0.072 | 0.139 | 0.096 | -0.054 | 0.223 | 0.345 | 0.847 | ... |
| RXJ1158.5-7754a | 0.209 | ... | 0.179 | 0.034 | 0.648 | ... | 1.584 | 0.561 |
| RXJ1159.7-7601 | 0.180 | 0.227 | 0.187 | 0.047 | 0.558 | 0.563 | 1.655 | 0.773 |
| RXJ1201.7-7859 | 0.01 | -0.01 | -0.012 | 0.031 | 0.031 | ... | ... | 0.510 |
| RXJ1239.4-7502 ^d | 0.107 | 0.083 | 0.036 | 0.058 | 0.332 | 0.206 | 0.319 | 0.952 |
| RXJ1239.4-7502 ^d | 0.027 | 0.013 | -0.003 | 0.058 | 0.084 | 0.032 | ... | 0.952 |
| Rho Ophiuchus | | | | | | | | |
| RXJ1620.7-2348 | 0.304 | 0.495 | 0.203 | 0.086 | 0.942 | 1.228 | 1.795 | 1.410 |
| RXJ1621.0-2352 | 0.002 | 0.005 | -0.041 | 0.002 | 0.006 | 0.012 | ... | 0.039 |
| RXJ1621.2-2347 | 1.312 | 1.809 | 0.746 | 0.418 | 4.067 | 4.486 | 6.608 | 6.828 |
| RXJ1623.1-2300 | 0.343 | 0.521 | 0.215 | 0.041 | 1.063 | 1.292 | 1.903 | 0.675 |
| RXJ1623.4-2425 | 0.513 | 0.962 | 0.379 | 0.220 | 1.590 | 2.386 | 3.361 | 3.594 |
| RXJ1623.5-2523 | 0.448 | 0.784 | 0.225 | 0.176 | 1.389 | 1.944 | 1.994 | 2.878 |
| RXJ1624.0-2456 | 0.757 | 1.250 | 0.452 | 0.209 | 2.347 | 3.100 | 4.005 | 3.416 |
| RXJ1624.8-2239 | 0.124 | 0.208 | 0.083 | 0.078 | 0.384 | 0.516 | 0.739 | 1.279 |
| RXJ1624.8-2359 | 0.840 | 1.509 | 0.671 | 0.300 | 2.604 | 3.742 | 5.943 | 4.902 |
| RXJ1625.0-2508 | 0.740 | 1.153 | 0.409 | 0.165 | 2.294 | 2.859 | 3.626 | 2.696 |
| RXJ1625.4-2346 | 0.388 | 0.777 | 0.336 | 0.141 | 1.203 | 1.927 | 2.981 | 2.307 |
| RXJ1625.6-2613 | -0.097 | 0.074 | 0.139 | 0.273 | ... | 0.184 | 1.233 | 4.447 |
| ROXR1 13 | 1.365 | 2.246 | 0.832 | 0.527 | 4.232 | 5.570 | 7.372 | 8.606 |
| RXJ1627.1-2419 | 1.151 | 2.103 | 0.979 | 0.710 | 3.568 | 5.215 | 8.676 | 11.591 |

a – Reddening vectors are calculated by subtracting appropriate photometric colours for each target (see Table 2) from corresponding theoretical values for dwarf stars (from KH95) based on their spectral types (see Table 3).

b – $E(J - H)$ and $E(H - K)$ vectors are based on KH95 JHK data which had been first transformed onto the 2MASS system using the [Carpenter \(2001\)](#) relations.

c – Extinction vectors [A_v], based on four colour-dependent reddening vectors, are calculated to be: For optical data, $A_v = 3.1 \times E(B - V)$ and $A_v = 2.48 \times E(V - Ic)$ (from [Bessell & Brett 1988](#)); For infrared data, $A_v = 8.86 \times E(J - H)$ and $A_v = 16.32 \times E(H - K)$ (from [Ramírez & Meléndez 2005](#)).

d – Two sets of reddening and extinction values are calculated, one for each of the two spectral sub-types.

disc-accretion ([Szegeedi-Elek et al. 2013](#); [Sousa et al. 2016](#)) and/or chromospheric magnetic activity ([Eibe 1998](#); [Barnes et al. 2001](#); [Bell et al. 2012](#)) can readily explain short- and long-term spectral line variations in the Balmer series H α species.

Comparing H α emission in the present sample to the J06 one (see Figure 6) reveals several interesting objects. In the two Rho Oph cases, there is convincing empirical evidence to suggest that both stars have circumstellar accretion discs (see § 4 and Figure 12), and high levels of extinction (at least $A_v > 4$), which naturally provides a physical environment with which to explain their Balmer series H α variable emission over widely-separated epochs.

In the case of Chamaeleon candidates, there are two clear cases of variable H α emission between the J06 and present study. The first arises from the very rapid rotator RXJ0951.9-7901, which is listed as a double-lined spectroscopic binary in J06, and will be re-classified in this study as a 45 Myr Tuc-Hor object (see discussion in § 3.6.1). Given its rapid rotation, modest extinction (see Table 4), post-T Tauri age and clean bare photosphere SED (see § 4 and Figure D2), its time variable H α emission is most likely due to a chromospherically-induced temporal event such as stellar activity

– and its cycle – and/or a magnetic activity flare. The second is a Cham I object (RXJ1112.7-7637), which exhibits high levels of extinction ($A_v > 5$) and shows clear evidence of near- and mid-infrared excess in its SED (see Figure 12). In this case, we feel comfortable attributing its H α emission variability to physical processes associated with its circumstellar accretion disc.

3.6 Hertzsprung-Russell Diagrams: Mass, Age

Placing observational parameters onto the theoretical plane is a well-established and well-calibrated method of determining fundamental stellar characteristics. Converting photometry and spectral types into bolometric luminosity and effective temperatures allows the construction of HRDs, which when combined with theoretical stellar models, yields mass and age determinations for a sample of stars.

Using main sequence bolometric corrections and spectral type-photometric colours & effective temperature relations from KH95, we calculate bolometric luminosity for each of our targets employing their V-magnitudes detailed in Table 2 and four sepa-

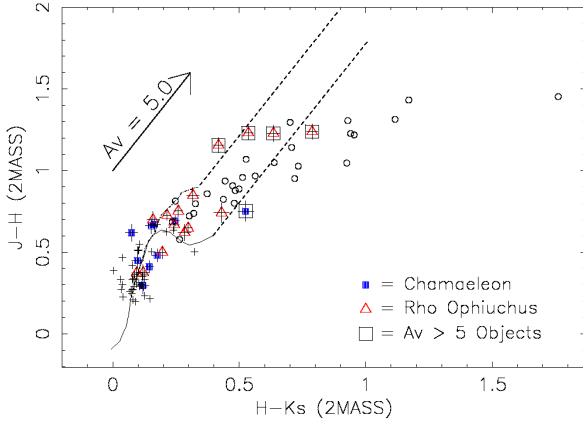


Figure 5. Colour-colour diagram using 2MASS JHK photometry representing our SFR candidate members. We include for comparison data representing field dwarfs (small crosses - Nidever et al. 2002), and Classical T Tauri stars in the Orion SFR (open circles - Neuhäuser et al. 1995). The solid and dot-dashed lines represent $J - H/H - K$ loci for the intrinsic colours of field dwarfs and giants (as detailed by Bessell & Brett 1988), transformed onto the 2MASS JHKs system. The two dashed lines represent reddening vectors originating from the extrema of the Bessel and Brett dwarf and giant sequences.

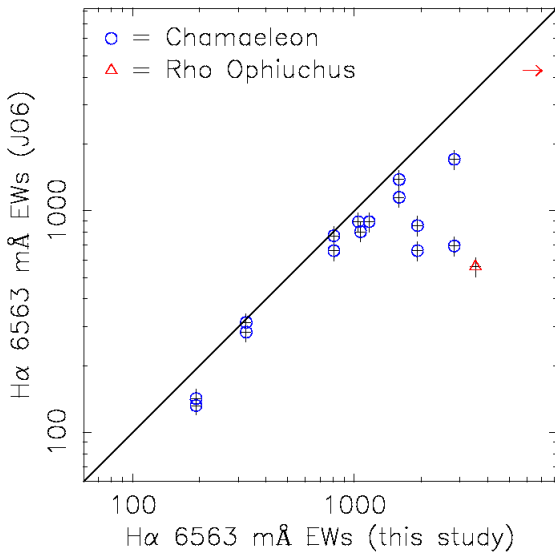


Figure 6. Comparison of Balmer series $H\alpha$ 6563 Å equivalent widths for stars in common between the present study and that of J06. Some stars are presented twice, representing multiple epochs of measurement in the J06 study. The solid line represents equality between the two studies and is not a fit to the data.

rate extinction values (A_v), based on $B - V$, $V - I$, $J - H$, and $H - K$ colour (see Table 4). Distances employed for luminosity calculations are detailed in the footnotes to Table 5, and all theoretical models are based on solar metallicity Padova and Trieste Stellar Evolution Code [PARSEC - (Bressan et al. 2012)] stellar evolution models in our analysis, a pre-main sequence Deuterium burning phase with initial abundance of 2.12×10^{-5} , and incorporating an initial helium fraction of $Y=0.249$. The results of our HRD anal-

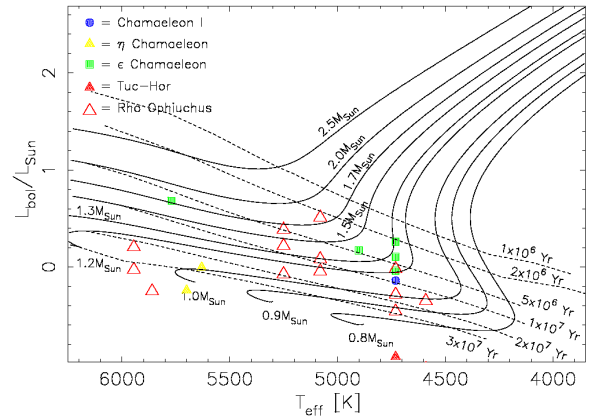


Figure 7. An Hertzsprung-Russell diagram, using A_v extinction values derived from $B - V$ colours (see Table 4), is plotted for Cham I (●), η Cham (▲), ϵ Cham (■), Tuc-Hor (▲) & Rho Ophiuchus (▲) candidates. Effective temperatures, bolometric corrections and reddening vectors are based on KH95 colour-spectral type relationships for dwarf stars, with distances to individual stellar groups cited in Table 5. Stellar isochrones (dashed tracks) and mass tracks (solid lines) are computed from PARSEC solar metallicity, theoretical stellar models (Bressan et al. 2012).

yses are detailed in Tables 5 & 6, and graphically represented in Figures 7–10.

Based on proper motion and radial velocity vectors (see § 3.1), we triage our Chamaeleon candidates into their parent kinematic group. However, in the case of RXJ1140.3-8321, in going forward we consider it more likely a member of the older ≈ 40 Myr Tuc-Hor association (Bell et al. 2015; Kraus et al. 2014; Elliott et al. 2014), and use the Elliott et al. (2014) distance of 48pc in calculating its bolometric luminosity. For RXJ0850.1-7554 and RXJ0951.9-7901, we start with the assumption that the objects are candidate members of the η Cha association. However, in light of the arguments presented in § 3.1– § 3.3, after having considered their HRD properties, we will re-evaluate their membership properties at the end of § 3.6.1.

It has occurred to us that we are using main sequence theoretical models to determine effective temperatures and bolometric corrections, which may not be wholly appropriate for stars in young SFRs. While we continue with this analysis, we also perform an HRD age and mass analysis using pre-main sequence empirically calibrated stellar parameters, the results of which are presented in § B.

3.6.1 HRD: Stellar Ages

While small number statistics for the individual Chamaeleon subgroups, as well as the Rho Ophiuchus sample, precludes a detailed analysis of their ages, a colour-dependent HRD analysis can be informative in the assessment of stellar youth. One *caveat lector* to bear in mind is that five stars, RXJ1112.7-7637 (Cham), ROXR1 13 (ρ Oph), RXJ1621.2-2347 (ρ Oph), RXJ1624.8-2359 (ρ Oph) and RXJ1627.1-2419 (ρ Oph) show evidence of elevated extinction ($A_v > 5$), as well as exhibiting strongly colour-dependent extinction vectors (see Table 4), characteristics likely to produce colour-dependent ages and masses in the HRDs.

HRDs ages of our limited numbers of stars across the Cham I and ϵ Chamaeleon regions are broadly consistent with young SFRs having ages $\lesssim 5$ -10 Myr. Both Cham I stars have mean ages

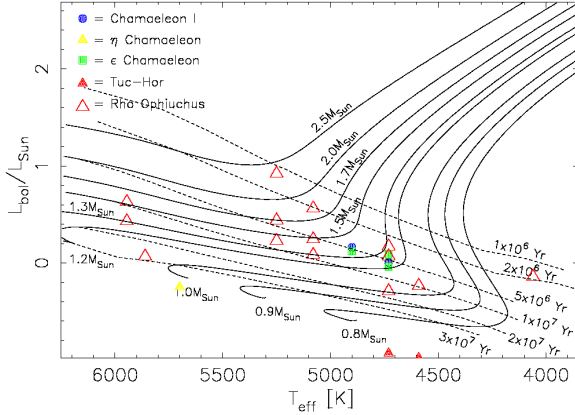


Figure 8. *Idem* to Figure 7, except A_v extinction values are derived from $V - I_c$ colours.

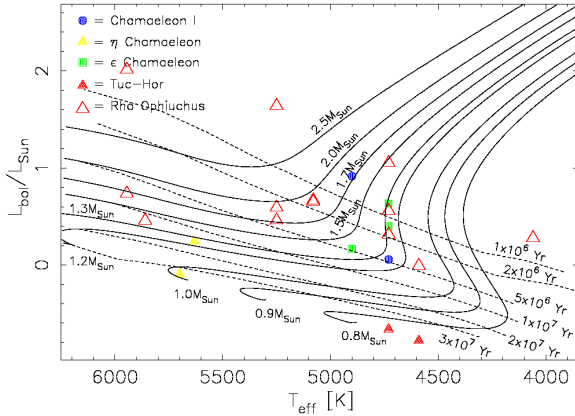


Figure 9. *Idem* to Figure 7, except A_v extinction values are derived from $J - H$ colours.

< 5 Myr, which are perfectly aligned with the results of [Luhman \(2007\)](#) and [Spina et al. \(2014\)](#). Interpreting the mean age determinations for our four ϵ Cham stars is also straightforward, as they all return consistent values of $\lesssim 5$ Myr, in agreement with the [Feigelson et al. \(2003\)](#) and [Murphy et al. \(2013\)](#) studies.

For the η Cham candidates, both RXJ0850.1-7554 and RXJ0951.9-7901 appear to be considerably older than the 5-10 Myr age of the group ([Lawson et al. 2001](#), [Luhman & Steeghs 2004](#)), having ages at least 25-30 Myr, more appropriate to those of post T-Tauri stars. This supposition for both of these objects is consistent with the [Elliott et al. \(2014\)](#) assertion that they are members of older associations (30 Myr Carina in the case of RXJ0850.1-7554, and the $\simeq 40$ Myr Tuc-Hor group in the case of RXJ0951.9-7901). For RXJ1140.3-8321, which was already assumed to be a Tuc-Hor member, its K95 HRD analysis unsurprisingly yields isochronal ages of ~ 50 Myr for both measurements of its K3 and K4 spectral types.

In the case of Rho Ophiuchus stars, their HRD mean ages show clear evidence of a group of young SFR objects broadly consistent with a $\simeq 1$ -10 Myr distribution, supporting conclusions found by [Luhman & Rieke \(1999\)](#), [Wilking et al. \(2005\)](#) & [Alves de Oliveira et al. \(2010\)](#). Several stars exhibit a spread in ages, based on different colour extinction relations in the L_{bol}/L_{\odot} calculation, of an order-of-magnitude or more, always decreas-

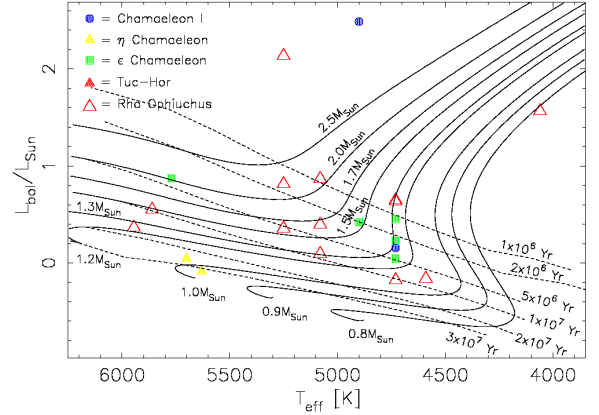


Figure 10. *Idem* to Figure 7, except A_v extinction values are derived from $H - K_s$ colours.

ing in age as the extinction relationships derived go from blue to red reddening vectors (*i.e.*, $E(B - V) \rightarrow E(H - K)$). Of these targets, RXJ1621.2-2347, RXJ1623.4-2425, RXJ1624.8-2359, RXJ1625.4-2346, RXJ1627.1-2419, three exhibit $A_v > 5$ values (see § 3.4). As to why the age determinations of RXJ1623.4-2425 especially, and RXJ1625.4-2346, change so markedly as a function of colour-dependent extinction we cannot explain. We also note that RXJ1623.4-2425 and RXJ1625.0-2508 appear to be considerably older than the remainder of the Rho Ophiuchus sample.

3.6.2 HRD: Stellar Masses

With the exception of three stars, RXJ1112.7-7637, ROXR1 13 and RXJ1627.1-2419, stellar masses derived from the HRDs are remarkably consistent (see Table 6), and show that our sample is essentially composed of stars 1 – 2 times the mass of the Sun. The masses for one Cham I, and three Rho Ophiuchus objects, are not constrained, which except for our coolest K7e star, is caused by strong ($A_v > 5$) and variable extinction across the four photometric colours we consider.

The observed age and mass dependence for some of our objects on the colour used to derive A_v is likely the product of excess emission from circumstellar discs. For instance, a target with excess emission in the red/infrared will appear older when using bluer colours, *i.e.* $B - V$ and $V - I$, due to a downward shift on the diagram. To further examine this disc hypothesis, in § 4 compare our Y4KCam and 2MASS photometry for each of our objects, as well as publicly available infrared photometry from several other instruments, with theoretical spectral energy distributions for young stellar objects with discs.

3.6.3 HRD: Comparing Stellar Models:

In an attempt to quantify the dependence of derived stellar masses and ages on our choice of stellar evolutionary model, we can easily compare our PARSEC results with those calculated using other stellar models. For convenience, we have chosen the isochrones and mass tracks of the Dartmouth group [Dotter et al. \(2008\)](#) and the [D'Antona & Mazzitelli \(1997\)](#) [DAM97] team, both of which are of solar-metallicity. The former has an initial He content of $Y=0.274$ and does not explicitly include Deuterium burning during the pre-main sequence, while the latter does include Deuterium burning on the PMS starting with an initial abundance of ^2H of

Table 5. Isochronal ages for Chamaeleon and Rho Ophiuchus candidates using four separate colour-dependent extinction laws (based on KH95 effective temperatures and bolometric corrections for dwarf stars) and PARSEC stellar models.

| Target ^a | T_{eff}^b [K] | $[L_{\text{bol}}/L_{\odot}]^c$ | Age ^a [Myr] | $[L_{\text{bol}}/L_{\odot}]^c$ | Age ^a [Myr] | $[L_{\text{bol}}/L_{\odot}]^c$ | Age ^a [Myr] | $[L_{\text{bol}}/L_{\odot}]^c$ | Age ^a [Myr] | Mean age [Myr] |
|---------------------------------------|---------------------------|--------------------------------|---------------------------|--------------------------------|---------------------------|--------------------------------|---------------------------|--------------------------------|---------------------------|-------------------|
| | | $^b E(B - V)$ | | $^b E(V - I)$ | | $^b E(J - H)$ | | $^b E(H - K)$ | | |
| Chamaeleon I (●) | | | | | | | | | | |
| RXJ1112.7-7637 | 4900 | 9.999 | ... | 0.161 | 5.0 | 0.915 | < 1 | 2.489 | < 1 | < 2.3 |
| RXJ1129.2-7546 | 4730 | −0.141 | 9.5 | 0.005 | 5.5 | 0.057 | 5.0 | 0.155 | 3.5 | 5.9 ± 1.3 |
| η Cham (▲) | | | | | | | | | | |
| RXJ0850.1-7554 | 5700 | −0.242 | > 30 | −0.251 | > 30 | −0.099 | > 30 | 0.042 | 27 | > 29 |
| RXJ0951.9-7901 | 5630 | −0.005 | 26 | 9.999 | ... | 0.241 | 15 | −0.089 | > 30 | > 24 |
| Tuc Hor (▲) | | | | | | | | | | |
| RXJ1140.3-8321 [†] | 4730 | −0.926 | > 30 | −0.932 | > 30 | −0.662 | > 30 | 9.999 | ... | > 30 |
| RXJ1140.3-8321 [‡] | 4590 | −1.030 | > 30 | −0.981 | > 30 | −0.780 | > 30 | 9.999 | ... | > 30 |
| ϵ Cham (■) | | | | | | | | | | |
| RXJ1158.5-7754a | 4730 | 0.260 | 2.0 | 9.999 | ... | 0.634 | < 1 | 0.225 | 2.5 | < 1.8 |
| RXJ1159.7-7601 | 4730 | −0.041 | 6.5 | −0.039 | 6.5 | 0.398 | 1.5 | 0.045 | 5.0 | 4.9 ± 1.2 |
| RXJ1201.7-7859 | 5770 | 0.681 | 6.5 | 9.999 | ... | 9.999 | ... | 0.872 | 4.5 | 5.5 ± 1.0 |
| RXJ1239.4-7502 [†] | 4900 | 0.172 | 4.5 | 0.121 | 5.5 | 0.166 | 5.0 | 0.420 | 2.0 | 4.3 ± 0.8 |
| RXJ1239.4-7502 [‡] | 4730 | 0.104 | 4.0 | 0.084 | 4.5 | 9.999 | ... | 0.452 | 1.0 | 3.2 ± 1.1 |
| Rho Ophiuchus (△) | | | | | | | | | | |
| RXJ1620.7-2348 | 4590 | −0.349 | 15 | −0.234 | 9.5 | −0.008 | 4.0 | −0.162 | 7.5 | 9.0 ± 2.3 |
| RXJ1621.0-2352 | 5080 | 0.081 | 9.5 | 0.084 | 9.0 | 9.999 | ... | 0.094 | 9.0 | 9.2 ± 0.2 |
| RXJ1621.2-2347 | 4730 | −0.458 | 29 | −0.290 | 16 | 0.559 | < 1 | 0.647 | < 1 | < 12 |
| RXJ1623.1-2300 | 4730 | −0.021 | 6.5 | 0.070 | 4.5 | 0.315 | 2.0 | −0.176 | 12 | 6.3 ± 2.1 |
| RXJ1623.4-2425 | 5860 | −0.250 | > 30 | 0.068 | 28 | 0.458 | 12 | 0.551 | 10 | > 20 |
| RXJ1623.5-2523 | 5250 | 0.218 | 8.5 | 0.440 | 4.5 | 0.460 | 4.5 | 0.814 | 2.0 | 4.9 ± 1.3 |
| RXJ1624.0-2456 | 5250 | −0.072 | 19 | 0.230 | 8.0 | 0.592 | 3.0 | 0.356 | 5.5 | 8.9 ± 3.5 |
| RXJ1624.8-2239 | 5080 | 0.511 | 2.5 | 0.564 | 2.0 | 0.653 | 1.5 | 0.869 | < 1 | < 1.8 |
| RXJ1624.8-2359 | 4730 | −0.284 | 16 | 0.172 | 3.5 | 1.052 | < 1 | 0.636 | < 1 | < 5.4 |
| RXJ1625.0-2508 | 5945 | 0.205 | 23 | 0.431 | 15 | 0.738 | 8.0 | 0.366 | 17 | 15.8 ± 3.1 |
| RXJ1625.4-2346 | 5080 | −0.045 | 15 | 0.245 | 5.5 | 0.666 | 1.5 | 0.397 | 3.5 | 6.4 ± 3.0 |
| RXJ1625.6-2613 | 4060 | 9.999 | ... | −0.140 | 2.0 | 0.279 | < 1 | 1.565 | < 1 | < 1.3 |
| ROXR1 13 | 5250 | 0.386 | 5.0 | 0.921 | 1.0 | 1.642 | < 1 | 2.136 | < 1 | < 2.0 |
| RXJ1627.1-2419 | 5945 | −0.028 | > 30 | 0.630 | 5.5 | 2.015 | < 1 | 3.181 | < 1 | $\simeq 9$ (?) |

a – Isochronal age determinations are segregated into stars comprising disparate young SFR regions, with symbols ●, ▲, ▲, ■ & △, matching those data presented in Figures 7 – 10, using solar metallicity PARSEC models (Bressan et al. 2012).
b – L_{bol}/L_{\odot} data are calculated using T_{eff} and reddening vectors based on KH95 colour-spectral types relationships for dwarf stars (see also Tables 3 & 4).
c – Distances used for L_{bol}/L_{\odot} calculations are as follows: Cham I (●) $d=160\text{pc}$ (Whittet et al. 1997); η Cham (▲) $d=97\text{pc}$ (Murphy et al. 2013; Bell, Mamajek & Naylor 2015); ϵ Cham (■) $d=115\text{pc}$ (Murphy et al. 2013); Tuc-Hor (▲) $d=48\text{pc}$ (Elliott et al. 2014); Rho Ophiuchus (△) $d=131\text{pc}$ (Mamajek 2008).
[†] – for a given star having two spectral types, calculations are made using earlier spectral type/higher T_{eff} .
[‡] – *Idem*, calculations are made using later spectral type/lower T_{eff} .

4.5×10^{-5} , and incorporates an initial He content of $Y=0.280$. We also note that the DAM97 model also relies upon a gray atmosphere approximation as an exterior boundary condition, which will have different effects on stellar effective temperatures and luminosities compared to the D08 and PARSEC models. For brevity, we restrict ourselves at the present time to a comparison of the models containing L_{bol}/L_{\odot} calculations using A_v extinction values derived from B-V colours and effective temperatures derived from KH95 main-sequence spectral types. The graphical and numerical results of their inter-comparability are presented in Figure 11 and Table 7.

Our analysis shows that for extinction based on B-V colours, the Dartmouth group isochrones return stellar ages that are on average 0.68 Myr (± 0.21) older than the PARSEC ones, whereas the DAM97 ones are 2.86 Myr (± 0.58) younger. For the Cham I, ϵ

Cha and Rho Ophiuchus stars, such a large PARSEC/DAM97 age differential actually represents a substantial fraction of the system age ($\simeq 30 - 50$ per cent). For extinction based on other colours (V-Ic, J-H, H-Ks), we find that Dartmouth models remain closely matched to their PARSEC counterparts being 0.68 ± 1.06 Myr younger, 0.08 ± 0.29 Myr older and 0.03 ± 0.44 Myr younger respectively. For the DAM97 model comparisons however, the other three colour-based extinctions again yield younger ages albeit at a lower level than their B-V colours (1.32 ± 2.06 , 0.68 ± 0.98 and 1.50 ± 1.56 Myr younger for V-Ic, J-H and H-Ks colours respectively).

In terms of masses, the Dartmouth models are essentially identical to the PARSEC ones across all four colour-based extinctions (0.00 ± 0.02 , 0.03 ± 0.09 , 0.02 ± 0.06 and $0.03 \pm 0.04 M_{\odot}$ - the

Table 6. PARSEC model masses for Chamaeleon and Rho Ophiuchus candidates using four separate colour-dependent extinction laws (based on KH95 effective temperatures and bolometric corrections for dwarf stars).

| Target | T_{eff} [K] | Mass [M_{\odot}] $E(B - V)$ | Mass [M_{\odot}] $E(V - I)$ | Mass [M_{\odot}] $E(J - H)$ | Mass [M_{\odot}] $E(H - K)$ | Mean Mass [M_{\odot}] |
|-----------------------------|-------------------------|---------------------------------------|---------------------------------------|---------------------------------------|---------------------------------------|------------------------------|
| Chamaeleon I (●) | | | | | | |
| RXJ1112.7-7637 | 4900 | ... | 1.4 | 1.7 | > 2.5 | > 1.9 |
| RXJ1129.2-7546 | 4730 | 1.1 | 1.2 | 1.2 | 1.3 | 1.2 ± 0.04 |
| η Cham (▲) | | | | | | |
| RXJ0850.1-7554 | 5700 | 1.0 | 1.0 | 1.0 | 1.0 | $1.0 \pm ...$ |
| RXJ0951.9-7901 | 5630 | 1.0 | ... | 1.2 | 1.0 | 1.07 ± 0.07 |
| Tuc Hor (▲) | | | | | | |
| RXJ1140.3-8321 [†] | 4730 | ... | ... | ... | ... | ... |
| RXJ1140.3-8321 [‡] | 4590 | ... | ... | ... | ... | ... |
| ϵ Cham (■) | | | | | | |
| RXJ1158.5-7754a | 4730 | 1.3 | ... | 1.3 | 1.3 | $1.3 \pm ...$ |
| RXJ1159.7-7601 | 4730 | 1.4 | 1.2 | 1.3 | 1.2 | 1.28 ± 0.05 |
| RXJ1201.7-7859 | 5770 | 1.7 | ... | ... | 2.0 | 1.85 ± 0.15 |
| RXJ1239.4-7502 [†] | 4900 | 1.4 | 1.3 | 1.4 | 1.5 | 1.40 ± 0.04 |
| RXJ1239.4-7502 [‡] | 4730 | 1.4 | 1.3 | ... | 1.3 | 1.33 ± 0.03 |
| Rho Ophiuchus (△) | | | | | | |
| RXJ1620.7-2348 | 4590 | 1.0 | 1.0 | 1.0 | 1.0 | $1.0 \pm ...$ |
| RXJ1621.0-2352 | 5080 | 1.3 | 1.3 | ... | 1.3 | $1.3 \pm ...$ |
| RXJ1621.2-2347 | 4730 | 0.9 | 1.0 | 1.3 | 1.3 | 1.13 ± 0.10 |
| RXJ1623.1-2300 | 4730 | 1.2 | 1.2 | 1.3 | 1.1 | 1.20 ± 0.04 |
| RXJ1623.4-2425 | 5860 | ... | 1.1 | 1.4 | 1.5 | 1.33 ± 0.12 |
| RXJ1623.5-2523 | 5250 | 1.4 | 1.5 | 1.7 | 2.2 | 1.70 ± 0.18 |
| RXJ1624.0-2456 | 5250 | 1.0 | 1.2 | 1.9 | 1.6 | 1.43 ± 0.20 |
| RXJ1624.8-2239 | 5080 | 1.7 | 1.8 | 1.9 | 2.0 | 1.85 ± 0.06 |
| RXJ1624.8-2359 | 4730 | 1.0 | 1.3 | 1.5 | 1.3 | 1.28 ± 0.10 |
| RXJ1625.0-2508 | 5945 | 1.1 | 1.3 | 1.7 | 1.2 | 1.33 ± 0.13 |
| RXJ1625.4-2346 | 5080 | 1.3 | 1.5 | 1.9 | 1.6 | 1.58 ± 0.13 |
| RXJ1625.6-2613 | 4060 | ... | < 0.8 | < 0.8 | 0.8 | < 0.8 |
| ROXR1 13 | 5250 | 1.6 | 2.4 | > 2.5 | > 2.5 | > 2.3 |
| RXJ1627.1-2419 | 5945 | 1.1 | 1.5 | > 2.5 | > 2.5 | > 1.9 |

Notes:

a— PARSEC model mass determinations are segregated into stars comprising disparate young SFR regions, with symbols ●, ▲, ■ & △, matching those data presented in Figures 7–10.

b— L_{bol}/L_{\odot} data are calculated using T_{eff} and reddening vectors based on KH95 colour-spectral types relationships for dwarf stars (see also Tables 3 & 4).

c— Distances used for L_{bol}/L_{\odot} calculations are the same as those presented in the footnotes to Table 5.

[†] — for a given star, calculations are made using earlier spectral type/higher T_{eff} .

[‡] — for a given star, calculations are made using later spectral type/lower T_{eff} .

latter three being more massive). For the DAM97 models, all four extinctions yield slightly lower mass HRD values on average but only at the $\simeq 0.1 M_{\odot}$ level (0.08 ± 0.03 , 0.06 ± 0.15 , 0.15 ± 0.12 and $0.13 \pm 0.13 M_{\odot}$).

4 PRESENCE OF DISC EMISSION: SPECTRAL ENERGY DISTRIBUTIONS

In order to confirm the presence of circumstellar disc material inferred from stellar positions in colour-colour space (see § 3.5), we construct SEDs and compare them to theoretical radiative transfer models. We combine optical photometry derived in this work (§ 2.1) with additional near- and mid-infrared photometry gathered from the literature; these data are presented in Tables 2, E1 and E2. Following the procedure described in Aarnio et al. (2010),

these photometric data were fit using the computed SED grid of Robitaille et al. (2007). These $\sim 200,000$ radiative transfer models include a central star surrounded by a flaring disc and envelope; the properties of these model components vary as described by a set of 14 parameters. Additional parameters used to constrain the fitter include A_v and distance: the allowed range of A_v was set to 0–10 mag for both SFRs, while the distance range for the different Chamaeleon regions was confined to 100–175 pc; Rho Ophiuchus member distances were constrained to be within 110–150 pc.

In those cases where substantial infrared excess was seen, we filtered the resulting best fit models based on known stellar properties. Spectral types reported in Table 3 were converted to effective temperatures via the KH95 relationships, and only models whose central star has T_{eff} within 5000 K of the estimated effective temperature were included. One should retain some level of caution with this approach, as young, solar-type stars can show photomet-

Table 7. A comparison of stellar ages and masses for our candidate sample, using using A_v extinction values derived from $B - V$ colours, for the PARSEC, Dartmouth group and D’Antona & Mazzitelli stellar models.

| Target ^a | T_{eff}^a [K] | $[L_{\text{bol}}/L_{\odot}]^{a,b}$ | Age ^c [Myr] | Mass ^c [M_{\odot}] | Age ^d [Myr] | Mass ^d [M_{\odot}] | Age ^e [Myr] | Mass ^e [M_{\odot}] | ΔAge^f [Myr] | ΔMass^f [M_{\odot}] |
|---------------------------------------|---------------------------|------------------------------------|---------------------------|--------------------------------------|---------------------------|--------------------------------------|---------------------------|--------------------------------------|-------------------------------|--|
| | | | PARSEC ^c | | Dartmouth08 ^d | | DAM97 ^e | | | |
| Chamaeleon I (●) | | | | | | | | | | |
| RXJ1112.7-7637 | 4900 | ... | ... | ... | ... | ... | ... | ... | ... | ... |
| RXJ1129.2-7546 | 4730 | −0.141 | 9.5 | 1.1 | 10 | 1.2 | 6.0 | 1.0 | −0.5, 3.5 | −0.1, 0.1 |
| η Cham (▲) | | | | | | | | | | |
| RXJ0850.1-7554 | 5700 | −0.242 | > 30 | 1.0 | > 30 | 1.0 | > 30 | 1.0 | ... | 0.0, 0.0 |
| RXJ0951.9-7901 | 5630 | −0.005 | 26 | 1.0 | 28 | 1.0 | 23 | 1.0 | −2.0, 3.0 | 0.0, 0.0 |
| Tuc Hor (▲) | | | | | | | | | | |
| RXJ1140.3-8321 [†] | 4730 | −0.926 | > 30 | ... | > 30 | ... | > 30 | ... | ... | ... |
| RXJ1140.3-8321 [‡] | 4590 | −1.030 | > 30 | ... | > 30 | ... | > 30 | ... | ... | ... |
| ϵ Cham (■) | | | | | | | | | | |
| RXJ1158.5-7754a | 4730 | 0.260 | 2.0 | 1.3 | 2.0 | 1.3 | 1.0 | 1.0 | 0.0, 1.0 | 0.0, 0.3 |
| RXJ1159.7-7601 | 4730 | −0.041 | 6.5 | 1.4 | 7.5 | 1.2 | 4.0 | 1.0 | −1.0, 2.5 | 0.2, 0.4 |
| RXJ1201.7-7859 | 5770 | 0.681 | 6.5 | 1.7 | 6.5 | 1.8 | 7.5 | 1.7 | 0.0, −1.0 | −0.1, 0.0 |
| RXJ1239.4-7502 [†] | 4900 | 0.172 | 4.5 | 1.4 | 5.0 | 1.4 | 3.5 | 1.3 | −0.5, 1.0 | 0.0, 0.1 |
| RXJ1239.4-7502 [‡] | 4730 | 0.104 | 4.0 | 1.4 | 4.5 | 1.3 | 2.0 | 1.0 | −0.5, 2.0 | 0.1, 0.4 |
| Rho Ophiuchus (△) | | | | | | | | | | |
| RXJ1620.7-2348 | 4590 | −0.349 | 15 | 1.0 | 18 | 1.0 | 9.5 | 0.9 | −3.0, 5.5 | 0.0, 0.1 |
| RXJ1621.0-2352 | 5080 | 0.081 | 9.5 | 1.3 | 10 | 1.3 | 7.0 | 1.3 | −0.5, 2.5 | 0.0, 0.0 |
| RXJ1621.2-2347 | 4730 | −0.458 | 29 | 0.9 | > 30 | 0.9 | 20 | 0.9 | ... | 0.0, 0.0 |
| RXJ1623.1-2300 | 4730 | −0.021 | 6.5 | 1.2 | 7.0 | 1.2 | 3.5 | 1.0 | −0.5, 3.0 | 0.0, 0.2 |
| RXJ1623.4-2425 | 5860 | −0.250 | > 30 | ... | > 30 | 1.0 | > 30 | 1.1 | ... | ... |
| RXJ1623.5-2523 | 5250 | 0.218 | 8.5 | 1.4 | 8.5 | 1.4 | 7.0 | 1.4 | 0.0, 1.5 | 0.0, 0.0 |
| RXJ1624.0-2456 | 5250 | −0.072 | 19 | 1.0 | 20 | 1.1 | 16 | 1.1 | −1.0, 3.0 | −0.1, −0.1 |
| RXJ1624.8-2239 | 5080 | 0.511 | 2.5 | 1.7 | 2.5 | 1.8 | 2.0 | 1.7 | 0.0, 0.5 | −0.1, 0.0 |
| RXJ1624.8-2359 | 4730 | −0.284 | 16 | 1.0 | 18 | 1.0 | 9.5 | 1.0 | −2.0, 6.5 | 0.0, 0.0 |
| RXJ1625.0-2508 | 5945 | 0.205 | 23 | 1.1 | 23 | 1.2 | 21 | 1.2 | 0.0, 2.0 | −0.1, −0.1 |
| RXJ1625.4-2346 | 5080 | −0.045 | 15 | 1.3 | 15 | 1.1 | 9.5 | 1.2 | 0.0, 5.5 | 0.2, 0.1 |
| RXJ1625.6-2613 | 4060 | ... | ... | ... | ... | ... | ... | ... | ... | ... |
| ROXR1 13 | 5250 | 0.386 | 5.0 | 1.6 | 5.0 | 1.6 | 4.5 | 1.6 | 0.0, 0.5 | 0.0, 0.0 |
| RXJ1627.1-2419 | 5945 | −0.028 | > 30 | 1.1 | > 30 | 1.1 | > 30 | 1.1 | ... | 0.0, 0.0 |

a – Chamaeleon, Tuc-Hor and Rho Ophiuchus candidates triaged into disparate young SFR regions, with symbols ●, ▲, ▲, ■ & △, matching those data presented in Figures 11.

b – L_{bol}/L_{\odot} calculated using photometric data, T_{eff} , A_v extinction values derived from $B - V$ colours and distances detailed in Tables 2–5.

c – Theoretical ages and masses based on the PARSEC (Bressan et al. 2012) models.

d – Theoretical ages and masses based on the Dartmouth group (Dotter et al. 2008) models.

e – Theoretical ages and masses based on the DAM97 (D’Antona & Mazzitelli 1997).

f – Differential values are PARSEC - Dartmouth and PARSEC - DAM97, respectively.

ric and spectroscopic temporal variations due some combination of on-going accretion, rapid rotation and extreme (and stochastic) chromospheric and coronal magnetic activity. The sample of best-fit models was further narrowed by accepting only cases in which the χ^2 fit value was within a 99.73 per cent confidence level ($\Delta\chi^2 = 11.8$) of the (post- T_{eff} rejection) best fit. Finally, models with disc masses $< 10^{-10} M_{\odot}$ were rejected.

Our SED analysis shows substantial excess for three Rho Ophiuchus objects and one Chamaeleon star (see Figure 12). In three additional Rho Ophiuchus stars, we see low to moderate mid-infrared excess (see Figure D1); the SEDs for the remainder of the sample are consistent with bare photospheres (see Figures D2 & D3). We compare our SED fit A_v values to those calculated via extinction laws in § 3.4 and Table 4, finding that for stars with evidence of circumstellar discs, extinction derived from

optical photometry best matches the SED-fit derived A_v values (especially for V-I), presumably due to the complications of active accretion or disc radiation in the infra-red. For stars without disc signatures, we find the near infrared reddening vector E(H-Ks) produces A_v values in better agreement with the SED results; to our mind, this is attributable to the variable and difficult-to-quantify effect (starspots, flares, etc.) of stellar magnetic activity on optical photometry.

In the four star+disc systems with the most near- to mid-infrared excess (see Figure 12), we find that the best-fit model parameters have the greatest disc masses, highest accretion rates, and all show some sign of emission (or blueshifted absorption) in their H α profiles, which are tell-tale indicators of ongoing activity, accretion, or outflow. In fact, all four stars exhibit narrow-lined neutral Oxygen [O I] 5577.3 Å emission in their UVES spectra,

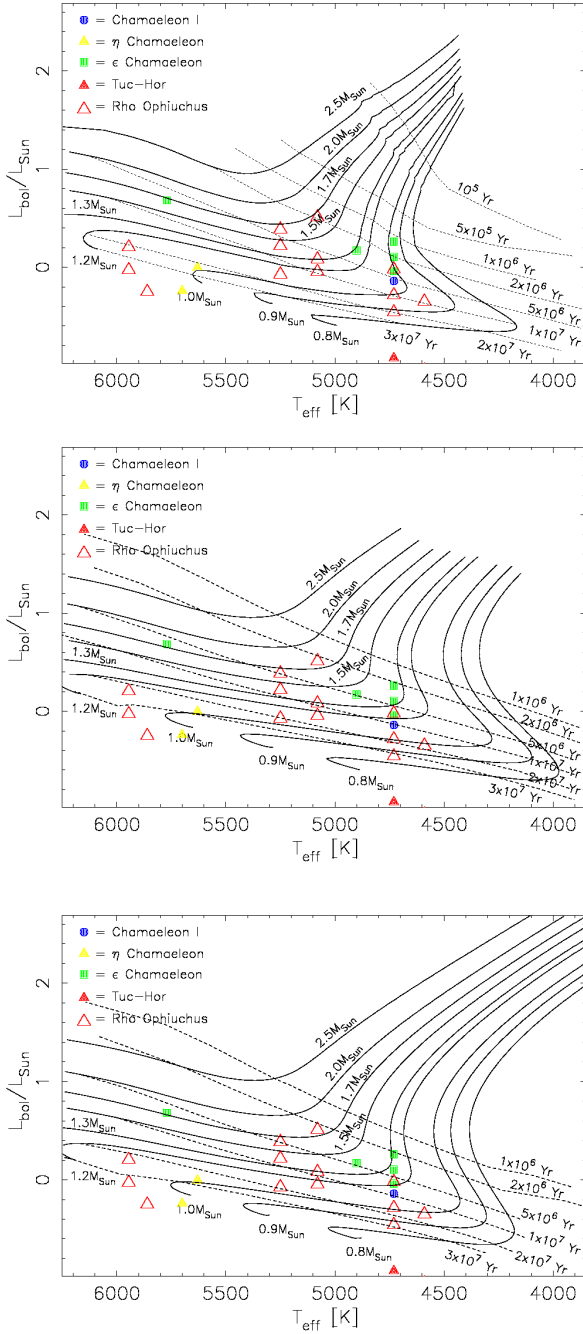


Figure 11. A triumvirate of Hertzsprung-Russell diagrams, using A_v extinction values derived from $B - V$ colours (see Table 4), is plotted for Cham I (●), η Cham (▲), ϵ Cham (■), Tuc-Hor (▲) & Rho Ophiuchus (△) candidates. Effective temperatures, bolometric corrections and reddening vectors are based on KH95 colour-spectral type relationships for dwarf stars, with distances to individual stellar groups cited in Table 5. Stellar isochrones (dashed tracks) and mass tracks (solid lines) are computed from theoretical pre-main sequence, solar metallicity stellar models by D’Antona & Mazzitelli (1997 - top plot), the Dartmouth group (Dotter et al. 2008 - middle plot) and the PARSEC group (Bressan et al. 2012 - lower plot).

oftentimes shown to originate in a circumstellar disc or envelope. For RXJ1627.1-2419, its O I profile is actually complex in nature, and looks double-peaked. Moreover, both RXJ1112.7-7637 and RXJ1627.1-2419 also show narrow O I emission lines at 6300.2 & 6363.9 Å. ROXR1 13 only produces a narrow 6363.9 Å emission feature as opposed to RXJ1625.6-2613 which only shows 6300.2 Å in emission.

Interestingly, the UVES spectra of ROXR1 13 and RXJ1627.1-2419 both show P Cygni like profiles in the neutral Sodium doublet at ≈ 5900 Å (Fraunhofer *D* lines), indicative of a dense magneto-hydrodynamical driven stellar wind and self-absorption through a circumstellar accretion disc (e.g., Israelian & de Groot 1999). For completeness, we note that RXJ1112.7-7637 also exhibits small narrow-lined emission features at 6410.1 Å, 6505.4 Å, 6523.5 Å and 6529.0 Å, while RXJ1627.1-2419 produces an emission feature at 5615.3 Å (all observing-frame wavelengths). Finally, RXJ1625.6-2613 has small emission features at 5875.1 Å and 6678.2 Å, which may be He I and/or O II species).

In three of four cases, the models indicate disc truncation at the dust destruction radius; in the sole case with a best-fit disc truncated beyond R_{trunc} , RXJ1627.1-2419, there is existing evidence that this object is characterized by a transition disc (McClure et al. 2010). We present best-fit model parameters for all seven (7) objects with moderate to substantial disc excess in Table C1, and we provide additional discussion of each object, including a review of extant observations garnered from the literature (see § C).

Except in the strongest two cases, we find no correlation between the residual $H\alpha$ equivalent width and disc excess indicators; this is perhaps unsurprising, given the youth of the sample stars and the wide range of $H\alpha$ fluxes observed in stars < 100 Myr of age (cf. Herbig 1985; Herbig & Bell 1988; Kenyon & Hartmann 1995).

5 CONCLUSIONS

We have obtained optical *BVIc* photometry and high-resolution spectroscopy for a modest sample of X-ray selected stars in the Chamaeleon and Rho Ophiuchus SFRs. We exploit our observational data in order to pursue five principle avenues of investigation with the goal of establishing fundamental properties of our target stars; (I:) RVs and Lithium detections are employed in assigning 1-d kinematic membership of the sample’s parent associations, as well as in the assessment of stellar youth; (II:) in combination with 2MASS near-IR photometry and optical spectral types, we use our optical *BVIc* data in order to calculate colour-dependent reddening vectors and A_v values; (III:) in an $J - H/H - K$ diagram, we search for evidence of IR-excess in our targets, which is the smoking gun evidence normally associated with viscous circumstellar discs; (IV:) transforming observational plane photometry and spectral types onto the theoretical plane of L_{bol}/L_{\odot} and T_{eff} , we construct HRDs based on four different colour-dependent A_v values, thereby allowing us to establish model-dependent stellar age and mass; (V:) we compare our optical photometry, as well as extant near- and mid-IR photometry in the literature, to radiative transfer models in order to construct SEDs for all of our targets, identifying and (re-)confirming systems consistent with circumstellar accretion discs.

For our Chamaeleon candidates, we *ab initio* took advantage of 2-d kinematics in order to triage stars into three distinct sub-groups in the region. Two stars, RXJ1112.7-7637 and RXJ1129.2-7546, have proper motions consistent with membership of the Cham I group. Three stars, RXJ0850.1-7554, RXJ0951.9-

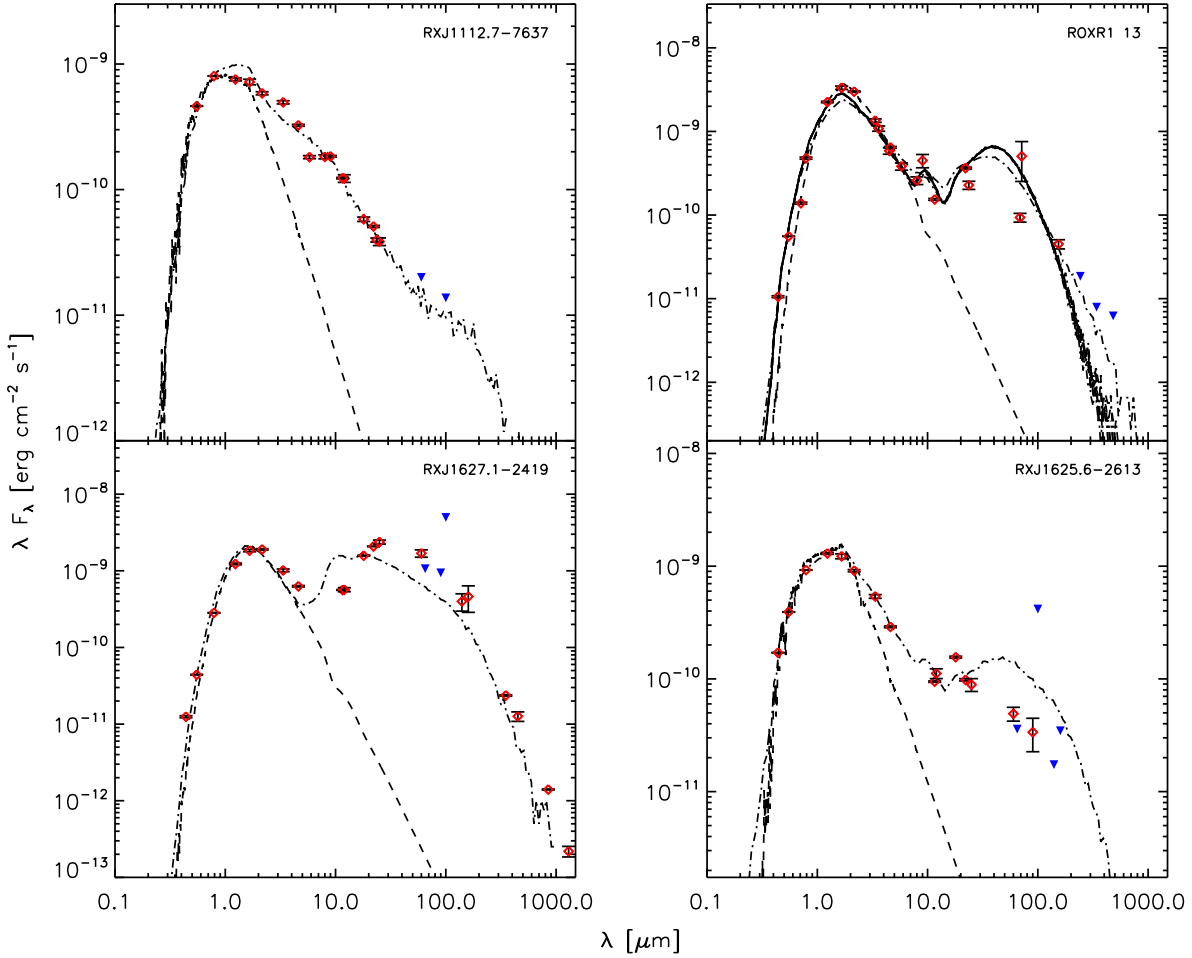


Figure 12. SEDs of Rho Ophiuchus and Chamaeleon candidates show, outwith the error budget, that significant departures from a bare photosphere are clear, *i.e.*, substantial infrared excess is evident. Red diamonds and blue triangles denote photometry from Tables 2, E1 & E2 - where blue triangles are upper limits. Dot-dashed lines are the best fit synthetic SEDs as determined via criteria defined in § 4, with dashed lines representing a stellar photospheric contribution matching spectral-type derived effective temperature.

7901 and RXJ1140.3-8321, have proper motions in broad agreement with membership of the η Cham population, well-aligned with the López Martí et al. findings. In the more recent Elliott et al. study however, they advocate allocating a 30 Myr Carina association membership for RXJ0850.1-7554 and a 45 Myr Tuc-Hor membership for both RXJ0951.9-7901 and RXJ1140.3-8321. Moving forward into the analysis of the spectroscopic data and theoretical HRDs, we retained η Cham tentative membership for these three objects, revisiting their membership status as each additional layer of analysis was added. RXJ1233.5-7523 is an obvious proper motion field star not associated with any of the Chamaeleon groups. The four remaining Chamaeleon stars (RXJ1158.5-7754a, RXJ1159.7-7601, RXJ1201.7-7859 and RXJ1239.4-7502) are kinematic members of the Eps Cham group.

With one exception, RXJ1303.5-7701, all of our Chamaeleon candidates yield UVES RVs consistent with membership of large samples of low-mass, young stars in the Chamaeleon region. Ex-

cept for RXJ1620.1-2348 and RXJ1624.0-2456, the majority of our Rho Ophiuchus sample also reflect this behaviour in presenting 1-d kinematics consistent with membership of the parent Rho Ophiuchus cloud. Our UVES data show that three Chamaeleon group stars are RV variable, with confirmation that RXJ1201.7-7859 and RXJ1303.5-7701 are SB1 systems. Our spectra do not confirm the J06 finding that RXJ0951.9-7901 is an SB2, and we suggest that further RV observations of this object are required to firmly establish its multiplicity status.

With four exceptions, our UVES spectra show that our sample stars are young by virtue of being Lithium rich, having Lithium I 6708Å equivalent widths at least as large as their similar T_{eff} counterparts in the 125-Myr Pleiades cluster, oftentimes far more. Three of the four Li-poorer stars are either early-type (RXJ1303.5-7701), or are proper motion non-members (RXJ1233.5-7523 & RXJ1620.1-2348) of their parent associations. The low-Lithium status of the fourth object, RXJ1140.3-8321, suggests that the star

is actually a post T-Tauri star considerably older than the $\simeq 5$ Myr Eta Cha group. This supposition supports the Elliott et al. claim that it is a member of the Tuc-Hor group, which going forward we endorse. With the exception of the rapidly rotating possible SB2 system RXJ0951.9-7901, there is little evidence to suggest that our objects have variable Lithium abundance over a two-year period.

One Chamaeleon star (RXJ1112.7-7637) and four Rho Ophiuchus stars (ROXR1 13, RXJ1621.2-2347, RXJ1624.8-2359 & RXJ1627.1-2419) show evidence of substantial, $A_v > 5$ infrared excess, as judged by their displaced positions compared to unreddened dwarf and giant loci in the $J - H/H - K$ colour-colour diagram. Nevertheless, for the vast majority of stars in our sample, the Balmer series residual $H\alpha$ emission is $< 5\text{\AA}$, except for RXJ1625.6-2613, which has an equivalent width $> 6\text{\AA}$. The majority of our sample are therefore consistent, in terms of Balmer series $H\alpha$ emission at least, with being weak-lined T-Tauri stars.

Employing main sequence models to derive bolometric corrections as well as calculate spectral type based photometric colours and effective temperatures, we derive stellar ages and masses based on theoretical HRDs for our targets using four separate extinction values based on B-V, V-Ic, J-H and H-K colours. By comparison to the PARSEC theoretical models, we show that our Cham I and ϵ Cham stars are consistent with membership of young SFRs, having ages $\lesssim 5$ Myr across all four colour-based extinction vectors – agreeing with several other studies across the literature. For both η Cham **candidates**, RXJ0850.1-7554 and RXJ0951.9-7901, post T-Tauri like ages of at least 25-30 Myr are calculated, and so in agreement with Elliott et al. (2014), we henceforth advocate their membership of the 30 Myr Carina and 45 Myr Tuc-Hor associations, respectively. Several stars exhibit a spread in ages, based on different colour extinction relations in the L_{bol}/L_{\odot} calculation, of an order-of-magnitude or more, always decreasing in age as the extinction relationships derived go from blue to red reddening vectors (*i.e.*, $E(B - V) \rightarrow E(H - K)$). With the exception of three stars, RXJ1112.7-7637, ROXR1 13 and RXJ1627.1-2419, HRDs stellar masses are consistent across blue to red reddening vectors, and reveal that our sample is mostly composed of objects 1 – 2 times the mass of the Sun. Three objects with determinable masses are not well constrained because of strong ($A_v > 5$) and variable extinction across the four photometric colours we consider.

We use our modest sample of X-ray selected stars in the Chamaeleon, Carina, Tuc-Hor and Rho Ophiuchus regions to benchmark the PARSEC stellar models against those of the DAM97 and Dartmouth groups. For extinction based on B-V colours, we find that there is good agreement between the PARSEC and Dartmouth models at the slightly-older $0.68 (\pm 0.21)$ Myr level, whereas the DAM97 models are younger by $2.86 (\pm 0.58)$ Myr – which is $\simeq 30 - 50$ per cent of the group's age for Cham I, ϵ Cha and Rho Ophiuchus. For extinction based on other colours (V-Ic, J-H, H-Ks), we find that Dartmouth models remain closely matched to their PARSEC counterparts being only 0.68 ± 1.06 Myr younger, 0.08 ± 0.29 Myr older and 0.03 ± 0.44 Myr younger respectively. For the DAM97 model comparisons however, the other three colour-based extinctions again yield younger ages albeit at a lower level than their B-V colours (1.32 ± 2.06 , 0.68 ± 0.98 and 1.64 ± 1.78 Myr – all younger – for V-Ic, J-H and H-Ks colours respectively). In terms of masses, PARSEC and Dartmouth agree almost perfectly across all four colour-based extinction at the $\simeq 2$ per cent level. The DAM97 comparison is also quite good, with PARSEC differences of $\lesssim 0.1 M_{\odot}$ level across all four extinctions.

Concerned with having employed dwarf-class (main sequence) models to derive effective temperatures and bolometric

corrections for HRD construction in the analysis of our mostly PMS objects, we repeated our analyses using spectral-type, colour and bolometric corrections from PMS theoretical models. In calculating differential colour-dependent extinction vectors for our sample, the two infrared colours yield A_v values based on $E(J - H)$ & $E(H - K) \simeq 3 - 5$ times their corresponding optical colour A_v values based on $E(B - V)$ & $E(V - I)$ for Chamaeleon stars, and $\simeq 4 - 10$ times in the case of the Rho Ophiuchus ensemble. This implies that our stars are considerably more red in the PMS models compared to the MS ones, in agreement with the findings of Pecaut & Mamajek (2013, their figure 4). An comparison of HRD ages using the main sequence and PMS model data shows that within the error bars, stellar age remains unaffected. In terms of mass however, the PMS input to the HRD models consistently yielded $0.1 - 0.3 M_{\odot}$ lower values than for the main sequence analysis.

Complementing our *BVIc* dataset with near- and mid-IR photometry has allowed us to construct spectral energy distributions for each star in our sample. Comparison of these distributions to radiative transfer models shows that most objects are consistent with a bare stellar photosphere. In the event that these stars are not too photospherically active (*i.e.*, starspots), our bare photosphere stars are bright enough, with well-characterized age and mass, that they will make prime transiting exoplanet host targets for the upcoming *TESS* mission.

Three stars (RXJ1623.1-2300, RXJ1623.5-2523 & RXJ1625.0-2508) exhibit marginal signs of mid-IR excess emission compared to their bare photosphere models. Of more interest however are the one Chamaeleon star (RXJ1112.7-7637) and three Rho Ophiuchus stars (ROXR1 13, RXJ1625.6-2613 & RXJ1627.1-2419) that exhibit strong evidence of excess infrared emission; the physical interpretation of this excess emission is predicated upon infrared radiation originating in the circumstellar accretion disc of a young star. These four stars are southerly enough, bright enough and have well-established stellar age and masses to lend themselves favourably to disc-imaging surveys using state of the art facilities such as ALMA. High-resolution, spatially resolved images of young stars hosting accretion discs are prime candidates for the detection and characterization of intra-disc gaps, and sites of active and on-going exoplanet formation.

ACKNOWLEDGMENTS

We are extremely grateful to the anonymous referee whose report was timely, thorough and fair. S/he made several important suggestions which have resulted in an improved body of work. Her/his neutrality, positive guidance and constructive criticism allowed us the academic freedom to fully concentrate on the amelioration of the manuscript, for which we are deeply grateful. This manuscript is based on observational data acquired using the 1.0m telescope at the Cerro Tololo InterAmerican Observatory (Programme ID: VANF-07A-02), operated by the SMARTS consortium, and the UT2 telescope operated by the European Southern Observatory at their Paranal site (programme ID: 075.C-0272). We are grateful to the staff and scientists at both observatories for their assistance. This publication also makes use of data products from the Two Micron All Sky Survey, which is a joint project of the University of Massachusetts and the Infrared Processing and Analysis Center/California Institute of Technology, funded by the National Aeronautics and Space Administration and the National Science Foundation. This publication makes use of data products from the

Wide-field Infrared Survey Explorer, which is a joint project of the University of California, Los Angeles, and the Jet Propulsion Laboratory/California Institute of Technology, funded by the National Aeronautics and Space Administration.

Our manuscript also makes use of the the Digitized Sky Surveys, which were produced at the Space Telescope Science Institute under U.S. Government grant NAG W-2166. The images of these surveys are based on photographic data obtained using the Oschin Schmidt Telescope on Palomar Mountain and the UK Schmidt Telescope. The plates were processed into the present compressed digital form with the permission of these institutions: The National Geographic Society - Palomar Observatory Sky Atlas (POSS-I) was made by the California Institute of Technology with grants from the National Geographic Society; The Second Palomar Observatory Sky Survey (POSS-II) was made by the California Institute of Technology with funds from the National Science Foundation, the National Geographic Society, the Sloan Foundation, the Samuel Oschin Foundation, and the Eastman Kodak Corporation. The Oschin Schmidt Telescope is operated by the California Institute of Technology and Palomar Observatory. The UK Schmidt Telescope was operated by the Royal Observatory Edinburgh, with funding from the UK Science and Engineering Research Council (later the UK Particle Physics and Astronomy Research Council), until 1988 June, and thereafter by the Anglo-Australian Observatory. The blue plates of the southern Sky Atlas and its Equatorial Extension (together known as the SERC-J), as well as the Equatorial Red (ER), and the Second Epoch [red] Survey (SES) were all taken with the UK Schmidt.

This research has also benefitted from the data, software and/or web tools obtained from the High Energy Astrophysics Science Archive Research Center (HEASARC), a service of the Astrophysics Science Division at NASA/GSFC and of the Smithsonian Astrophysical Observatory's High Energy Astrophysics Division. This research has further made use of the SIMBAD database, operated at the CDS, Strasbourg, France. Finally, this research has made use of the VizieR catalogue access tool, CDS, Strasbourg, France. The original description of the VizieR service was published in [Ochsenbein et al. \(2000\)](#).

For A.N.A., this work was partially supported by the National Science Foundation grants AST-0808072 and AST-1311698, as well as NASA award NNX09AB87G, for which she is grateful. For N.C.S., this work was supported by Fundação para a Ciência e a Tecnologia (FCT) through the research grant UID/FIS/04434/2013. He also acknowledge the support from FCT through Investigador FCT contract of reference IF/00169/2012 respectively, and POPH/FSE (EC) by FEDER funding through the program *Programa Operacional de Factores de Competitividade - COMPETE*, as well as from project reference PTDC/FIS-AST/1526/2014. This work results within the collaboration of the COST Action TD 1308. For P.A.C., this work was partially supported by NASA grant NNX13AI46G.

REFERENCES

- Aarnio A. N., Weinberger A. J., Stassun K. G., Mamajek E. E., James D. J., 2008, *AJ*, 136, 2483
- Aarnio A. N., Stassun K. G., Matt S. P., 2010, *ApJ*, 717, 93
- Alcalá J. M., Terranegra L., Wichmann R., Chavarría-K. C., Krautter J., Schmitt J. H. M. M., Moreno-Corral M. A., de Lara E., Wagner R. M., 1996, *A&AS*, 119, 7
- Alcalá J. M., Covino E., Sterzik M. F., Schmitt J. H. M. M., Krautter J., Neuhäuser R., 2000, *A&A*, 355, 629
- Altenhoff W. J., Thum C., Wendker H. J., 1994, *A&A*, 281, 161
- Alves de Oliveira C., Moraux E., Bouvier J., Bouy H., Marmo C., Albert L., 2010, *A&A*, 515, 75
- André P., Ward-Thompson D., Barsony M., 1993, *ApJ*, 406, 122
- Andrews S. M., Williams J. P., 2007, *ApJ*, 671, 1800
- Andrews S. M., Wilner D. J., Hughes A. M., Qi C., Dullemond C. P., 2009, *ApJ*, 700, 1502
- Armitage P. J., 2003, *ApJ*, 582, L47
- Barnes J. R., Collier Cameron A., James D. J., Steeghs D., 2001, *MNRAS*, 326, 1057
- Barnes S. A., 2007, *ApJ*, 669, 1167
- Barrado y Navascués D., Martín E. L., 2003, *AJ*, 126, 2997
- Basri G., Marcy G. W., Graham J. R., 1996, *ApJ*, 458, 600
- Bate M. R., 1998, *ApJ*, 508, L95
- Bate M. R., 2011, *MNRAS*, 417, 2036
- Bell K. J., Hilton E. J., Davenport J. R. A., Hawley S. L., West A. A., Rogel A. B., 2012, *PASP*, 124, 14
- Bell C. P. M., Mamajek E. E., Naylor T., 2015, *MNRAS*, 454, 593
- Bessell M. S., Brett J. M., 1988, *PASP*, 100, 1134
- Biazzo K., Alcalá J. M., Covino E., Frasca A., Getman F., Spezzi L., 2012, *A&A*, 547, A104
- Bodenheimer P., 1965, *ApJ*, 142, 451
- Bressan A., Marigo P., Giradi L., Salasnich B., Dal Cero C., Rubele S., Nanni A., 2012, *MNRAS*, 427, 127
- Brogan C. L., Perez L. M., Hunter T. R., et al. 2015, *ApJ*, 808, L3
- Cargile P. A., James D. J., Platais I., 2009, *AJ*, 137, 3230
- Cargile P. A., James D. J., 2010, *AJ*, 140, 677
- Carpenter J. M., 2001, *AJ*, 121, 2851
- Cieza L. A., Padgett D. L., Stapelfeldt K. R., et al. 2007, *ApJ*, 667, 308
- Cieza L. A., Olofsson J., Harvey P. M., Evans II N. J., Najita, J., Henning T., Merin B., Liebhart A., Güdel M., Augereau J.-C., Pinte C., 2013, *ApJ*, 452, 736
- Condon J. J., Cotton W. D., Greisen E. W., Yin Q. F., Perley R. A., Taylor G. B., Broderick J. J., 1998, *AJ*, 115, 1693
- Covino E., Alcalá J. M., Allain S., Bouvier J., Terranegra L., Krautter J., 1997, *A&A*, 328, 187
- Cowan N. B., Greene T., Angerhausen D., Batalha N. E., Clampin M., Colón K., Crossfield I. J. M., Fortney J. J., Gaudi B. S., Harrington J., Iro N., Lillie C. F., Linsky J. L., Lopez-Morales M., Mandell A. M., Stevenson K. B., ExoPAG SAG-10, 2015, *PASP*, 127, 311
- Cutri R. M., et al. 2012, WISE All-Sky Data Release - VizieR Online Data Catalogue.
- D'Antona F., & Mazzitelli I., 1997, *Mem. Soc. Astron. Ital.*, 68, 807
- Dotter A., Chaboyer B., Jevremović D., Kostov V., Baron E., Ferguson J. W., 2008, *ApJS*, 178, 89
- Ducourant C., Teixeira R., Périé J. P., Lecampion J. F., Guibert J., Satori M. J., 2005, *A&A*, 438, 769
- Dzib S. A., Loinard L., Mioduszewski A. J., et al., 2013, *ApJ*, 775, 63
- Eibe M. T., 1998, *A&A*, 337, 757
- Elliott P., Bayo A., Melo C. H. F., Torres C. A. O., Sterzik M., Quast G. R., 2014, *A&A*, 568, 26
- Feigelson E. D., Montmerle T., 1999, *ARA&A*, 37, 363
- Feigelson E. D., Lawson W. A., Garmike G. P., 2003, *ApJ*, 599, 1207
- Flock M., Ruge J. P., Dzyurkevich N., Henning Th., Klahr H., Wolf S., 2015, *A&A*, 574, 68
- Forest W. J., Sargent B., Furlan E., D'Alessio P., Calvet N., Hartmann L., Uchida K. I., Green J. D., Watson D. M., Chen C. H., Kemper F., Keller L. D., Sloan G. C., Herter T. L., Brandl B. R., Houck J. R., Barry D. J., Hall P., Morris P. W., Najita J., Myers P. C., 2004, *ApJS*, 154, 433
- Frasca A., Biazzo K., Lanzafame A. C., Alcalá J. M., Brugaletta E., Klutsch A., Stelzer B., Sacco G. G., Spina L., Jeffries R. D., Montes D., Alfaro E. J., Barentsen G., Bonito R., Gameiro J. F., López-Santiago J., Pace G., Pasquini L., Prisinzano L., Sousa S. G., Gilmore G., Randich S., Micela G., Bragaglia A., Flaccomio E., Bayo A., Costado M. T., Franciosini E., Hill V., Hourihane A., Jofré P., Lardo C., Maiorca E., Masseron T., Morbidelli L., Worley C. C., 2015, *A&A*, 575, 4
- Furlan E., Watson D. M., McClure M. K., Manoj P., Espaillat C., D'Alessio P., Calvet N., Kim K. H., Sargent B. A., Forrest W. J., Hartmann L.,

- 2009, *ApJ*, 703, 1964
- Gagné M., Skinner S. L., Daniel K. J., 2004, *ApJ*, 613, 393
- Girard T. M., van Altena W. F., Zacharias N., Vieira K., Casetti-Dinescu D. I., Castillo D., Herrera D., Sun Lee Y., Beers T. C., Monet D. G., Lopez C. E., 2011, *AJ*, 142, 15
- Gray, D. F., 1992, *The Observation and Analysis of Stellar Photospheres* 2nd edn, Cambridge: University Press
- Guenther E. W., Esposito M., Mundt R., Covino E., Alcalá J. M., Cusano F., Stecklum B., 2007, *A&A*, 467, 1147
- Haisch K. E., Lada E. A., Lada C. J., 2001, *ApJ*, 553, 153
- Hartigan P., Edwards S. Ghandour L., 1995, *ApJ*, 452, 736
- Hatchell J., Terebey S., Huard T., Mamajek E. E., Allen L., Bourke T. L., Dunham M. M., Gutermuth R., Harvey P. M., Jørgensen J. K., Merín B., Noriega-Crespo A., Peterson D. E., 2012, *ApJ*, 754, 104
- Hempelmann A., Schmitt J. H. M. M., Schultz M., Ruediger G., Stępień K., 1995, *A&A*, 294, 515
- Herbig G. H., 1985, *ApJ*, 289, 269
- Herbig G. H., Bell K. R., 1988, in G.H. Herbig and K.R. Bell eds, *Third catalog of emission-line stars of the Orion population*, Lick Observatory Bulletin #1111, Santa Cruz: Lick Observatory, June 1988, P. 90
- Hernández J., Hartmann L., Megeath T., Gutermuth R., Muzerolle J., Calvet N., Vivas A. K., Briceño C., Allen L., Stauffer J. R., Young E., Fazio G., 2007a, *ApJ*, 662, 1067
- Hernández J., Calvet N., Briceño C., Hartmann L., Vivas A. K., Muzerolle J., Downes J., Allen L., Gutermuth R., 2007b, *ApJ*, 671, 1784
- Ishihara D., et al. 2010, *A&A*, 514, A1
- Israeli G., de Groot M., 1999, *Space Science Review*, 90, 493
- James D. J., Jeffries R. D., 1997, *MNRAS*, 292, 252
- James D. J., Jardine M. J., Jeffries R. D., Randich S., Collier Cameron A., Ferreira F., 2000, *MNRAS*, 318, 1217
- James D. J., Melo C., Santos N. C., Bouvier J., 2006, *A&A*, 446, 971
- James D. J., 2013, *PASP*, 125, 1087
- Jeffries R. D., Totten E. J., James D. J., 2000, *MNRAS*, 316, 950
- Jeffries R. D., Jackson R. J., James D. J., Cargile P. A., 2009, *MNRAS*, 400, 317
- Jensen E. L. N., Cohen D. H., Gagné M., 2009, *ApJ*, 703, 252
- Kenyon S. J., Hartmann L., 1995, *ApJS*, 101, 117
- Köhler R., 2001, *AJ*, 122, 3325
- Kraus A. L., Shkolnik E. L., Allers K. N., Liu M. C., 2014, *AJ*, 147, 146
- Kurosawa R., Harries T. J., Littlefair S. P., 2006, *MNRAS*, 372, 1879
- Lada C. J., 1987, in Peimbert M., Jugaku J., eds, *Star Forming Regions* Vol. 115 of IAU Symposium, Star formation - From OB associations to protostars. pp 1–17
- Landolt A. U., 1992, *AJ*, 104, 340
- Lawson W. A., Crause L. A., Mamajek E. E., Feigelson E. D., 2001, *MNRAS*, 321, 57
- López Martí B., Jiménez Esteban F., Bayo A., Barrado D., Solano E., Rodrigo C., 2013, *A&A*, 551, 46
- López Martí B., Jiménez Esteban F., Bayo A., Barrado D., Solano E., Bout H., Rodrigo C., 2013, *A&A*, 556, 144
- Luhman K. L., Rieke G. H., 1999, *ApJ*, 525, 440
- Luhman K. L., 2004, *ApJ*, 602, 816
- Luhman K. L., 2007, *ApJ*, 173, 104
- Luhman K. L., Allen L. E., Allen P. R., Gutermuth R. A., Hartmann L., Mamajek E. E., Megeath S. T., Myers P. C., Fazio G. G., 2008, *ApJ*, 675, 1375
- Luhman K. L., Steeghs D., 2004, 609, 917
- Luhman K. L., Loutrel N. P., McCurdy N. S., Mace G. N., Melso N. D., Star K. M., Young M. D., Terrien R. C., McLean I. S., Kirkpatrick J. D., Rhode K. L., 2012, *ApJ*, 760, 152
- Mamajek E. E., 2008, *Astron. Nachr.*, 329, 10
- Malo L., Doyon R., Lafrenière D., Artigau É., Gagné J., Baron F., Riedel, A., 2013, *ApJ*, 762, 88
- Manoj P., Kim K. H., Furlan E., McClure M. K., Luhman K. L., Watson D. M., Espaillat C., Calvet N., Najita J. R., D'Alessio P., Adame L., Sargent B. A., Forrest W. J., Bohac C., Green J. D., Arnold L. A., 2011, *ApJS*, 193, 11
- Malaroda S., Levato H., Galliani S., 2006, *VizieR Online Data Catalog: Stellar radial velocities bibliographic catalog*
- Martín E. L., Montmerle T., Gregorio-Hetem J., Casanova S., 1998, *MNRAS*, 300, 733
- McClure M. K., Furlan E., Manoj P., Luhman K. L., Watson D. M., Forrest W. J., Espaillat C., Calvet N., D'Alessio P., Sargent B., Tobin J. J., Chiang H.-F., 2010, *ApJS*, 188, 75
- Motte F., André P., Neri R., 1998, *A&A*, 336, 150
- Murphy S. J., Lawson W. A., Bessell M. S., 2013, *MNRAS*, 435, 1325
- Nelson A. F., Benz W., 2003a, *ApJ*, 589, 556
- Nelson A. F., Benz W., 2003b, *ApJ*, 589, 578
- Neuhäuser R., Sterzik M. F., Schmitt J. H. M. M., Wichmann R., Krautter J., 1995, *A&A*, 297, 391
- Nguyen D. C., Brandeker A., van Kerkwijk M. H., Jayawardhana R., 2012, *ApJ*, 745, 119
- Nidever D. L., Marcy G. W., Butler R. P., Fischer D. A., Vogt S. S., 2002, *ApJS*, 141, 503
- Nordström B., Mayor M., Andersen J., Holmberg J., Pont F., Jørgensen B. R., Olsen E. H., Udry S., Mowlavi N., 2004, *A&A*, 418, 989
- Ochsenbein F., Bauer P., Marout J., 2000, *A&AS*, 143, 23
- Pecaut M. J., Mamajek E. E., 2013, *ApJS*, 208, 9
- Pollack J. B., Hubickyi O., Bodenheimer P., Lissauer J. J., Podolak M., Greenzweig Y., 1996, *Icarus*, 124, 62
- Prato L., 2007, *ApJ*, 657, 338
- Ramírez I., Meléndez J., 2005, *ApJ*, 626, 465
- Robitaille T. P., Whitney B. A., Indebetouw R., Wood K., 2007, *ApJS*, 169, 328
- Rojas G., Gregorio-Hetem J., Hetem A., 2008, *MNRAS*, 387, 1335
- Santos N. C., Melo C., James D. J., Gameiro J. F., Bouvier J., Gomes J. I., 2008, *A&A*, 480, 889
- Sartori M. J., Lépine J. R. D., Dias W. S., 2003, *A&A*, 404, 913
- Skemer A. J., Marley M. S., Hinz P. M., Morzinski K. M., Skrutskie M. F., Leisenring J. M., Close L. M., Saumon D., Bailey V. P., Briguglio R., Defrere D., Esposito S., Follette K. B., Hill J. M., Males J. R., Puglisi A., Rodigas T. J., Xompero M., 2014, *ApJ*, 792, 17
- Soderblom D. R., Stauffer J. R., Hudon J. D., Jones B. F., 1993, *ApJS*, 85, 315
- Soderblom D. R., Jones B. F., Balachandran S., Stauffer J. R., Duncan D. K., Fedele S. B., Hudon J. D., 1993, *ApJ*, 106, 1059
- Soubiran C., Jasiewicz G., Chemin L., Crifo F., Udry S., Hestroffer D., Katz D., 2013, *A&A*, 552, 64
- Sousa A., Alencar S., Bouvier J., Stauffer J., Venuti L., Hillenbrand L., Cody C., Teixeira P., Guimarães M., McGinnis P., Rebull L., Flaccomio E., Fűrész G., Micela G., Gameiro J., 2016, *A&A*, *accepted*
- Spina L., Randich S., Palla F., Biazzo K., Sacco G. G., Alfaro E. J., Francosini E., Magrini L., Morbidelli L., Frasca A., Adibekyan V., Delgado-Mena E., Sousa S. G., González Hernández J. I., Montes D., Taberner H., Tautvaišienė G., Bonito R., Lanzafame A. C., Gilmore G., Jeffries R. D., Vallenari A., Bensby T., Bragaglia A., Flaccomio E., Korn A. J., Pancino E., Recio-Blanco A., Smiljanic R., Bergemann M., Costado M. T., Damiani F., Hill V., Hourihane A., Jofré, P., de Laverny P., Lardo C., Masseron T., Prisinzano L., Worley C. C., 2015, *A&A*, 568, A2
- Stauffer J. R., Schultz G., Kirkpatrick J. D., 1998, *ApJ*, 499, L199
- Stetson P. B., 1993, in Butler C. J., Elliott I., eds, *IAU Colloq. 136: Stellar Photometry - Current Techniques and Future Developments* Further Progress in CCD Photometry. p. 291
- Stetson P. B., Davis L. E., Crabtree D. R., 1990, in Jacoby G. H., ed., *CCDs in astronomy* Vol. 8 of Astronomical Society of the Pacific Conference Series, Future development of the DAOPHOT crowded-field photometry package. pp 289–304
- Szegedi-Elek E., Kun M., Reipurth B., Pál A., Balázs L. G., Willman M., 2013, *ApJS*, 208, 28
- Tonry J., Davis M., 1979, *AJ*, 84, 1511
- Torres C. A. O., Quast G. R., Da Silva L., De La Reza R., Melo C. H. F., Sterzik M., 2006, *A&A*, 460, 695
- Trilling D. E., Benz W., Guillot T., Lunine J. I., Hubbard W. B., Burrows A., 1998, *ApJ*, 500, 428

- Tsakamoto Y., Machida M. N., Inutsuka S., 2013, MNRAS, 436 1667
- Valenti J. A., Fallon A. A., Johns-Krull C. M., 2003, ApJS, 147, 305
- Wahhaj Z., Cieza L., Koerner D. W., Stapelfeldt K. R., Padgett D. L., Case A., Keller J. R., Merín B., Evans II N. J., Harvey P., Sargent A., van Dishoeck E. F., Allen L., Blake G., Brooke T., Chapman N., Mundy L., Myers P. C., 2010, ApJ, 724, 835
- Whittet D. C. B., Prusti T., Franco G. A. P., Gerakines P. A., Kilkenny D., Larson K. A., Wesseliuss P. R., A&A, 327, 1194
- Willing B. A., Meyer M. R., Robinson J. G., Greene T. P., 2005, AJ, 130, 1733
- Wolf S., Malbet F., Alexander R., Berger J.-P., Creech-Eakman M., Duchêne G., Dutrey A., Mordasini C., Pantin E., Pont F., Pott J.-U., Tatulli E., Testi L., 2012, The Astronomy and Astrophysics Review, 20, 52
- Wright J. T., Marcy G. W., Butler R. P., Vogt S. S., 2004, ApJS, 152, 261
- Wuchterl G., Tscharnuter W. W., 2003, A&A, 398, 1081
- Yamamura I., Makiuti S., Ikeda N., Fukuda Y., Oyabu S., Koga T., White G. J., 2010, AKARI/FIS All-Sky Survey Point Source Catalogues (ISAS/JAXA, 2010) - VizieR Online Data Catalogue.
- Zacharias N., Finch C. T., Girard T. M., Henden A., Bartlett J. L., Monet D. G., Zacharias M. I., 2012, AJ, 145, 44
- Yamamura I., Makiuti S., Ikeda N., Fukuda Y., Oyabu S., Koga T., White G. J., 2010, AKARI/FIS All-Sky Survey Point Source Catalogues (ISAS/JAXA, 2010) - VizieR Online Data Catalogue.

APPENDIX A: OBSERVING LOGS FOR PHOTOMETRIC AND SPECTROSCOPIC OBSERVING CAMPAIGNS

Logs for the photometric (Y4KCAM - see Table A1) and spectroscopic (UVES - see Table A2) observing campaigns of Chamaeleon and Rho Ophiuchus candidate members are presented, and are referenced in § 2.

APPENDIX B: REDDENING VECTORS AND HRDS USING PRE-MAIN SEQUENCE SPECTRAL-TYPE VS COLOUR RELATIONSHIPS

Historically, studying properties of star forming region members has oftentimes been benchmarked against samples of similar effective temperature main sequence stars and mixed suites of theoretical pre-main and main-sequence models (e.g. Neuhäuser et al. 1995, Covino et al. 1997, Martín et al. 1998, Luhman 2004, James et al. 2006). In our own research programme, we too have adopted this philosophy, all the while pondering how appropriate it is to employ dwarf-class effective temperatures and bolometric corrections for use in HRDs for stars still on the pre-main sequence.

In this section, we therefore provide a reddening/extinction analysis for our SFR candidate members based on recent pre-main sequence models as opposed to dwarf star properties, and adopt their pre-main sequence effective temperatures and bolometric corrections in constructing HRDs. We subsequently compare and contrast the derived physical properties of our SFR candidate members with those derived from main-sequence model parameters.

In Table B1, we present the results of the reddening/extinction analysis, detailing wavelength-dependent vectors derived from the Pecaut & Mamajek (2013) pre-main sequence spectral-type versus photometric colour values. As in the case for the main sequence analysis (see Table 4), we prefer not to derive extinction values for those stars with negative reddening values, which occurred five times, and once, for Chamaeleon and Rho Ophiuchus stars, respectively, in the main sequence properties section. In this pre-main se-

quence analysis however, such cases jump to thirteen and five cases, respectively - representing a marked increase in invalid values.

While this feature is noteworthy, it is not altogether surprising given how photometrically variable these magnetically active stars are (probably at the $\simeq 10$ per cent level). However, when one examines the difference in extinction values based on the four photometric colours we employ (see Table B2), the two infrared colours yield A_v values based on $E(J - H)$ & $E(H - K) \simeq 3 - 5$ times their corresponding optical colour A_v values based on $E(B - V)$ & $E(V - I)$ for Chamaeleon stars, and $\simeq 4 - 10$ times in the case of the Rho Ophiuchus ensemble. This suggests that the stars are considerably more red in the PMS models compared to the MS ones. We note however that the PM13 PMS models cover the 5 - 30 Myr age range, which encompasses a broad age range of surface stellar conditions during this rapidly variable stage of stellar evolution.

B1 HRDs properties using PM13 colours, effective temperatures and bolometric corrections

We re-construct our series of multi-colour HRDs using the extinction corrections (see Table B1) and bolometric corrections from the PM13 empirically-calibrated PMS models, and perform an age-mass analysis similar to that presented in § 3.6. The ages and masses that we derive are detailed in Tables B3 & B4.

A comparison of stellar ages for our sample between the KH95 and PM13 analysis reveals the following properties: (a) Chamaeleon I and ϵ Cha stars show no difference in age; (b) For the two former η Cha candidates, RXJ0850.1-7554 & RXJ0951.9-7901, we present discussion in § 3.6.1 supporting the supposition that these stars are in fact likely members of the older Carina and Tuc-Hor associations, respectively. The PM13 HRD analysis, retaining a 97pc distance, confirms this assertion for the RXJ0850.1-7554 object returning an age of > 29 Myr, although the case for RXJ0951.9-7901 is weaker. Either way, the PM13 mean age of RXJ0951.9-7901 is 16.0 ± 5.0 Myr, older than the 5-10 Myr age reported in the literature for η Cha (Lawson et al. 2001; Luhman & Steeghs 2004); (c) For the Rho Ophiuchus stars, within the error bars, there is no discernible difference between the KH95 and PM13 analysis. Finally, with one or two exceptions, Chamaeleon and Rho Ophiuchus stars have stellar masses derived in the PM13 analysis consistently $0.1 - 0.3 M_{\odot}$ lower than for the KH95 analysis.

APPENDIX C: RESEARCH NOTES ON OBJECTS WITH EXCESS

We have gathered below observations and notes from the literature for the seven objects which have marginal to high levels of infrared excess emission in their SEDs. Three of the four objects with substantial excess have been observed by multiple other authors, from sub-mm disc observations/modeling to detailed SED modeling. One object, RXJ1625.6-2613 has been relatively unobserved, with only one set of previous H α /Li EW measurements, and its assignation of WTTS status, having been reported (Martín et al. 1998) is at odds with our analysis (see § C4). We have compared our isochrone-derived stellar masses with those from our SED models (see Table C1), and generally find good agreement; the sole exception to such an agreement is RXJ1625.6-2613. In this case, our sole model fit which meets the selection criteria (defined in § 4) is subject to a degeneracy in stellar luminosity and inclination.

Table A1. Log of Y4Kcam Chamaeleon and Rho Ophiuchus photometric observations on UT20070630

| Object ^a | RA(2000) Y4Kcam | DEC(2000) Field Centre | RA(2000) [2MASS] ^b | DEC(2000) | Filter | Exp Time [s] | Airmass | Julian Date [days] |
|---------------------|--------------------|---------------------------|----------------------------------|--------------|--------|-----------------|---------|-----------------------|
| Chamaeleon | | | | | | | | |
| RXJ0850.1–7554 | 08 50 14.8 | −75 56 59 | 08 50 05.41 | −75 54 38.07 | B | 7.0 | 1.73 | 2454282.4678 |
| | | | | | V | 7.0 | 1.73 | 2454282.4697 |
| | | | | | I | 7.0 | 1.74 | 2454282.4707 |
| RXJ0951.9–7901 | 09 51 59.8 | −79 05 00 | 09 51 50.70 | −79 01 37.72 | B | 7.0 | 1.67 | 2454282.4719 |
| | | | | | V | 7.0 | 1.68 | 2454282.4734 |
| | | | | | I | 7.0 | 1.68 | 2454282.4742 |
| RXJ1112.7–7637 | 11 12 28.9 | −76 41 00 | 11 12 24.41 | −76 37 06.41 | I | 7.0 | 1.52 | 2454282.4752 |
| | | | | | V | 7.0 | 1.52 | 2454282.4768 |
| | | | | | B | 7.0 | 1.52 | 2454282.4777 |
| RXJ1129.2–7546 | 11 29 16.0 | −75 50 00 | 11 29 12.62 | −75 46 26.32 | B | 7.0 | 1.49 | 2454282.4791 |
| | | | | | V | 7.0 | 1.49 | 2454282.4805 |
| | | | | | I | 7.0 | 1.49 | 2454282.4814 |
| RXJ1140.3–8321 | 11 40 21.1 | −83 25 00 | 11 40 16.59 | −83 21 00.38 | I | 7.0 | 1.71 | 2454282.4834 |
| | | | | | V | 7.0 | 1.71 | 2454282.4849 |
| | | | | | B | 7.0 | 1.71 | 2454282.4859 |
| RXJ1158.5–7754a | 11 58 32.0 | −77 59 00 | 11 58 28.17 | −77 54 29.48 | B | 7.0 | 1.53 | 2454282.4873 |
| | | | | | V | 7.0 | 1.53 | 2454282.4887 |
| | | | | | I | 7.0 | 1.53 | 2454282.4898 |
| RXJ1159.7–7601 | 11 59 46.0 | −76 06 00 | 11 59 42.27 | −76 01 26.08 | I | 7.0 | 1.48 | 2454282.4909 |
| | | | | | V | 7.0 | 1.48 | 2454282.4927 |
| | | | | | B | 7.0 | 1.49 | 2454282.4939 |
| RXJ1233.5–7523 | 12 33 34.9 | −75 26 59 | 12 33 29.81 | −75 23 11.25 | B | 7.0 | 1.45 | 2454282.4956 |
| | | | | | V | 5.0 | 1.45 | 2454282.4999 |
| | | | | | I | 5.0 | 1.45 | 2454282.5008 |
| RXJ1239.4–7502 | 12 39 24.9 | −75 07 00 | 12 39 21.24 | −75 02 39.16 | I | 5.0 | 1.44 | 2454282.5026 |
| | | | | | V | 7.0 | 1.44 | 2454282.5046 |
| | | | | | B | 7.0 | 1.44 | 2454282.5057 |
| Rho Ophiuchus | | | | | | | | |
| RXJ1620.1–2348 | 16 20 15.9 | −23 51 59 | 16 20 10.57 | −23 48 12.22 | I | 7.0 | 1.06 | 2454282.6612 |
| | | | | | V | 8.0 | 1.07 | 2454282.6642 |
| | | | | | B | 20.0 | 1.07 | 2454282.6651 |
| RXJ1621.0–2352 | 16 21 01.8 | −23 55 59 | 16 20 57.87 | −23 52 34.38 | B | 20.0 | 1.16 | 2454282.6878 |
| | | | | | V | 8.0 | 1.14 | 2454282.6909 |
| | | | | | I | 7.0 | 1.14 | 2454282.6918 |
| RXJ1621.2–2347 | 16 21 19.9 | −23 49 59 | 16 21 16.24 | −23 47 21.99 | I | 10.0 | 1.20 | 2454282.7160 |
| | | | | | V | 25.0 | 1.25 | 2454282.7188 |
| | | | | | B | 40.0 | 1.26 | 2454282.7198 |
| RXJ1623.1–2300 | 16 23 11.9 | −23 04 59 | 16 23 07.83 | −23 00 59.67 | I | 10.0 | 1.14 | 2454282.6935 |
| | | | | | V | 14.0 | 1.15 | 2454282.6952 |
| | | | | | B | 20.0 | 1.15 | 2454282.6961 |
| RXJ1623.4–2425 | 16 23 25.9 | −24 28 00 | 16 23 21.81 | −24 24 57.79 | B | 7.0 | 1.01 | 2454282.6308 |
| | | | | | V | 7.0 | 1.02 | 2454282.6323 |
| | | | | | I | 7.0 | 1.02 | 2454282.6340 |
| RXJ1623.5–2523 | 16 23 11.9 | −23 04 59 | 16 23 32.34 | −25 23 48.53 | I | 8.0 | 1.15 | 2454282.6984 |
| | | | | | V | 12.0 | 1.16 | 2454282.7005 |
| | | | | | B | 18.0 | 1.16 | 2454282.7016 |
| RXJ1624.0–2456 | 16 24 11.4 | −25 00 00 | 16 24 06.32 | −24 56 46.81 | B | 20.0 | 1.02 | 2454282.6355 |
| | | | | | V | 20.0 | 1.02 | 2454282.6371 |
| | | | | | I | 12.0 | 1.02 | 2454282.6385 |

C1 ROXR1 13 (a.k.a DoAr 21/RXJ1626.03-2423)

Being the most extensively, and thoroughly, observed object of our sample abundant photometric data are available for ROXR1 13. In our modeling of these data, however, we noted inconsistencies likely due to variability; indeed, previous authors have noted in the farther wavelengths specifically, there is likely contamina-

tion from nearby extended sources. ROXR1 13 was observed by [Cieza et al. \(2013\)](#) with Herschel, disc excess seen in both the PACS 70 μ m and 160 μ m bands. Their H α line profile appears to be simply in absorption, but earlier work has shown this line to be highly variable ([Jensen et al., 2009](#)). [McClure et al. \(2010\)](#) obtained Spitzer IRS spectra and saw PAH features. The Spitzer c2d survey also observed this object, providing IRAC and MIPS pho-

Table A1 – *continued*

| Object ^a | RA(2000) DEC(2000) Y4Kcam Field Centre | RA(2000) DEC(2000) [2MASS] ^b | Filter | Exp Time [s] | Airmass | Julian Date [days] |
|----------------------|---|--|--------|-----------------|---------|-----------------------|
| Rho Ophiuchus | | | | | | |
| RXJ1624.8–2359 | 16 24 52.4 –24 04 00 | 16 24 48.40 –23 59 16.02 | B | 75.0 | 1.02 | 2454282.6401 |
| | | | V | 30.0 | 1.03 | 2454282.6425 |
| | | | I | 14.0 | 1.03 | 2454282.6436 |
| RXJ1624.8–2239 | 16 24 55.9 –22 42 59 | 16 24 51.36 –22 39 32.54 | B | 18.0 | 1.18 | 2454282.7035 |
| | | | V | 10.0 | 1.19 | 2454282.7051 |
| | | | I | 7.0 | 1.19 | 2454282.7068 |
| RXJ1625.0–2508 | 16 25 09.9 –25 12 59 | 16 25 04.49 –25 09 11.49 | I | 7.0 | 1.03 | 2454282.6452 |
| | | | V | 7.0 | 1.03 | 2454282.6467 |
| | | | B | 25.0 | 1.03 | 2454282.6480 |
| RXJ1625.4–2346 | 16 25 33.0 –23 49 59 | 16 25 28.64 –23 46 26.55 | B | 25.0 | 1.04 | 2454282.6496 |
| | | | V | 10.0 | 1.04 | 2454282.6512 |
| | | | I | 8.0 | 1.04 | 2454282.6527 |
| RXJ1625.6–2613 | 16 25 43.0 –26 17 00 | 16 25 38.49 –26 13 54.03 | I | 7.0 | 1.19 | 2454282.7109 |
| | | | V | 12.0 | 1.20 | 2454282.7121 |
| | | | B | 15.0 | 1.20 | 2454282.7136 |
| ROXR1 13 | 16 26 09.9 –24 27 00 | 16 26 03.02 –24 23 36.04 | B | 50.0 | 1.01 | 2454282.6206 |
| | | | I | 20.0 | 1.01 | 2454282.6255 |
| | | | V | 20.0 | 1.01 | 2454282.6272 |
| RXJ1627.1–2419 | 16 27 14.9 –24 22 59 | 16 27 10.28 –24 19 12.74 | I | 7.0 | 1.04 | 2454282.6542 |
| | | | V | 10.0 | 1.04 | 2454282.6556 |
| | | | B | 30.0 | 1.04 | 2454282.6573 |

a – Nomenclature based on Rosat All-Sky Survey detections. [<http://www.xray.mpe.mpg.de/cgi-bin/rosat/rosat-survey>]

b – Astrometric data taken from the 2MASS All-Sky Release Point Source catalogue (March 2003). [<http://irsa.ipac.caltech.edu/applications/Gator/>]

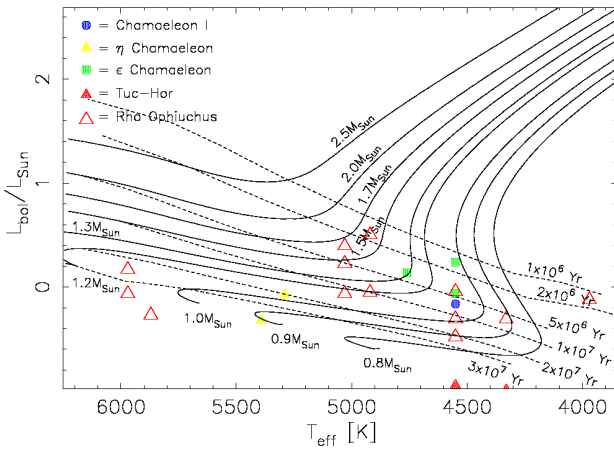


Figure B1. Similar to Figure 7, we plot an Hertzsprung-Russell diagram, using extinction values derived based on $B - V$ colours (see Table B1), for Cham I (●), η Cham (▲), Tuc-Hor (▲), ϵ Cham (■) & Rho Ophiuchus (△) objects. Effective temperatures, bolometric corrections and reddening vectors are based on the pre-main sequence colour-spectral type relationships presented in PM13, with distances to individual stellar groups cited in Table 5. Stellar isochrones (dashed tracks) and mass tracks (solid lines) are computed from theoretical solar metallicity PARSEC stellar models by (Bressan et al. 2012).

tometry (Wahhaj et al. 2010). Our SED for this $A_v > 5$ object (see Figure 12) clearly shows that its photometric data are incompatible with a bare photosphere $> 10\mu\text{m}$, and it is obviously consistent with a circumstellar disc model (e.g. see Table C1); such a finding

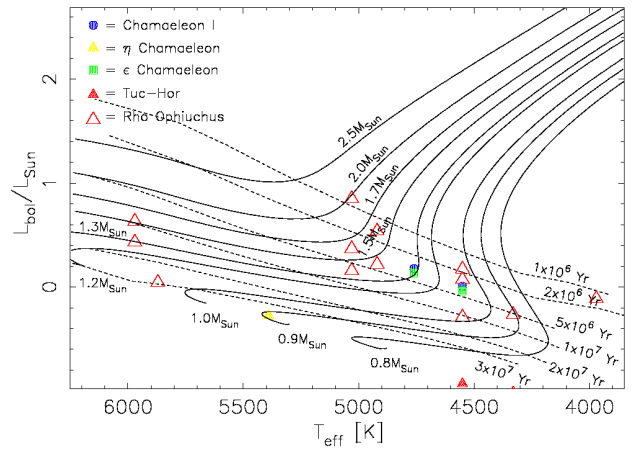


Figure B2. *Idem* to Figure B1, except extinction values are derived from $V - I_c$ colours.

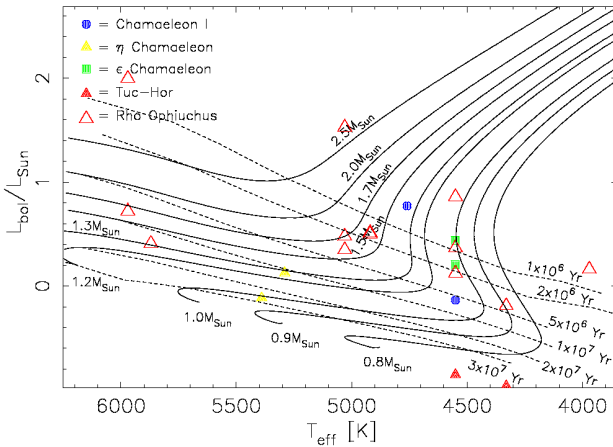
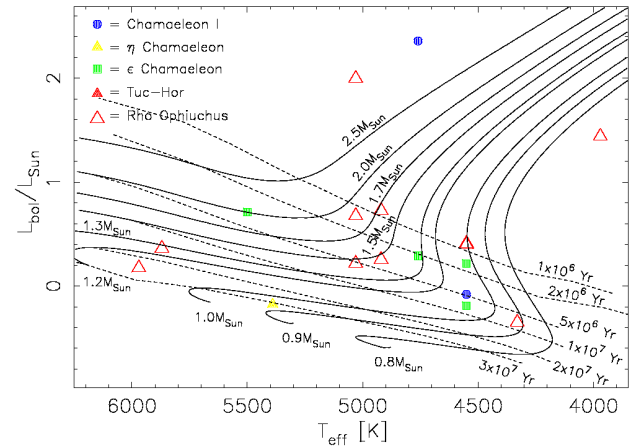
agrees well with its Spitzer c2d result (Cieza et al. 2007), although at odds with the Valenti et al. (2003) *naked T-Tauri star* (NTTS) status and class III assignment by Dzib et al. (2013).

C2 RXJ1627.1-2419 (a.k.a. SR 21 AB)

Furlan et al. (2009) and McClure et al. (2010) both modeled the SED of this object and proposed it is a transitional disc based upon its steep spectral slope from 13 to $31\mu\text{m}$. The spectra of Martín et al. (1998) indicated no ongoing accretion, but our spectra show some $H\alpha$ emission; this is unsurprising given the high

Table A2. Log of UVES spectroscopic observations of Chamaeleon and Rho Ophiuchus candidate members.

| Object | UT Date | UT Time | Exp Time [s] | Heliocentric Julian Date [days] | Airmass |
|-----------------|------------|----------|--------------|---------------------------------|---------|
| Chamaeleon | | | | | |
| RXJ0951.9-7901 | 2005-03-23 | 03:24:07 | 282 | 2453452.6444 | 1.729 |
| RXJ1112.7-7637 | 2005-03-24 | 00:56:49 | 1487 | 2453453.5495 | 1.783 |
| RXJ1129.2-7546 | 2005-03-24 | 01:24:59 | 1487 | 2453453.5691 | 1.735 |
| RXJ1140.3-8321 | 2005-03-24 | 04:37:35 | 649 | 2453453.6973 | 1.924 |
| RXJ1158.5-7754a | 2005-03-24 | 04:51:24 | 712 | 2453453.7078 | 1.672 |
| RXJ1159.7-7601 | 2005-03-24 | 05:06:38 | 540 | 2453453.7176 | 1.607 |
| RXJ1201.7-7859 | 2005-03-24 | 05:31:55 | 71 | 2453453.7322 | 1.729 |
| RXJ1233.5-7523 | 2005-03-24 | 05:37:23 | 163 | 2453453.7368 | 1.584 |
| RXJ1239.4-7502 | 2005-03-24 | 05:44:30 | 410 | 2453453.7432 | 1.573 |
| RXJ1303.5-7701 | 2005-03-24 | 05:54:31 | 149 | 2453453.7485 | 1.638 |
| Rho Ophiuchus | | | | | |
| RXJ1620.1-2348 | 2005-03-24 | 09:29:36 | 236 | 2453453.8995 | 1.010 |
| RXJ1620.7-2348 | 2005-03-27 | 05:12:57 | 2145 | 2453456.7326 | 1.486 |
| RXJ1621.0-2352 | 2005-03-24 | 09:36:42 | 341 | 2453453.9050 | 1.014 |
| RXJ1623.1-2300 | 2005-03-27 | 05:52:02 | 1128 | 2453456.7538 | 1.298 |
| RXJ1623.4-2425 | 2005-03-27 | 06:13:56 | 2585 | 2453456.7774 | 1.213 |
| RXJ1623.5-2523 | 2005-04-06 | 08:19:39 | 492 | 2453466.8534 | 1.001 |
| RXJ1624.0-2456 | 2005-04-06 | 08:32:08 | 1961 | 2453466.8706 | 1.005 |
| RXJ1624.8-2359 | 2005-04-21 | 03:39:35 | 3107 | 2453481.6751 | 1.479 |
| RXJ1624.8-2239 | 2005-05-04 | 03:00:29 | 781 | 2453494.6352 | 1.416 |
| RXJ1625.0-2508 | 2005-04-06 | 09:11:05 | 1237 | 2453466.8934 | 1.032 |
| RXJ1625.4-2346 | 2005-05-04 | 03:23:06 | 125 | 2453494.6471 | 1.303 |
| RXJ1625.4-2346 | 2005-05-05 | 02:56:40 | 1128 | 2453495.6345 | 1.413 |
| RXJ1625.6-2613 | 2005-04-16 | 06:31:49 | 781 | 2453476.7809 | 1.027 |
| ROXR1 13 | 2005-05-15 | 04:35:20 | 2357 | 2453505.7105 | 1.030 |
| ROXR1 13 | 2005-05-15 | 06:42:51 | 2357 | 2453505.7991 | 1.037 |
| RXJ1627.1-2419 | 2005-05-15 | 03:46:42 | 2585 | 2453505.6780 | 1.104 |

**Figure B3.** *Idem* to Figure B1, except extinction values are derived from $J - H$ colours.**Figure B4.** *Idem* to Figure B1, except extinction values are derived from $H - K$ colours.

frequency of variability seen in YSO spectral lines generally. Sub-millimeter imaging of [Andrews et al. \(2009\)](#) resolved a ~ 37 AU gap in the inner disc in the dust continuum, indicating some clearing has taken place. We too find that this $A_v > 5$ object shows clear evidence of infrared excess longward of $5\mu\text{m}$, supporting its class II status reported by ([Andrews & Williams 2007](#)).

C3 RXJ1112.7-7637 (a.k.a. Cha T 2-51/T-51)

For this $A_v > 5$ object, we again find clear evidence in its SED of a circumstellar disc, with strong infrared excess longward of a couple of microns. This object was also included in the survey of [Furlan et al. \(2009\)](#), and based on the shallow $13\text{--}31\mu\text{m}$ spectral slope, it is not likely a transition disc object. Both [Furlan et al.](#)

Table B1. Reddening and extinction vectors for Chamaeleon and Rho Ophiuchus targets based on empirically calibrated theoretical pre-main sequence photometric colours (Pecaut & Mamajek 2013).

| Target | $E(B - V)^a$ | $E(V - Ic)^a$ | $E(J - H)^a$ | $E(H - K)^a$ | A_v^b [$E(B - V)$] | A_v^b [$E(V - Ic)$] | A_v^b [$E(J - H)$] | A_v^b [$E(H - K)$] |
|-----------------------------|--------------|---------------|--------------|--------------|---------------------------|----------------------------|---------------------------|---------------------------|
| Chamaeleon | | | | | | | | |
| RXJ0850.1-7554 | 0.007 | 0.055 | 0.061 | 0.024 | 0.022 | 0.136 | 0.540 | 0.392 |
| RXJ0951.9-7901 | 0.061 | ... | 0.079 | -0.022 | 0.189 | ... | 0.700 | ... |
| RXJ1112.7-7637 | ... | 0.334 | 0.261 | 0.385 | ... | 0.828 | 2.312 | 6.283 |
| RXJ1129.2-7546 | 0.387 | 0.654 | 0.143 | 0.086 | 1.200 | 1.622 | 1.267 | 1.404 |
| RXJ1140.3-8321 ^c | 0.122 | 0.169 | 0.069 | -0.086 | 0.378 | 0.419 | 0.611 | ... |
| RXJ1140.3-8321 ^c | 0.032 | 0.019 | 0.019 | -0.096 | 0.099 | 0.047 | 0.168 | ... |
| RXJ1158.5-7754a | 0.159 | ... | 0.113 | -0.008 | 0.493 | ... | 1.001 | ... |
| RXJ1159.7-7601 | 0.130 | 0.187 | 0.121 | 0.005 | 0.403 | 0.464 | 1.072 | 0.082 |
| RXJ1201.7-7859 | -0.030 | -0.010 | -0.034 | 0.009 | ... | ... | ... | 0.147 |
| RXJ1239.4-7502 ^c | 0.067 | 0.083 | -0.009 | 0.036 | 0.208 | 0.206 | ... | 0.588 |
| RXJ1239.4-7502 ^c | -0.023 | -0.027 | -0.069 | 0.016 | ... | ... | ... | 0.261 |
| Rho Ophiuchus | | | | | | | | |
| RXJ1620.7-2348 | 0.264 | 0.375 | 0.126 | 0.044 | 0.818 | 0.930 | 1.116 | 0.718 |
| RXJ1621.0-2352 | -0.008 | -0.025 | -0.085 | -0.020 | ... | ... | ... | ... |
| RXJ1621.2-2347 | 1.262 | 1.769 | 0.680 | 0.376 | 3.912 | 4.387 | 6.025 | 6.136 |
| RXJ1623.1-2300 | 0.293 | 0.481 | 0.149 | -0.001 | 0.908 | 1.193 | 1.320 | ... |
| RXJ1623.4-2425 | 0.533 | 0.982 | 0.378 | 0.198 | 1.652 | 2.435 | 3.349 | 3.231 |
| RXJ1623.5-2523 | 0.448 | 0.704 | 0.191 | 0.154 | 1.389 | 1.746 | 1.692 | 2.513 |
| RXJ1624.0-2456 | 0.757 | 1.170 | 0.418 | 0.187 | 2.347 | 2.902 | 3.703 | 3.052 |
| RXJ1624.8-2239 | 0.114 | 0.178 | 0.039 | 0.056 | 0.353 | 0.441 | 0.346 | 0.914 |
| RXJ1624.8-2359 | 0.790 | 1.469 | 0.605 | 0.258 | 2.449 | 3.643 | 5.360 | 4.211 |
| RXJ1625.0-2508 | 0.750 | 1.203 | 0.418 | 0.143 | 2.325 | 2.983 | 3.703 | 2.334 |
| RXJ1625.4-2346 | 0.378 | 0.747 | 0.292 | 0.119 | 1.172 | 1.853 | 2.587 | 1.942 |
| RXJ1625.6-2613 | 0.003 | 0.014 | 0.081 | 0.240 | 0.009 | 0.035 | 0.718 | 3.917 |
| ROXR1 13 | 1.365 | 2.166 | 0.798 | 0.505 | 4.232 | 5.372 | 7.070 | 8.242 |
| RXJ1627.1-2419 | 1.161 | 2.153 | 0.988 | 0.688 | 3.599 | 5.339 | 8.754 | 11.228 |

- a – Reddening vectors are calculated by subtracting appropriate photometric colours for each target (see Table 2) from corresponding theoretical values for pre-main sequence stars (from table 6 in Pecaut & Mamajek 2013) based on spectral types (see Table 3).
- b – Extinction vectors [Av], based on four colour-dependent reddening vectors, are calculated to be: For optical data, $A_v = 3.1 \times E(B - V)$ and $A_v = 2.48 \times E(V - Ic)$ (from Bessell & Brett 1988); For infrared, $A_v = 8.86 \times E(J - H)$ and $A_v = 16.32 \times E(H - K)$ (from Ramírez & Meléndez 2005). For negative reddening values, we do not calculate an extinction value.
- c – Two sets of reddening and extinction values are calculated, one for each of the two spectral types.

(2009) and Manoj et al. (2011) discuss the likeliness, based on the shallow slope in the 13-31 μ m window, clearing of the outer disc, but RXJ1112.7-7637 lacks a sub-arcsecond companion that could do it.

C4 RXJ1625.6-2613 (a.k.a. PDS 83, V* V896 Sco, CD-25 1150.4, IRAS 16225-2607)

This target has been previously observed spectroscopically by (Martín et al. 1998), who classified as a WTTS, and detected H α emission at the $\simeq 4.6\text{\AA}$ level as well as a strong Li I 6708 \AA absorption line ($\simeq 450\text{ m\AA}$). Our UVES Li I EW measurement agree very well with this earlier datum, but we cannot easily, directly at least, compare our H α EWs since we measure the residual line profile (observed - template), whereas the study of Martín et al. (1998) solely measures the observed profile. We note that in our UVES spectrum however, we observe a very strong H α emission feature ($> 6.4\text{\AA}$), as well as indications of a wind in a redshifted self-absorption feature of the H α feature. Similarly, Rojas et al. (2008) also observe a very strong and complex H α emission feature in

this object (EW=-12.8 \AA) as well as compelling evidence for IRAS infra-red emission. Furlan et al. (2009) present a SED of this object which shows clear evidence of mid infra-red excess emission and a conspicuous silicon feature at 10 μ m, consistent with circumstellar material. For this $A_v > 4.5$ object, our own SED shows clear evidence of disc-like infrared emission; combined with the Rojas et al. and Furlan et al. results, these observations are clearly at odds with its Martín et al. WTTS assignment.

C5 Marginal infrared excess targets

RXJ1625.0-2508 and RXJ1623.5-2523, whose SEDs are shown in Figure D1, were both included in the survey of Martín et al. (1998); our Li I EW values are consistent with the earlier measurements within error.

Luhman et al. (2012) suggest RXJ1623.1-2300 is a potential Upper Sco member, further noting that excess in the W2 band could mean this object has a debris or evolved transitional disc. We see excess in W3 and W4, as well as a strong, narrow H α emission feature.

Table B2. Differential Extinction Vectors for our Chamaeleon and Rho Ophiuchus Targets (KH95 main sequence values - PM13 PMS values).

| Target | ΔA_v^a [$E(B - V)$] | ΔA_v^a [$E(V - Ic)$] | ΔA_v^a [$E(J - H)$] | ΔA_v^a [$E(H - K)$] |
|---|----------------------------------|-----------------------------------|----------------------------------|----------------------------------|
| Chamaeleon | | | | |
| RXJ0850.1-7554 | 0.186 | 0.050 | 0.027 | 0.526 |
| RXJ0951.9-7901 | 0.186 | ... | 0.291 | ... |
| RXJ1112.7-7637 | ... | 0.000 | 0.399 | 0.365 |
| RXJ1129.2-7546 | 0.155 | 0.099 | 0.583 | 0.691 |
| RXJ1140.3-8321 ^b | 0.155 | 0.099 | 0.583 | ... |
| RXJ1140.3-8321 ^b | 0.124 | 0.298 | 0.679 | ... |
| RXJ1158.5-7754a | 0.155 | ... | 0.583 | ... |
| RXJ1159.7-7601 | 0.155 | 0.099 | 0.583 | 0.691 |
| RXJ1201.7-7859 | ... | ... | ... | 0.363 |
| RXJ1239.4-7502 ^b | 0.124 | 0.000 | ... | 0.364 |
| RXJ1239.4-7502 ^b | ... | ... | ... | 0.691 |
| Mean (all stars) ($\pm 1\sigma$) | 0.155 ± 0.023 | 0.092 ± 0.101 | 0.466 ± 0.216 | 0.527 ± 0.164 |
| Mean ($A_v < 5$) ($\pm 1\sigma$) | 0.155 ± 0.023 | 0.108 ± 0.101 | 0.476 ± 0.232 | 0.554 ± 0.161 |
| Rho Ophiuchus | | | | |
| RXJ1620.7-2348 | 0.124 | 0.298 | 0.679 | 0.692 |
| RXJ1621.0-2352 | ... | ... | ... | ... |
| RXJ1621.2-2347 | 0.155 | 0.099 | 0.583 | 0.692 |
| RXJ1623.1-2300 | 0.155 | 0.099 | 0.583 | ... |
| RXJ1623.4-2425 | -0.062 | -0.049 | 0.012 | 0.363 |
| RXJ1623.5-2523 | 0.000 | 0.198 | 0.302 | 0.365 |
| RXJ1624.0-2456 | 0.000 | 0.198 | 0.302 | 0.364 |
| RXJ1624.8-2239 | 0.031 | 0.075 | 0.393 | 0.365 |
| RXJ1624.8-2359 | 0.155 | 0.099 | 0.583 | 0.691 |
| RXJ1625.0-2508 | -0.031 | -0.124 | -0.077 | 0.362 |
| RXJ1625.4-2346 | 0.031 | 0.074 | 0.394 | 0.365 |
| RXJ1625.6-2613 | ... | 0.149 | 0.515 | 0.530 |
| ROXR1 13 | 0.000 | 0.198 | 0.302 | 0.364 |
| RXJ1627.1-2419 | -0.031 | -0.124 | -0.078 | 0.363 |
| Mean (all stars) ($\pm 1\sigma$) | 0.044 ± 0.081 | 0.092 ± 0.127 | 0.346 ± 0.256 | 0.460 ± 0.148 |
| Mean ($A_v < 5$) ($\pm 1\sigma$) | 0.031 ± 0.074 | 0.102 ± 0.130 | 0.345 ± 0.249 | 0.426 ± 0.122 |

Notes:

a – For each SFR target, differential A_v vectors, as a function of photometric colour, are calculated by subtracting spectral type-colour dependent A_v values derived from main sequence (KH95) and pre-main sequence (Pecaut & Mamajek 2013) theoretical models.

b – Two sets of differential extinction values are calculated, one for each of the two spectral types.

C6 Remaining $A_v > 5$ Objects

SEDs for the two remaining $A_v > 5$ objects, RXJ1621.2-2347 & RXJ1624.8-2359, are consistent with bare photospheres, and out to the WISE W4 band, exhibit essentially no infrared excess emission whatsoever. Visual inspection of DSS optical and 2MASS infrared images show that these two stars lie in heavily-extincted regions of the Rho Ophiuchus SFR. We therefore posit that both systems are WTTs experiencing heavy *in situ* visual and near-infrared extinction.

APPENDIX D: SEDS FOR FULL SAMPLE

For completeness, we plot the SEDs of those Chamaeleon and Rho Ophiuchus stars that are consistent with WTTs in Figures D2 & D3.

APPENDIX E: ANCILLARY INFRARED PHOTOMETRIC DATA

In constructing our SEDs, we exploited mid-infrared and sub-mm photometric datasets for the Chamaeleon and Rho Ophiuchus stars obtained using the AKARI, Herschel, IRAM, SCUBA, Spitzer, VLA

Table B3. Isochronal ages for Chamaeleon and Rho Ophiuchus candidates stars using four separate colour-dependent extinction laws (based on PM13 effective temperatures and bolometric corrections for pre-main sequence stars) and PARSEC stellar models.

| Target ^a | T_{eff}^b [K] | $[L_{\text{bol}}/L_{\odot}]^c$ | Age [Myr] | $[L_{\text{bol}}/L_{\odot}]^c$ | Age [Myr] | $[L_{\text{bol}}/L_{\odot}]^c$ | Age [Myr] | $[L_{\text{bol}}/L_{\odot}]^c$ | Age [Myr] | Mean age [Myr] |
|-----------------------------|---------------------------|--------------------------------|--------------|--------------------------------|--------------|--------------------------------|--------------|--------------------------------|--------------|-------------------|
| | | ${}^bE(B-V)$ | | ${}^bE(V-I)$ | | ${}^bE(J-H)$ | | ${}^bE(H-K)$ | | |
| Chamaeleon I (●) | | | | | | | | | | |
| RXJ1112.7-7637 | 4760 | 9.999 | ... | 0.177 | 3.5 | 0.771 | < 1 | 2.359 | < 1 | < 1.8 |
| RXJ1129.2-7546 | 4550 | −0.163 | 7.0 | 0.006 | 4.0 | −0.136 | 6.0 | −0.081 | 5.0 | 5.5 ± 0.6 |
| η Cham (▲) | | | | | | | | | | |
| RXJ0850.1-7554 | 5390 | −0.325 | > 30 | −0.279 | > 30 | −0.117 | 27 | −0.177 | > 30 | > 29 |
| RXJ0951.9-7901 | 5290 | −0.080 | 21 | 9.999 | ... | 0.125 | 11 | 9.999 | ... | 16.0 ± 5.0 |
| Tuc Hor (▲) | | | | | | | | | | |
| RXJ1140.3-8321 [†] | 4550 | −0.948 | > 30 | −0.932 | > 30 | −0.855 | > 30 | 9.999 | ... | > 30 |
| RXJ1140.3-8321 [‡] | 4330 | −0.992 | > 30 | −1.012 | > 30 | −0.964 | > 30 | 9.999 | ... | > 30 |
| ε Cham (■) | | | | | | | | | | |
| RXJ1158.5-7754a | 4550 | 0.238 | 1.5 | 9.999 | ... | 0.441 | < 1 | 9.999 | ... | < 1.3 |
| RXJ1159.7-7601 | 4550 | −0.063 | 4.5 | −0.038 | 4.5 | 0.205 | 2.0 | −0.191 | 7.5 | 4.6 ± 1.1 |
| RXJ1201.7-7859 | 5500 | 9.999 | ... | 9.999 | ... | 9.999 | ... | 0.711 | 3.5 | 3.5 |
| RXJ1239.4-7502 [†] | 4760 | 0.138 | 4.0 | 0.137 | 4.0 | 9.999 | ... | 0.290 | 2.0 | 3.3 ± 0.7 |
| RXJ1239.4-7502 [‡] | 4550 | 9.999 | ... | 9.999 | ... | 9.999 | ... | 0.215 | 2.0 | 2.0 |
| Rho Ophiuchus (△) | | | | | | | | | | |
| RXJ1620.7-2348 | 4330 | −0.310 | 7.0 | −0.266 | 5.0 | −0.191 | 4.0 | −0.350 | 7.5 | 5.9 ± 0.8 |
| RXJ1621.0-2352 | 4920 | 9.999 | ... | 9.999 | ... | 9.999 | ... | 9.999 | ... | ... |
| RXJ1621.2-2347 | 4550 | −0.480 | 22 | −0.290 | 11 | 0.366 | < 1 | 0.410 | < 1 | < 8.8 |
| RXJ1623.1-2300 | 4550 | −0.043 | 4.5 | 0.071 | 3.0 | 0.122 | 2.0 | 9.999 | ... | 3.2 ± 0.7 |
| RXJ1623.4-2425 | 5870 | −0.270 | > 30 | 0.044 | 30 | 0.409 | 14 | 0.362 | 16 | > 23 |
| RXJ1623.5-2523 | 5030 | 0.226 | 5.0 | 0.369 | 3.5 | 0.348 | 4.0 | 0.676 | 1.5 | 3.5 ± 0.7 |
| RXJ1624.0-2456 | 5030 | −0.064 | 14 | 0.158 | 6.5 | 0.479 | 2.5 | 0.218 | 5.0 | 7.0 ± 2.5 |
| RXJ1624.8-2239 | 4920 | 0.502 | 2.0 | 0.538 | 1.5 | 0.500 | 2.0 | 0.727 | < 1 | < 1.6 |
| RXJ1624.8-2359 | 4550 | −0.306 | 11 | 0.172 | 2.0 | 0.859 | < 1 | 0.399 | < 1 | < 3.8 |
| RXJ1625.0-2508 | 5970 | 0.169 | 25 | 0.432 | 16 | 0.720 | 8.5 | 0.173 | 25 | 18.6 ± 4.0 |
| RXJ1625.4-2346 | 4920 | −0.053 | 10 | 0.219 | 4.5 | 0.513 | 2.0 | 0.255 | 4.0 | 5.1 ± 1.7 |
| RXJ1625.6-2613 | 3970 | −0.122 | 1.5 | −0.112 | 1.5 | 0.161 | < 1 | 1.441 | < 1 | < 1.3 |
| ROXR1 13 | 5030 | 0.394 | 3.5 | 0.850 | < 1 | 1.529 | < 1 | 1.998 | < 1 | < 1.6 |
| RXJ1627.1-2419 | 5970 | −0.064 | > 30 | 0.632 | 10 | 1.998 | < 1 | 2.988 | < 1 | ≈ 10 (?) |

^a— Isochronal age determinations are segregated into stars comprising disparate young SFR regions, with symbols ●, ▲, ▲, ■ & △, matching those data presented in Figures B1–B4.

^b— L_{bol}/L_{\odot} data are calculated using T_{eff} and reddening vectors based on PM13 colour-spectral types relationships for pre-main sequence stars (see also Tables 3 & B1).

^c— Distances used for L_{bol}/L_{\odot} calculations are the same as those used in § 3.6 and Table 5.

[†] — for a given star, calculations are made using earlier spectral type/higher T_{eff} .

[‡] — for a given star, calculations are made using later spectral type/lower T_{eff} .

and WISE facilities; all data are detailed and referenced in Tables E1 & E2.

Table B4. Theoretical PARSEC masses for Chamaeleon, Tuc-Hor and Rho Ophiuchus candidates using four separate colour-dependent extinction laws (based on PM13 effective temperatures, colours and bolometric corrections for PMS stars corresponding to each target's spectral type).

| Target | T_{eff} [K] | Mass [M_{\odot}] $E(B - V)$ | Mass [M_{\odot}] $E(V - I)$ | Mass [M_{\odot}] $E(J - H)$ | Mass [M_{\odot}] $E(H - K)$ | Mean Mass [M_{\odot}] |
|-----------------------------|-------------------------|---------------------------------------|---------------------------------------|---------------------------------------|---------------------------------------|------------------------------|
| Chamaeleon I (●) | | | | | | |
| RXJ1112.7-7637 | 4760 | ... | 1.3 | 1.4 | > 2.5 | > 1.7 |
| RXJ1129.2-7546 | 4550 | 1.1 | 1.1 | 1.1 | 1.1 | 1.1 ± ... |
| η Cham (▲) | | | | | | |
| RXJ0850.1-7554 | 5390 | 0.9 | 0.9 | 1.0 | 0.9 | 0.93 ± 0.03 |
| RXJ0951.9-7901 | 5290 | 1.0 | ... | 1.3 | ... | 1.15 ± 0.15 |
| Tuc Hor (▲) | | | | | | |
| RXJ1140.3-8321 [†] | 4550 | ... | ... | ... | ... | ... |
| RXJ1140.3-8321 [‡] | 4330 | ... | ... | ... | ... | ... |
| ϵ Cham (■) | | | | | | |
| RXJ1158.5-7754a | 4550 | 1.0 | ... | 1.0 | ... | 1.0 ± ... |
| RXJ1159.7-7601 | 4550 | 1.1 | 1.1 | 1.0 | 1.1 | 1.08 ± 0.03 |
| RXJ1201.7-7859 | 5500 | ... | ... | ... | 2.0 | 2.0 ± ... |
| RXJ1239.4-7502 [†] | 4760 | 1.3 | 1.3 | ... | 1.3 | 1.3 ± ... |
| RXJ1239.4-7502 [‡] | 4550 | ... | ... | ... | 1.0 | 1.0 ± ... |
| Rho Ophiuchus (△) | | | | | | |
| RXJ1620.7-2348 | 4330 | 0.8 | 0.9 | 0.8 | 0.9 | 0.85 ± 0.03 |
| RXJ1621.0-2352 | 4920 | ... | ... | ... | ... | ... |
| RXJ1621.2-2347 | 4550 | 0.9 | 1.0 | 1.0 | 1.0 | 0.98 ± 0.03 |
| RXJ1623.1-2300 | 4550 | 1.1 | 1.1 | 1.0 | ... | 1.07 ± 0.03 |
| RXJ1623.4-2425 | 5870 | ... | 1.1 | 1.3 | 1.3 | 1.23 ± 0.07 |
| RXJ1623.5-2523 | 5030 | 1.5 | 1.6 | 1.6 | 2.2 | 1.73 ± 0.16 |
| RXJ1624.0-2456 | 5030 | 1.1 | 1.4 | 1.7 | 1.5 | 1.43 ± 0.13 |
| RXJ1624.8-2239 | 4920 | 1.6 | 1.6 | 1.6 | 1.7 | 1.63 ± 0.03 |
| RXJ1624.8-2359 | 4550 | 1.0 | 1.0 | 1.0 | 1.0 | 1.0 ± ... |
| RXJ1625.0-2508 | 5970 | 1.1 | 1.3 | 1.6 | 1.1 | 1.28 ± 0.12 |
| RXJ1625.4-2346 | 4920 | 1.2 | 1.4 | 1.6 | 1.5 | 1.43 ± 0.09 |
| RXJ1625.6-2613 | 3970 | < 0.8 | < 0.8 | < 0.8 | < 0.8 | < 0.8 |
| ROXR1 13 | 5030 | 1.6 | 2.0 | > 2.5 | > 2.5 | > 2.2 |
| RXJ1627.1-2419 | 5970 | 1.1 | 1.5 | > 2.5 | > 2.5 | > 1.9 |

Notes:

a— PARSEC model mass determinations are segregated into stars comprising disparate young SFR regions, with symbols ●, ▲, ■ & △, matching those data presented in Figures B1–B4.

b— L_{bol}/L_{\odot} data are calculated using T_{eff} and reddening vectors based on PM13 colour-spectral types relationships for PMS stars (see also Table B1).

c— Distances used for L_{bol}/L_{\odot} calculations are the same as those presented in the footnotes to Table 5.

[†]— for a given star, calculations are made using earlier spectral type/higher T_{eff} .

[‡]— for a given star, calculations are made using later spectral type/lower T_{eff} .

Table C1. Best fitting star+disc parameters for our SED models of stars with substantial NIR excess.

| Target | Best fit model ID | T_{eff} [K] | Stellar Mass [M_{\odot}] | Stellar Radius [R_{\odot}] | Disc Mass [M_{\odot}] | Inclination [°] |
|----------------|----------------------|-------------------------|---------------------------------|-----------------------------------|------------------------------|--------------------|
| RXJ1112.7-7637 | 3018851 | 5090 | 2.52 | 3.60 | 1.16×10^{-2} | 87 |
| ROXR1 13 | 3007238 | 4974 | 3.52 | 6.41 | 4.46×10^{-5} | 81 |
| RXJ1625.6-2613 | 3015710 | 5683 | 3.02 | 5.53 | 5.16×10^{-3} | 87 |
| RXJ1627.1-2419 | 3011961 | 5865 | 2.46 | 4.18 | 6.25×10^{-2} | 32 |
| RXJ1623.1-2300 | 3001684 | 4274 | 1.01 | 1.79 | 5.62×10^{-8} | 87 |
| RXJ1623.5-2523 | 3012187 | 5039 | 1.85 | 2.30 | 1.39×10^{-8} | 63 |
| RXJ1625.0-2508 | 3015211 | 5403 | 1.50 | 1.84 | 5.25×10^{-9} | 18 |

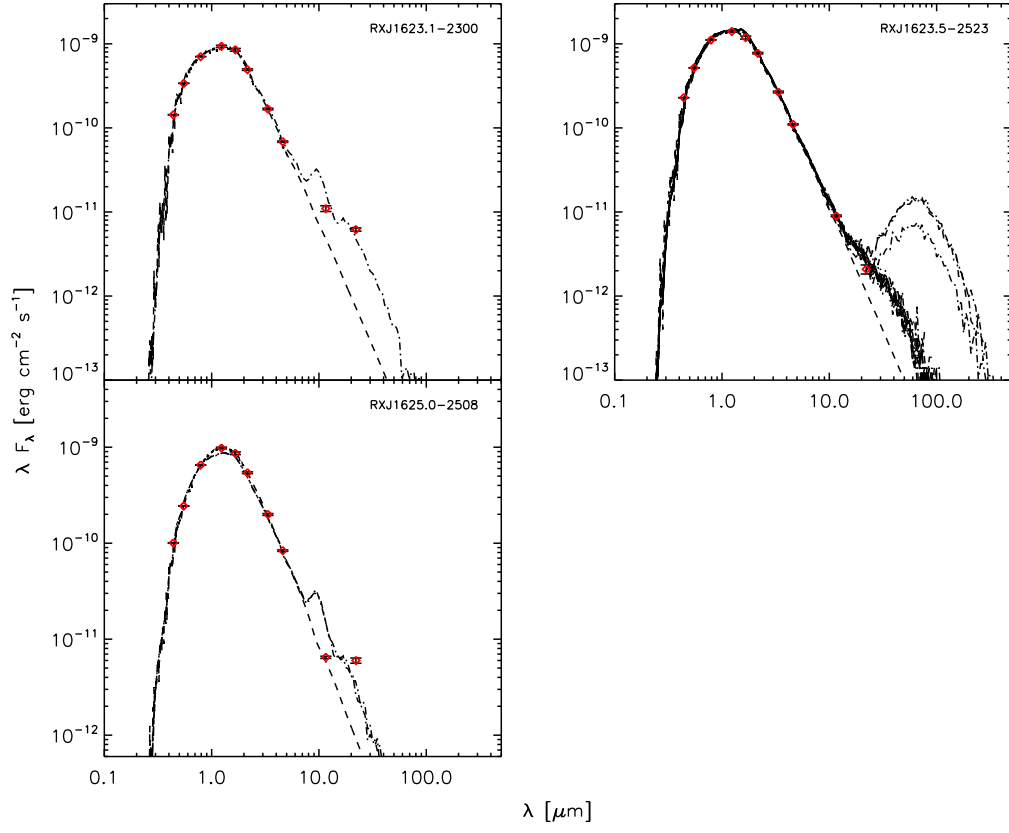


Figure D1. *Idem* to Figure 12, however we now plot SEDs of Rho Ophiuchus targets with marginal signatures of mid-infrared excesses.

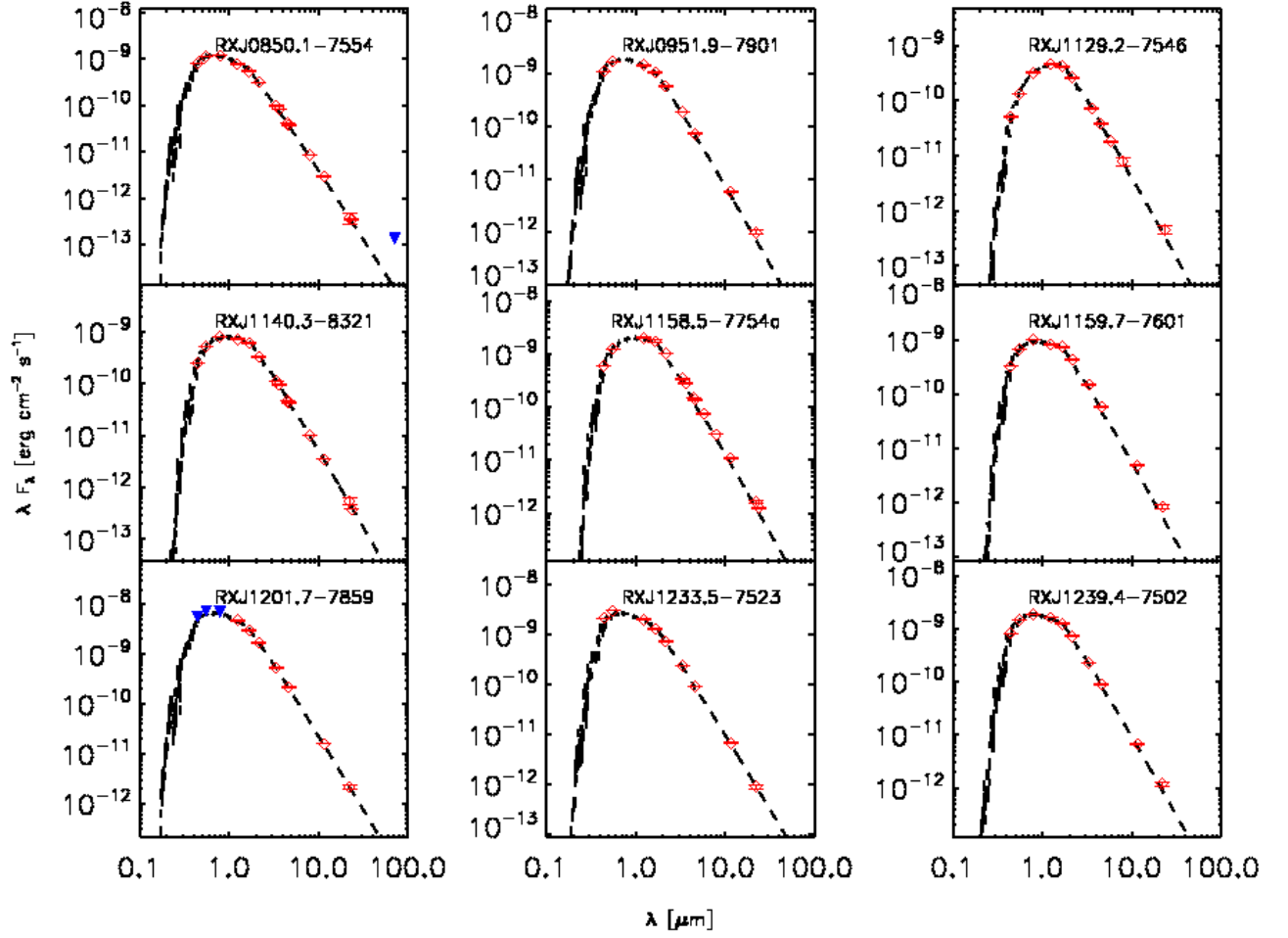


Figure D2. *Idem* to Figure 12, we now plot SEDs of Chamaeleon candidates that are consistent with bare photospheres.

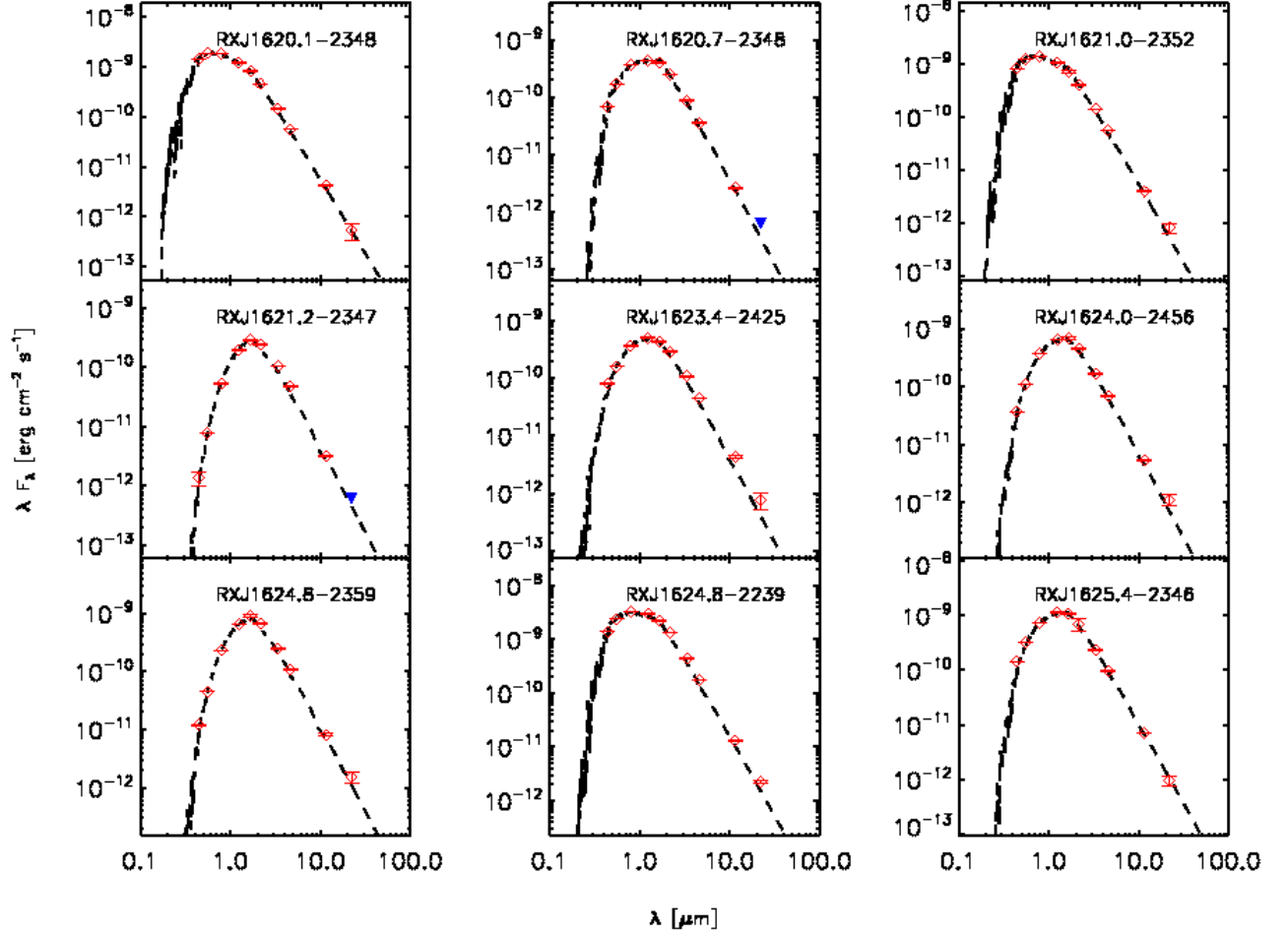


Figure D3. *Idem* to Figure 12, however we now plot SEDs of Rho Ophiuchus candidates that are consistent with bare photospheres.

Table E1. WISE data for our Chamaeleon and Rho Ophiuchus candidates (Cutri et al. 2012).

| Target | WISE 3.4 μ m [mag] | WISE 4.6 μ m [mag] | WISE 12 μ m [mag] | WISE 22 μ m [mag] | Error Code |
|----------------------|---------------------------|---------------------------|--------------------------|--------------------------|---------------|
| Chamaeleon | | | | | |
| RXJ0850.1-7554 | 8.646 \pm 0.022 | 8.684 \pm 0.020 | 8.588 \pm 0.021 | 8.582 \pm 0.227 | AAAB |
| RXJ0951.9-7901 | 7.995 \pm 0.196 | 7.986 \pm 0.021 | 7.921 \pm 0.019 | 7.833 \pm 0.144 | BAAB |
| RXJ1112.7-7637 | 6.611 \pm 0.053 | 6.200 \pm 0.023 | 4.536 \pm 0.014 | 3.365 \pm 0.020 | AAAA |
| RXJ1129.2-7546 | 8.815 \pm 0.092 | 8.766 \pm 0.021 | 8.549 \pm 0.022 | 7.476 \pm 0.116 | AAAB |
| RXJ1140.3-8321 | 8.509 \pm 0.023 | 8.540 \pm 0.020 | 8.442 \pm 0.022 | 8.371 \pm 0.209 | AAAB |
| RXJ1158.5-7754a | 6.946 \pm 0.024 | 7.166 \pm 0.019 | 7.169 \pm 0.016 | 7.095 \pm 0.092 | AAAA |
| RXJ1159.7-7601 | 8.168 \pm 0.023 | 8.198 \pm 0.020 | 8.099 \pm 0.019 | 7.894 \pm 0.155 | AAAB |
| RXJ1201.7-7859 | 6.823 \pm 0.060 | 6.792 \pm 0.022 | 6.785 \pm 0.017 | 6.677 \pm 0.065 | AAAA |
| RXJ1233.5-7523 | 7.666 \pm 0.027 | 7.738 \pm 0.021 | 7.695 \pm 0.017 | 7.641 \pm 0.143 | AAAB |
| RXJ1239.4-7502 | 7.725 \pm 0.026 | 7.753 \pm 0.021 | 7.702 \pm 0.017 | 7.400 \pm 0.092 | AAAA |
| Rho Ophiuchus | | | | | |
| RXJ1620.1-2348 | 8.230 \pm 0.023 | 8.255 \pm 0.021 | 8.241 \pm 0.032 | 7.850 \pm ... | AAAU |
| RXJ1620.7-2348 | 8.786 \pm 0.021 | 8.769 \pm 0.019 | 8.750 \pm 0.042 | 7.953 \pm ... | AAAU |
| RXJ1621.0-2352 | 8.256 \pm 0.024 | 8.263 \pm 0.019 | 8.313 \pm 0.028 | 8.024 \pm 0.279 | AAAB |
| RXJ1621.2-2347 | 8.555 \pm 0.023 | 8.412 \pm 0.020 | 8.524 \pm 0.033 | 8.506 \pm ... | AAAU |
| RXJ1623.1-2300 | 8.056 \pm 0.024 | 8.036 \pm 0.020 | 7.710 \pm 0.081 | 7.100 \pm 0.120 | AAAB |
| RXJ1623.4-2425 | 8.528 \pm 0.024 | 8.497 \pm 0.021 | 8.488 \pm 0.042 | 7.878 \pm ... | AAAU |
| RXJ1623.5-2523 | 7.509 \pm 0.030 | 7.509 \pm 0.020 | 7.396 \pm 0.023 | 6.941 \pm 0.161 | AAAB |
| RXJ1624.0-2456 | 8.073 \pm 0.025 | 8.018 \pm 0.021 | 7.966 \pm 0.021 | 7.354 \pm 0.168 | AAAB |
| RXJ1624.8-2239 | 6.999 \pm 0.054 | 6.997 \pm 0.020 | 6.983 \pm 0.020 | 6.882 \pm 0.091 | AAAA |
| RXJ1624.8-2359 | 7.610 \pm 0.030 | 7.533 \pm 0.019 | 7.431 \pm 0.053 | 7.248 \pm 0.156 | AAAB |
| RXJ1625.0-2508 | 7.846 \pm 0.026 | 7.816 \pm 0.021 | 7.784 \pm 0.030 | 6.708 \pm 0.105 | AAAA |
| RXJ1625.4-2346 | 7.701 \pm 0.029 | 7.661 \pm 0.020 | 7.690 \pm 0.022 | 8.125 \pm 0.323 | AAAB |
| RXJ1625.6-2613 | 6.812 \pm 0.072 | 6.493 \pm 0.022 | 4.840 \pm 0.015 | 2.668 \pm 0.024 | AAAA |
| ROXR1 13 | 5.840 \pm 0.169 | 5.678 \pm 0.070 | 4.431 \pm 0.043 | 1.562 \pm 0.054 | BAAA |
| RXJ1627.1-2419 | 6.102 \pm 0.083 | 5.499 \pm 0.044 | 2.925 \pm 0.013 | -0.669 \pm 0.010 | AAAA |

Table E2. Supplemental, longer-wavelength photometry for five objects with IR excesses.

| Band | Flux [mJy] | Band | Flux [mJy] | Band | Flux [mJy] | Band | Flux [mJy] | Band | Flux [mJy] |
|-----------------------------|--------------------|-----------------------|------------------|-----------------------|------------------|-----------------------|------------------|-----------------------|-----------------|
| ROXR1 13 | | RXJ1627.1-2419 | | RXJ1625.6-2613 | | RXJ1112.7-7637 | | RXJ1129.2-7546 | |
| IRAC 3.4 μ m | 1300 \pm 93 | IRAS 12 μ m | 2270 \pm 136.2 | IRAS 12 μ m | 447 \pm 44.7 | AKARI 9 μ m | 552 \pm 8.95 | IRAC 3.4 μ m | 8.78 \pm 0.02 |
| IRAC 4.5 μ m | 880 \pm 79 | IRAS 25 μ m | 19800 \pm 1188 | AKARI 18 μ m | 936.1 \pm 18 | AKARI 18 μ m | 348.5 \pm 14.2 | IRAC 4.5 μ m | 8.76 \pm 0.02 |
| IRAC 5.8 μ m | 740 \pm 74 | IRAS 60 μ m | 33800 \pm 3718 | IRAS 25 μ m | 741 \pm 96.33 | IRAS 12 μ m | 491 \pm 34.37 | IRAC 5.8 μ m | 8.79 \pm 0.03 |
| IRAC 8.0 μ m | 690 \pm 73 | IRAS 100 μ m | 166000 (UL) | IRAS 60 μ m | 982 \pm 137.48 | IRAS 25 μ m | 321 \pm 22.47 | IRAC 8.0 μ m | 8.72 \pm 0.04 |
| AKARI 9 μ m | 1347 \pm 244 | AKARI 18 μ m | 9460 \pm 108 | AKARI 65 μ m | 777.4 (UL) | IRAS 60 μ m | 400 (UL) | MIPS 24 μ m | 8.27 \pm 0.2 |
| MIPS 24 μ m | 1800 \pm 200 | AKARI 65 μ m | 23080 (UL) | AKARI 90 μ m | 1010 \pm 332 | IRAS 100 μ m | 458 (UL) | ... | ... |
| MIPS 70 μ m | 12000 \pm 6000 | AKARI 90 μ m | 28210 (UL) | IRAS 100 μ m | 13900 (UL) | IRAC 5.8 μ m | 7.28 \pm 0.02 | ... | ... |
| PACS 70 μ m | 2150 \pm 258 | AKARI 140 μ m | 18640 \pm 4750 | AKARI 140 μ m | 809.8 (UL) | IRAC 8.0 μ m | 6.72 \pm 0.02 | ... | ... |
| PACS 160 μ m | 2310 \pm 291 | AKARI 160 μ m | 24630 \pm 9330 | AKARI 160 μ m | 1849 (UL) | MIPS 24 μ m | 6.29 \pm 0.03 | ... | ... |
| SPIRE 250 μ m | 1500 (UL) | SCUBA 350 μ m | 2761 \pm 57 | ... | ... | ... | 5.30 \pm 0.04 | ... | ... |
| SPIRE 350 μ m | 900 (UL) | SCUBA 450 μ m | 1896 \pm 268 | ... | ... | ... | 3.4 \pm 0.04 | ... | ... |
| SPIRE 500 μ m | 1000 (UL) | SCUBA 850 μ m | 397 \pm 6 | ... | ... | ... | ... | ... | ... |
| IRAM 250 GHz (1200 μ m) | 21.0 (UL) | IRAM 230 GHz (1.3mm) | 95 \pm 15 | ... | ... | ... | ... | ... | ... |
| VLA 6cm | 12.404 \pm 0.043 | ... | ... | ... | ... | ... | ... | ... | ... |
| VLA 1.4 GHz (2.1CM) | 6.1 (UL) | ... | ... | ... | ... | ... | ... | ... | ... |

Notes:

AKARI infrared camera all-sky survey 9 μ m and 18 μ m data from [Ishihara et al. \(2010\)](#).90 μ m, 140 μ m, and 160 μ m from [Yamamura et al. \(2010\)](#).Spitzer IRAC and MIPS data from [Luhman et al. \(2008\)](#).Herschel PACS and SPIRE data from [Cieza et al. \(2013\)](#).SCUBA data from [Andrews & Williams \(2007\)](#).250MHz data from [Altenhoff et al. \(1994\)](#), 1.3mm data from [Motte et al. \(1998\)](#).1.4GHz data from [Condon et al. \(1998\)](#).6-cm data from [Gagné et al. \(2004\)](#).

This paper has been typeset from a \LaTeX file prepared by the author.